NTIA TR-25-579

U.S. Department of Commerce
National Telecommunications and Information Administration

Institute for Telecommunication Sciences
Technical Report

2024 McMurdo Area Radio Noise Measurements and Analysis

Robert J. Achatz, Adam C. Hicks, Sarah L. Vasel, Ryan S. McCullough

September 2025
Boulder, Colorado
its.ntia.gov

Institute for Telecommunication Sciences
Technical Report
NTIA TR-25-579
September 2025

2024 McMurdo Area Radio Noise Measurements and Analysis

Robert J. Achatz, Adam C. Hicks, Sarah L. Vasel, Ryan S. McCullough

United States Department of Commerce

National Telecommunications and Information Administration

Institute for Telecommunication Sciences
325 Broadway, Boulder CO 80305
its.ntia.gov

This publication is available free of charge from:
https://doi.org/10.70220/lfcj7dpl

About the Institute for Telecommunication Sciences

The Institute for Telecommunication Sciences (ITS) is the research and engineering laboratory of the National Telecommunications and Information Administration (NTIA), an agency of the U.S. Department of Commerce (DoC). ITS manages the telecommunications technology research programs of NTIA and the DoC-owned Table Mountain Radio Quiet Zone. ITS works closely with other NTIA Line Offices to support Administration and Agency needs.

The mission of ITS is to ADVANCE innovation in communications technologies, INFORM spectrum and communications policy for the benefit of all stakeholders, and INVESTIGATE our Nation's most pressing telecommunications challenges through research that employees are proud to deliver.

ITS publishes fundamental research communications as part of its Technology Transfer efforts. We are committed to ensuring that our publications are substantive, technically sound, accurate, and clear. A rigorous peer review process, documented in the "ITS Publications Handbook Volume I: Policies (Third Edition)," safeguards the scientific integrity of ITS technical publications, journal articles, and conference papers. The principles for technical peer review of manuscripts guide parallel peer review processes for the publication of software and datasets.

ITS reports authored by NTIA employees are subject to 17 U.S.C. §105 are U.S. Government works and generally not subject to copyright protection in the United States. ITS publications, including software and datasets, are freely and openly available at its.ntia.gov or github.com/NTIA.

Principal NTIA Formal Publication Series Published by ITS

NTIA Technical Report (TR): Important contributions to existing knowledge of less breadth than a monograph, such as results of completed projects and major activities.

NTIA Technical Memorandum (TM): Technical information typically of less breadth than an NTIA Technical Report. The series includes data, preliminary project results, and information for a specific, limited audience.

NTIA Special Publication (SP): Conference proceedings, bibliographies, course and instructional materials, or major scientific studies mandated by Congress.

NTIA Monograph (MG): A scholarly, professionally oriented publication dealing with state-of-the-art research, or an authoritative treatment of a broad area. Expected to have long-lasting value.

NTIA Handbook (HB): Information pertaining to technical procedures; reference and data guides; and formal user's manuals that are expected to be pertinent for a long time.

For more information about NTIA fundamental research publications, contact the ITS Publications Office at 325 Broadway, Boulder, CO, 80305 Tel. 303-497-3572 or email ITSinfo@ntia.gov.

Disclaimer

Certain commercial equipment and materials are identified in this report to specify adequately the technical aspects of the reported results. In no case does such identification imply recommendation or endorsement by the National Telecommunications and Information Administration, nor does it imply that the material or equipment identified is the best available for this purpose.

Contents

Figures

Tables

Acknowledgments

This work was completed in support of the NSF Spectrum Innovation Initiative (SII) under an interagency agreement between the National Telecommunications and Information Administration Institute for Telecommunication Sciences (NTIA ITS) and the National Science Foundation (NSF) Spectrum Innovation Initiative (SII).

The authors wish to acknowledge the following organizations and individuals, without whose support and assistance the research reported here could not have been completed.

NSF, for sponsorship and continual engagement, specifically Patrick Smith, Technology Development Manager, Polar Research Support.

Naval Information Warfare Center (NIWC) Atlantic Office of Polar Programs for continued collaboration, assistance, and coordination, specifically Matt Rushing, Polar Program IPT Manager; Ean Schroeder, Chief Engineer; and Sarah Conner, Communications and Network Engineer.

NIWC contractor engineers for "on-ice" logistics, technical, and measurement support, specifically Michael Goad, Steve Hidden, Matt Frazier, John Gomez, and Graeme Fluerty.

Chris Cianflone, ASC, for providing necessary equipment and access to the MACOPS and Ham Shack locations; Shelly Campbell, ASC, for providing access to the Arrival Heights location; and Jenn Dougherty, NASA, for providing access to the MGS location.

Dr. Robert Johnk, formerly with ITS, for Numerical Electromagnetic Code (NEC) modeling and simulation of short vertical monopole (SVM) on ground. Nicholas DeMinco of ITS for NEC modeling and simulation of SVM on ground and predictions of ground wave propagation loss.

Abbreviations/Acronyms

Acronym	Definition
AHFMS	Antarctica high-frequency monitoring system
ASC	Antarctic support contract
ATC	air traffic control
BITF	Black Island telecommunication facility
CDF	cumulative distribution function
CCDF	complementary CDF
CM	conical monopole
EM	electromagnetic
D-RAP	D Region Absorption Prediction
dB	decibel
dBi	decibel relative to isotropic radiator
dBm	decibel relative to a milliwatt
EMC	electromagnetic compatibility
FFT	fast Fourier transform
hr	hour or hours
HF	high frequency (3–30 MHz)
HP	Hewlett Packard
IAA	Interagency Agreement
IP3	third-order intercept point
I/Q	in-phase/quadrature
ITS	Institute for Telecommunication Sciences
ITU	International Telecommunication Union
J	joules
kHz	kilohertz
km	kilometer
kS/s	kilo samples per second

m	meter
M4	minimum, median, mean, and maximum
MACOPS	McMurdo Communications and Operations
mi	statute mile
min	minute or minutes
MHz	megahertz
MMN	man-made radio noise
ms	milliseconds
MS	McMurdo Station
MS/s	mega samples per second
NA	not available or applicable (depending on context)
NEC	Numerical Electromagnetic Code
NIWC	Naval Information Warfare Center
NOAA	National Oceanic and Atmospheric Administration
NTIA	National Telecommunications and Information Administration
NSF	National Science Foundation
OPP	Office of Polar Programs
PCA	polar cap absorption
PR	portable rod
PSD	power spectral density
R&D	research and development
R-S	Rhode-Schwarz
RF	radio frequency
RMS	root mean square
S/s	samples/second
SDR	software-defined radio
sec	second or seconds
SII	Spectrum Innovation Initiative
SME	subject matter expert
SNR	signal-to-noise ratio

SuperDARN	Super Dual Auroral Radar Network
SVM	short vertical monopole
TDRSS	tracking and data relay satellite system
TMRQZ	Table Mountain Radio Quiet Zone
USAP	United States Antarctic Program
USN	United States Navy
V	volts

Executive Summary

The Institute for Telecommunication Sciences (ITS) performed high frequency (HF) band (3–30 MHz) radio noise power measurements at six locations in the McMurdo Station (MS), Antarctica (AQ), area and one location at the Black Island Telecommunication Facility (BITF) 32 km (20 mi) from MS. The primary purpose of the measurements is to compare MS and BITF radio noise powers so that HF radio system designers can assess the feasibility of relocating BITF air traffic control (ATC) and field party communication HF antennas and receivers to MS.

This work is funded through a multi-year interagency agreement (IAA) with the National Science Foundation (NSF) Spectrum Innovation Initiative (SII). Under the IAA, ITS is to provide subject matter expertise (SME) on spectrum engineering issues across the Antarctica continent, including at McMurdo Station (MS), the South Pole, and the Palmer research station on the peninsula. Currently ITS is focused on providing HF radio band SME to the NSF Office of Polar Programs (OPP) and the Naval Information Warfare Center (NIWC) HF Radio Modernization Project which is considering consequential changes to the Antarctica HF radio system.

HF band receiver performance is impacted greatly by man-made radio noise (MMN) generated by electrical devices. MMN power is correlated to the types and numbers of electrical devices in an environment so, in order of increasing noise power, MMN is categorized as that found in quiet rural, rural, residential, and urban noise environments. More than 35 years ago HF ATC radio receivers were moved from McMurdo Station (MS) to the Black Island Telecommunication Facility (BITF) to minimize MMN and radio signal shadowing by Ross Island terrain.

Because of changes in electrical device technologies and use, it is conceivable that MMN power has decreased enough to consider moving the HF ATC receivers back to MS where they can be more easily maintained during the Antarctica winter. This report summarizes the findings of a December 2024 ITS HF noise measurement campaign, the goal of which was to answer that question.

Our approach was to assemble a portable radio noise measurement system; characterize the measurement system at the ITS Table Mountain Radio Quiet Zone (TMRQZ) in Boulder, CO; transport the measurement system to Antarctica; and measure radio noise power at the BITF, where the HF receivers are currently located, and at six sites in and around MS where the HF receivers might be relocated. Measurement durations ranged from 1 to 24 hours.

The portable measurement system used a short vertical monopole (SVM) or portable rod (PR) antenna placed on a radial ground plane. Impedance matching was provided by an “active” (transistorized) circuit. Characterization measurements demonstrated the system capable of measuring noise powers as low as those in rural environments.

The 24-hour measurement data was processed to show spectrum occupancy from 3.8 to 32 MHz at the BITF and MS MTRS-2 facility on the bluffs above MS. Most signals occupied the lower part of the HF band below 15 MHz, but the signal population differed between

locations. As an example, the powerful SuperDARN radar was much less prominent at the BITF than at MS MTRS-2.

Noise power was analyzed on off-route (OR) ATC frequency channels that are unoccupied most of the day. Results show noise power to be generally higher at MS than at BITF. Noise at the BITF was close to that of a quiet rural environment. Noise at MS in-town locations varied between rural and residential. Locations on the bluff surrounding MS varied between residential and urban. The most concerning finding was that 9 MHz noise was comparable to that of an urban setting. Lower rural noise power was found in a brief measurement at the MS Ham Shack (HS) location. However, times when these lower powers were present were interrupted by times with strong, nearby noise sources.

BITF and MS T-Site results were also compared to those of a prior ITS study using only fixed conical monopole (CM) antennas. The prior CM results showed that T-Site had considerably more noise than the BITF. The current measurements corroborate the prior CM results including much higher noise at 9 MHz.

Until we performed our measurements, the Stanford University (SU) study performed in 1970[1] was the most comprehensive study of MS HF radio noise. The goal of those measurements was to locate a radio quiet MS location for noise sensitive measurements. Our measurements showed noise powers considerably lower than the SU measurements. This suggests that MS noise power may have decreased from that time.

Inevitably problems occur during measurement campaigns. The measurement plan called for two systems being used simultaneously. One of the systems was battery powered and capable of operating away from buildings that are a source of MMN. The shipment with the battery powered system did not arrive, so we collected less data using a system tethered to a building power supply.

Recommendations for future work include

- On-ice measurements at more in-town, on-bluff, and remote MS locations
- Automated measurements throughout the year to determine ionospheric effects
- Analysis of radio noise instantaneous amplitude statistics
- On-ice investigations into the causes of the odd spectral bumps and spikes in this measurement data set

This work focused primarily on the effect of radio noise on ATC communications. Antarctica is a vital hub for international scientific research. In many cases the reliability of the research results depends on knowing what signals and noise are present. Following through with these recommendations will bolster the reliability of research results.

[1] M.J. Sites and G.F. Stuart, "An Electromagnetic Survey of the Hut Point Peninsula and Adjacent Regions," Radioscience Laboratory, Stanford Electronics Laboratory, Stanford University, Stanford, California, Technical Report 3640-1, October 1971. (Prepared for The Office of Polar Programs, National Science Foundation under NSF Grant GA-19603.)

2024 McMurdo Area Radio Noise Measurements and Analysis

Robert J. Achatz, Adam C. Hicks, Sarah L. Vasel, Ryan S. McCullough[2]

Abstract: The Institute for Telecommunication Sciences (ITS) performed high frequency (HF) band (3–30 MHz) radio noise power measurements at six locations in the McMurdo Station (MS), Antarctica (AQ), area and one location at the Black Island Telecommunication Facility (BITF) 32 km (20 mi) from MS. The primary purpose of the measurements is to compare MS and BITF radio noise powers so that HF radio system designers can assess the feasibility of relocating BITF air traffic control (ATC) and field party communication HF antennas and receivers to MS. Measurements were performed with portable rod (PR) and fixed conical monopole (CM) antennas. Twenty-four–hour spectrum occupancy plots show most signals below 15 MHz at BITF and MS. Differences in signal populations between locations were observed. Taking into account the location variability endemic to radio noise, noise at the ATC channel frequencies was found to be generally higher at MS than at BITF. BITF noise was similar to what would be expected of a quiet rural noise environment. MS noise was similar to what would be expected of a rural or residential noise environment, although noise at 9 MHz was comparable to that of an urban setting.

Keywords: active rod antenna, air traffic control communications, Antarctica, high frequency radio, HF, man-made radio noise, McMurdo Station, radio noise, spectrum occupancy, Table Mountain Radio Quiet Zone

1. Introduction

The Institute for Telecommunication Sciences (ITS) performed high frequency (HF) band (3-30 MHz) radio noise power measurements at six locations in the McMurdo Station (MS), Antarctica (AQ), area and one location at the Black Island Telecommunication Facility (BITF) 32 km (20 mi) from MS. The primary purpose of the measurements is to compare MS and BITF radio noise powers so that HF radio system designers can assess the feasibility of relocating BITF air traffic control (ATC) and field party communication HF antennas and receivers to MS.

[2] The authors are with the Institute for Telecommunication Sciences, National Telecommunications and Information Administration, U.S. Department of Commerce, Boulder, CO 80305.

This work is funded through a multi-year interagency agreement (IAA) with the National Science Foundation (NSF) Spectrum Innovation Initiative (SII) Center. Under the IAA, ITS is to provide subject matter expertise (SME) on spectrum engineering issues across the Antarctica continent, including at McMurdo Station (MS), the South Pole, and the Palmer research station on the peninsula. Currently ITS is focused on providing HF radio band SME to the NSF Office of Polar Programs (OPP) and the Naval Information Warfare Center (NIWC) HF Radio Modernization Project which is considering consequential changes to the Antarctica HF radio system.

1.1 Problem with Current HF ATC Radio Links

Figure 1 depicts how current MS ATC radio links use the HF radio band to establish voice communications between an aircraft and the MS Communications and Operations (MACOPS) center. The aircraft transmits an HF signal to receivers located at the remote Black Island Telecommunications Facility (BITF) approximately 32 km (20 mi) from MS. The received HF signal is then processed for retransmission at microwave frequencies to the MACOPS. The BITF HF and microwave antennas are shown in Figure 2. Signals from the MACOPS are transmitted to the aircraft from HF transmitters located at the transmitter site (T-Site) on a bluff above MS.

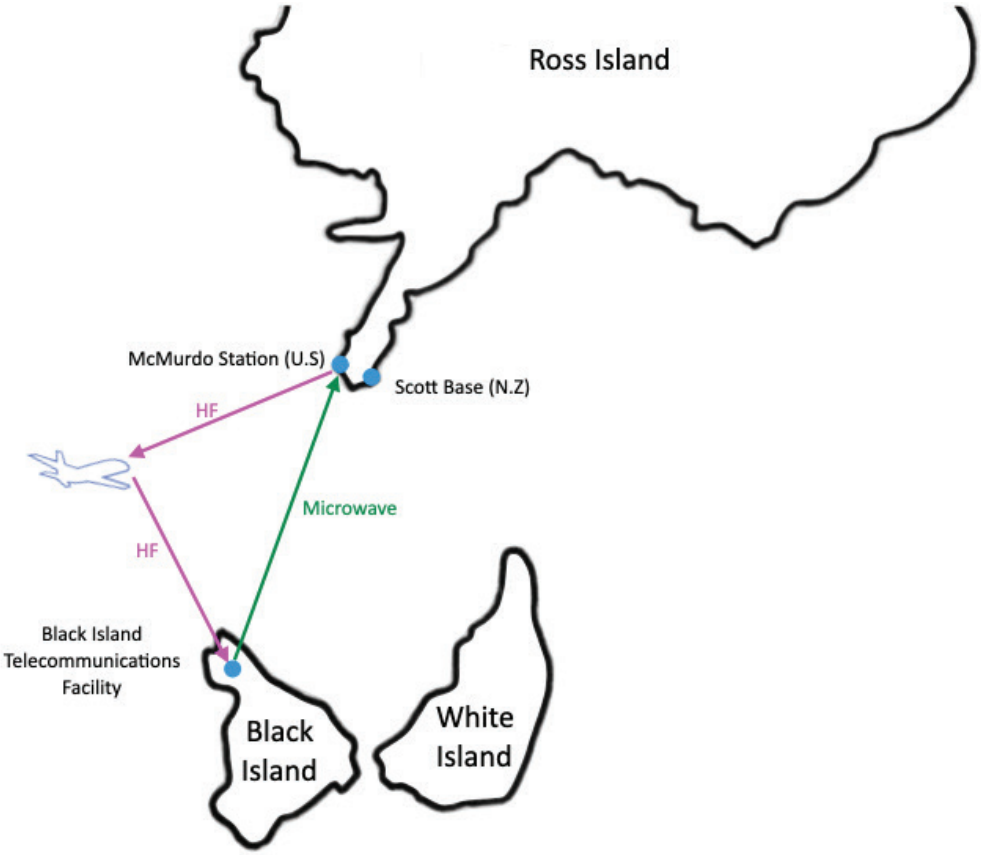

Figure 1. Current MS ATC radio links. (Credit: Kenneth Tilley)

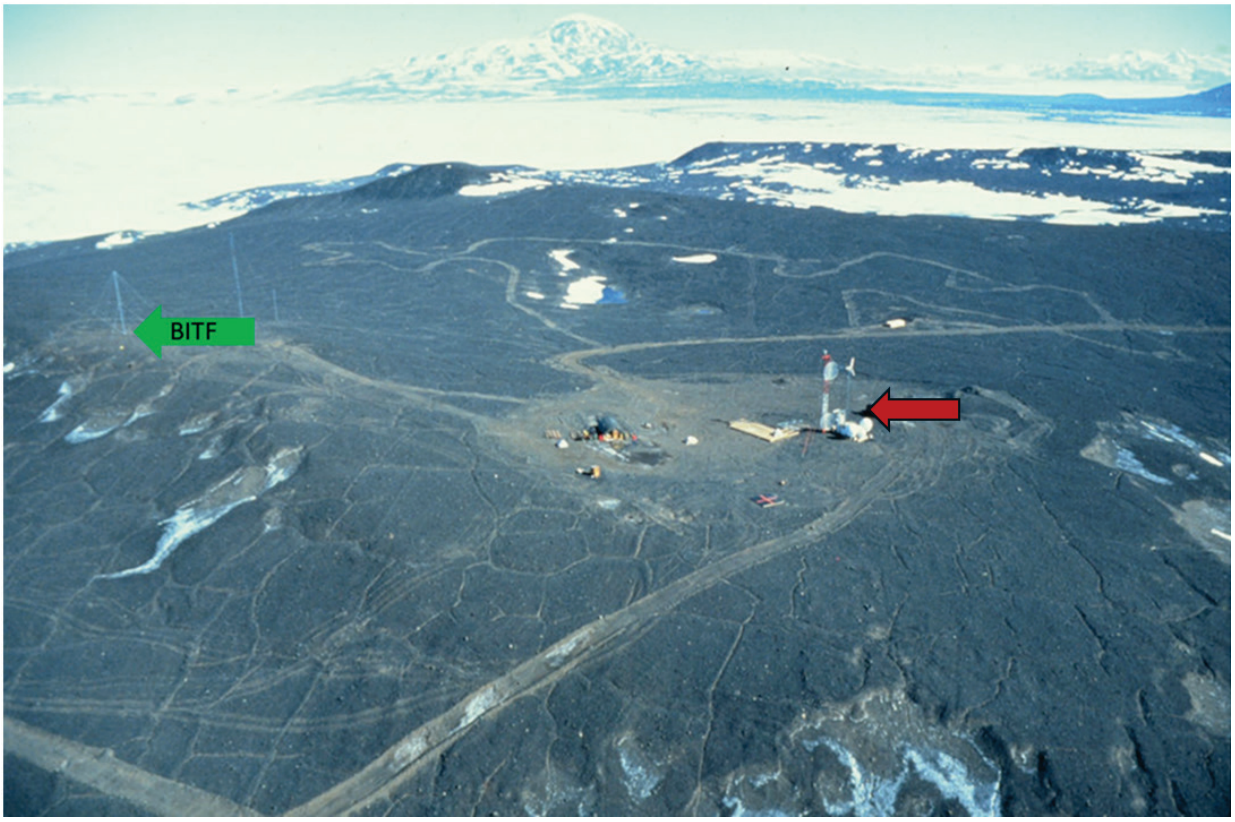

Figure 2. BITF with HF receive and microwave transmit antennas. The HF receive antenna is on a hill and identified by the green arrow. The microwave transmit antenna is at the top of the tall red and white tower and identified by the red arrow. (Credit: NIWC 1989/90)

The HF receivers were moved from MS to the BITF more than 35 years ago to minimize man-made noise (MMN) radiated by electrical devices and radio signal shadowing by such Ross Island terrain as Mount Erebus and Mount Terror. The former HF receive antenna field was located near the present-day Ham Shack location. Although the move MS to the BITF improved HF ATC receiver performance, it also hindered the repair and maintenance of the receivers during the Antarctic winter. In the austral summer the trip to the BITF is a quick helicopter ride. The same trip in the winter is a dark, long, and dangerous tractor ride.

The decision to locate HF ATC receivers on Black Island was informed in part by radio noise measurements that showed there was no practical radio quiet MS location for the receivers [1]. Because of changes in electrical device technologies and use, it is conceivable that MMN power has decreased enough to consider moving the HF ATC receivers back to MS. This report summarizes the findings of a December 2024 HF radio noise measurement campaign, the goal of which was to answer that question.

1.2 HF Radio Noise

Radio noise in the HF band consists of atmospheric, galactic, and MMN components. Atmospheric radio noise is created by lightning. Galactic radio noise is created by our Milky

Way galaxy. MMN is incidentally generated by electrical and electronic devices, such as power lines and power distribution equipment shown in Figure 3, automotive ignition systems, electric motors, and electronic power supplies.

Figure 3. Power lines and power distribution equipment in gray metal cabinets in front of MS power generator buildings 196 and 198. (Credit: Robert Achatz)

Figure 4 shows the International Telecommunication Union (ITU) median noise figure model [2] predictions, described in Appendix A, for Antarctica. The model shows that the Antarctica atmospheric median noise figure is expected to vary by month and time of day and the MMN median noise figure is expected to vary with setting or environment. In order of increasing noise power, the environments are *quiet rural*, *rural*, *residential*, and *urban*. Noise power corresponding to these environments is often referred to by the environment name. For example, residential noise refers to the noise power typically found in a residential environment.

Rural, residential, and urban noise is modeled to 250 MHz. Quiet rural noise is modeled to only 30 MHz because it consists of noise generated distantly and, like atmospheric noise, propagated around the world by skywaves reflected by the earth's ionospheric layers. Skywave reflection only occurs at frequencies below the F2 layer critical frequency, which depends on time-of-day, season, and sunspot cycle. Above the critical frequency, the ionosphere gradually becomes transparent, atmospheric and man-made noise propagate to

outer space, and galactic noise is all that remains. Skywave propagated noise is also vulnerable to absorption by the D-layer.

D-layer absorption and F2 layer critical frequency increase during the day and decrease during the night. This prompts radio operators to transmit at higher frequencies during the day and lower at night. Similarly, we would expect skywave propagated noise to be higher frequency during the day and lower at night.

Locally generated MMN propagated along a ground path can be separated from distantly generated noise propagated along a skywave path with two antenna measurements [3]. The antennas are separated by 500 m to 10 km so local sources have different ground paths but distance sources have the same skywave path.

High latitude ionospheric propagation differs from the other, i.e. mid and low, latitudes [4]. Noise propagating from other latitudes to the MS area will therefore have different characteristics than noise propagating completely within the other latitudes. The most significant difference is the chance for high D-layer polar cap absorption (PCA) events that are caused by major solar flares and can persist for days. The NOAA Space Weather Prediction Center provides historical D-Region Absorption Prediction (D-RAP) model data for determining the presence of a PCA event [5].

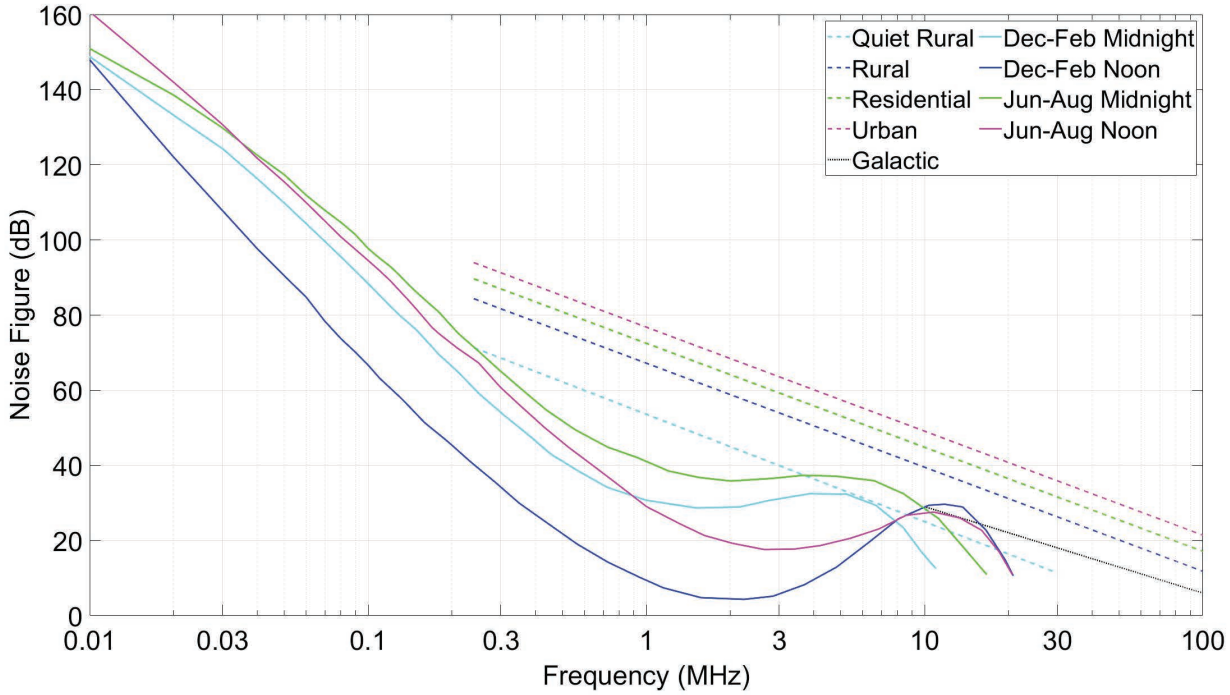

Figure 4. ITU median man-made and atmospheric noise figures.

The differences in MMN environment median noise figures, shown in Table 1, are independent of frequency. However, as shown in Table 2, this median noise figure is expected to vary in a frequency dependent manner from location to location within an environment. Location variability is an important consideration in our measurement analysis.

Table 1. Noise figure differences in dB between MMN environments.

	Rural	Residential	Urban
Quiet Rural	14.8	20.1	24.4
Rural	–	5.3	9.6
Residential	-5.3	–	4.3

Table 2. MMN median noise figure standard deviation in dB.

Frequency (MHz)	Rural	Residential	Urban
2.5	8.0	8.1	9.1
5.0	7.7	5.5	6.1
10.0	4.0	2.9	4.2
20.0	4.5	4.7	4.9

1.3 Approach

Our approach was to assemble a portable HF radio noise measurement system, characterize the measurement system at the Table Mountain Radio Quiet Zone (TMRQZ) in Boulder, CO, U.S.A.; transport the measurement system to Antarctica; measure noise at the BITF where the ATC receivers are currently located, and at six sites in and around MS where the ATC receivers could be relocated.

While most measurements used a portable short (1 m) vertical monopole (SVM) antenna – referred to as the portable rod (PR) – the measurement system could also be connected to fixed and much taller conical monopole (CM) antennas used by the MS HF radio system.

This report provides spectrum survey and noise figure results. The spectrum survey results span the entire 3.8–32 MHz BITF CM antenna frequency range. Noise figure results focus on the off-route (OR) ATC channel frequencies listed in Table 3. While critical in everyday ATC operations, the channels are unused for much of the day. This makes them ideal for noise measurement. The 9.032 MHz ATC channel was reported to be the primary channel and thus is highlighted in our results.

Indications of measurement quality are derived from standard frequency and time reference (SFTR) signals [6] transmitted by services such as the USA WWV, Chinese BPM, Indian ATA, and Argentinian LOL. No attempt was made to demodulate these signals to determine their origin.

Data processing converted the measured power spectral densities (PSD) to the noise figure needed by HF radio system engineers. Results were also compared to those from previous measurement campaigns to investigate whether the MS HF radio noise environment had changed over the years.

Table 3. ATC and SFTR channels.

Type	Frequency (MHz)	Note
ATC	4.718	
SFTR	5	WWV, BPM, ATA, LOL
ATC	5.726	
ATC	6.708	
ATC	9.032	US 5, primary channel
SFTR	10	WWV, BPM, ATA, LOL
ATC	11.256	US 5
ATC	13.251	US 5
SFTR	15	WWV, BPM, ATA, LOL
ATC	18.000	
SFTR	20	WWV

2. Methods

2.1 Measurement System

The general measurement system, shown in Figure 5, consists of an antenna, impedance matching circuit, transmission line, receiver, and computer to control the measurement and store data.

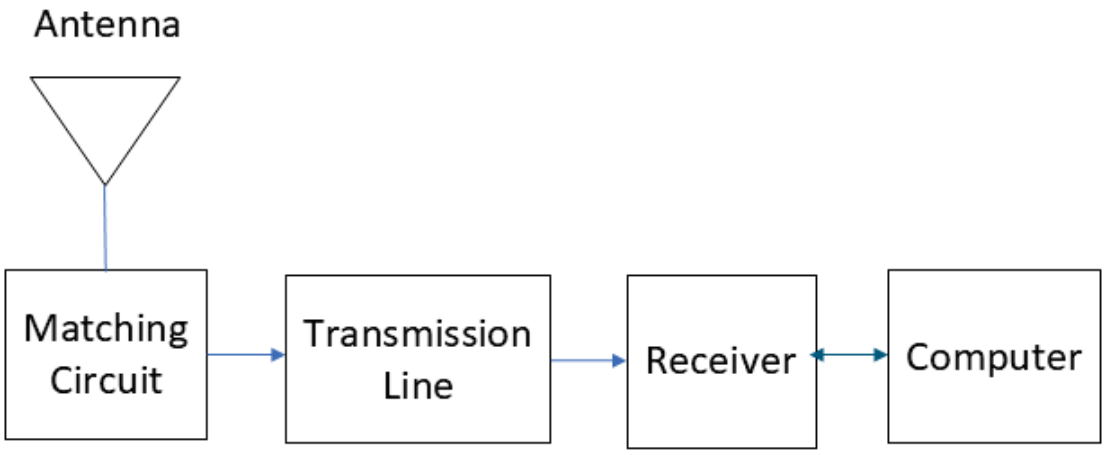

Figure 5. General measurement system.

The antenna, matching circuit, and transmission lines were configured in three ways, as summarized in Table 4. The entire portable system ITS brought to Antarctica consisted of a PR antenna, "active" i.e. transistorized matching circuit, and transmission line with bias unit to supply power to the matching circuit. The MACOPS and BITF systems consisted of existing fixed HF radio system antennas, passive matching circuits, and transmission lines. A picture of the filters and receiver, common to all systems, is shown in Figure 6.

Table 4. Measurement system configurations.

System	Antenna	Matching Circuit	Transmission Line
Portable	PR	Active	30.48 m (100 ft) with antenna bias unit
MACOPS	"Backup" CM	Passive	45.7 m (150 ft)
BITF	"Out of Service" CM	Passive	167.64 m (550 ft) with multi-coupler

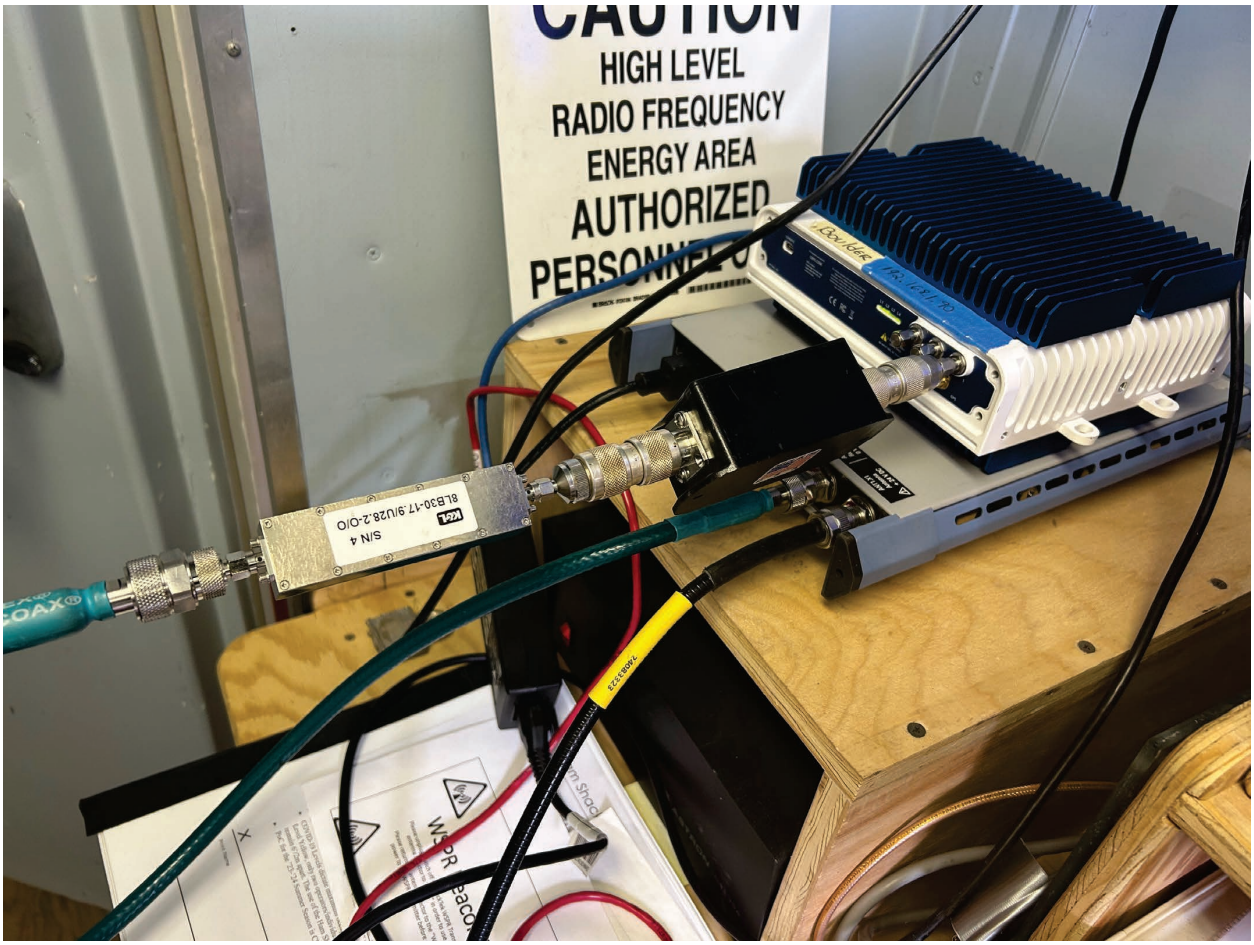

Figure 6. Typical receiver setup at MS Ham Shack location. Receiver with dark blue cooling fins is on top of a PR bias unit that supplies power to the active matching circuit. The black cable from PR antenna enters the bias unit. The green cable exits the bias unit and is connected to the filters that are attached to the receiver. A laptop computer is beyond the frame of the picture. (Credit: Robert Achatz)

2.1.1 Antennas

Antenna specifications are summarized in Table 5. A drawing of a typical CM antenna is shown in Figure 7 [7], [8]. This antenna is permanently mounted in the ground and surrounded by a radial ground plane, similar to that shown in Figure 8. The antenna's impedance is comparable to the transmission line's impedance, and so passive impedance matching is used.

A photograph of the PR antenna is shown in Figure 9 [9], [10]. This antenna is composed of a 1 m rod attached to the housing of an "active" or transistorized impedance matching circuit recommended for use by the ITU [3]. The rod's impedance can be considerably less than the transmission line's. Active impedance matching is used because it achieves wider bandwidths and higher efficiencies than a passive impedance matching circuit while limiting its transistor noise to that of a rural noise environment. The active circuity is not protected from overload by a bandpass filter but is designed to withstand high low-frequency atmospheric noise power.

Pre-trip numerical electromagnetic code (NEC) simulations and TMRQZ field experiments showed how important it is to operate the PR antenna on a quarter-wavelength radius radial ground plane [11],[12]. Benefits include maximizing directivity on the horizon, minimizing ground loss, and rendering the impedance matching circuit the antenna impedance it expects. Additionally, the measurement must be conducted on a ground plane since manufacturer antenna factors, used to convert measured power to field strength, are determined on a ground plane.

We used a relatively easy to set up and tear down radial ground plane consisting of 20 15.24 m (50 ft) long radials and shown in Figure 10. This radial length is ideal at 4.9 MHz and is only slightly less than the recommended 15.9 m (52.1 ft) radius at the lowest 4.718 MHz ATC channel frequency.

Bonding the ground plane to the antenna and a metallic rod driven deep into the ground, i.e. a ground rod, is the best practice for fixed HF antennas. Because of Antarctica ground conditions it was not practical to install a ground rod at every PR measurement location. Furthermore, in our TMRQZ tests, we did not notice any improvement with a metallic rod driven a practical 0.3 m (1 ft) into the ground. Therefore we did not use a ground rod during the Antarctica measurements.

Figure 11 compares theoretical realized or practical gains, i.e., antenna gains with impedance matching circuit loss, of CM and PR antennas on a ground plane.

Table 5. Antenna characteristics.

Antenna	Manufacturer Model Number	Dimensions	Frequency Range (MHz)	Practical Gain (dBi)
PR	R&S HE010E	1 m	8.3 kHz to 100 MHz	-28.7 at 3.8 MHz -10 at 32 MHz
MACOPS	TCI-506-6N	9.8 m (32 ft) high 20.1 m (66 ft) diameter at guy points	5.0–30.0	4.8
BITF	TCI-550-4	18.9 m (62 ft.) high 40.7 m (133.5 ft.) diameter at guy points	3.8–32.0	4.8

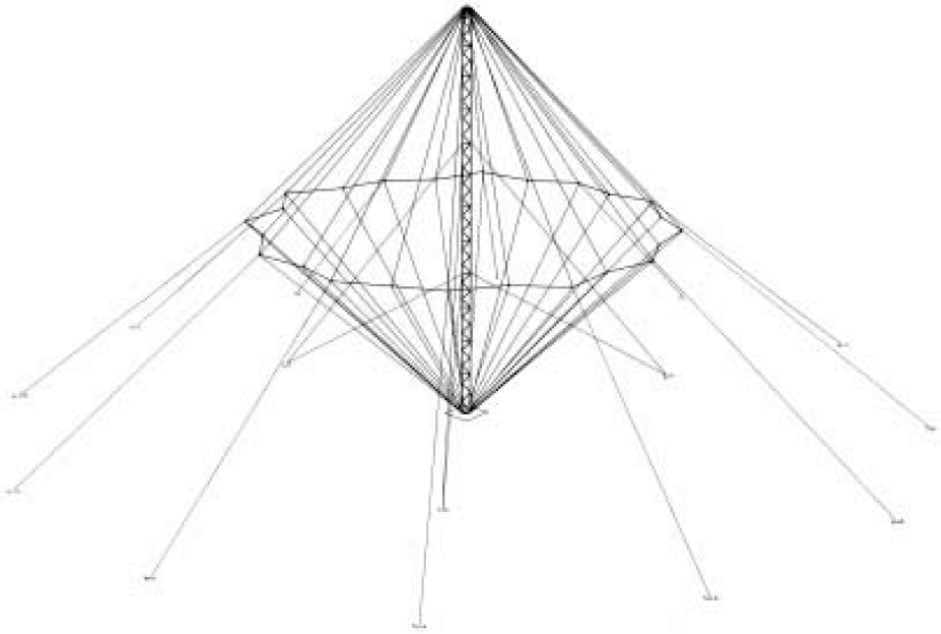

Figure 7. TCI Model 550 -4 CM antenna. (Credit: TCI International, Inc)

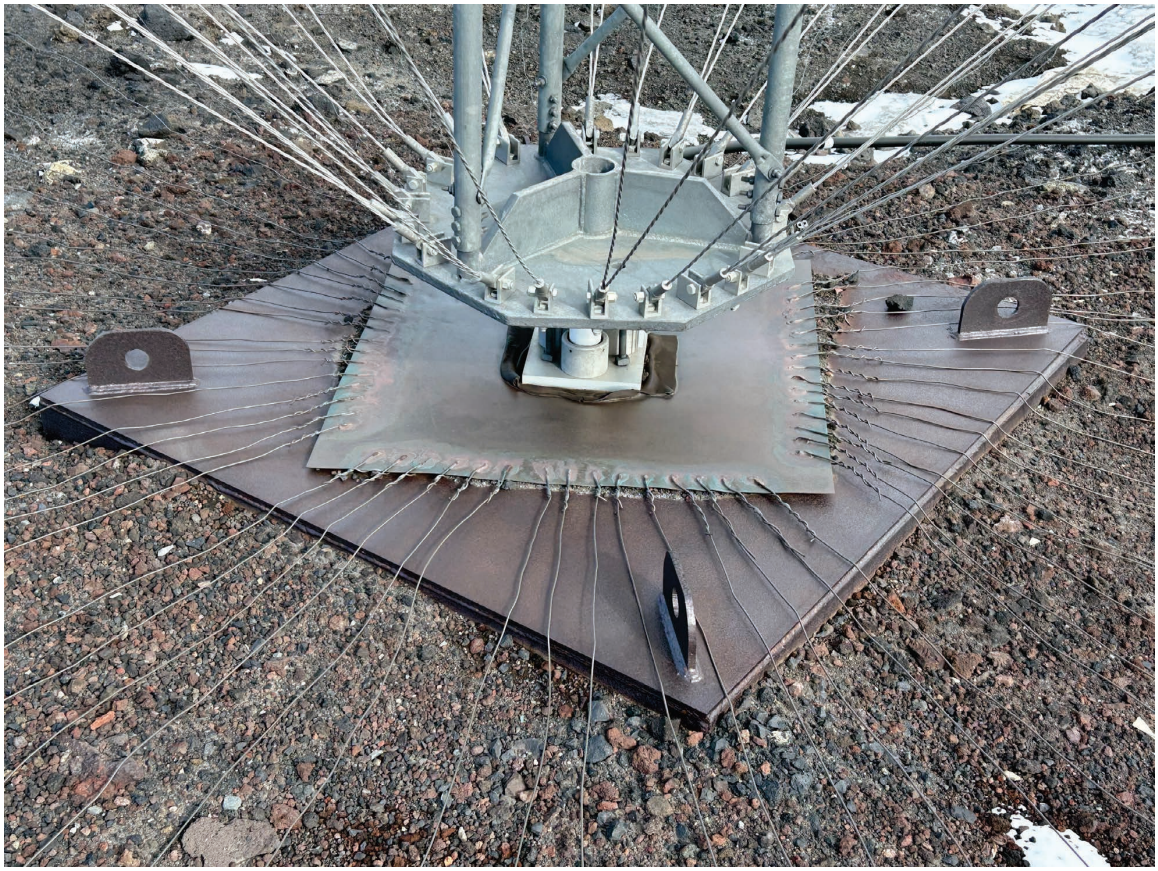

Figure 8. CM antenna base and radial ground plane. The ground plane has 60 radials 19.7 m, or 65 ft, long. (Credit: Robert Achatz)

Figure 9. R&S®HE010E active rod antenna, the PR antenna ITS used. It is approximately 1 m high. (Credit: Rhode & Schwarz Inc.)

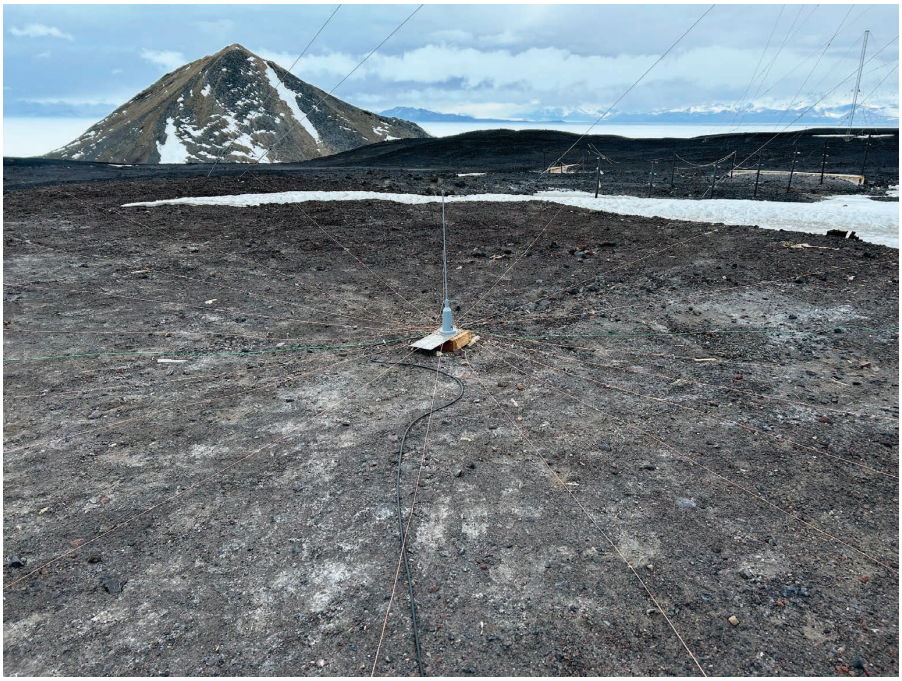

Figure 10. PR and radial ground plane at T-Site location. (Credit: Robert Achatz)

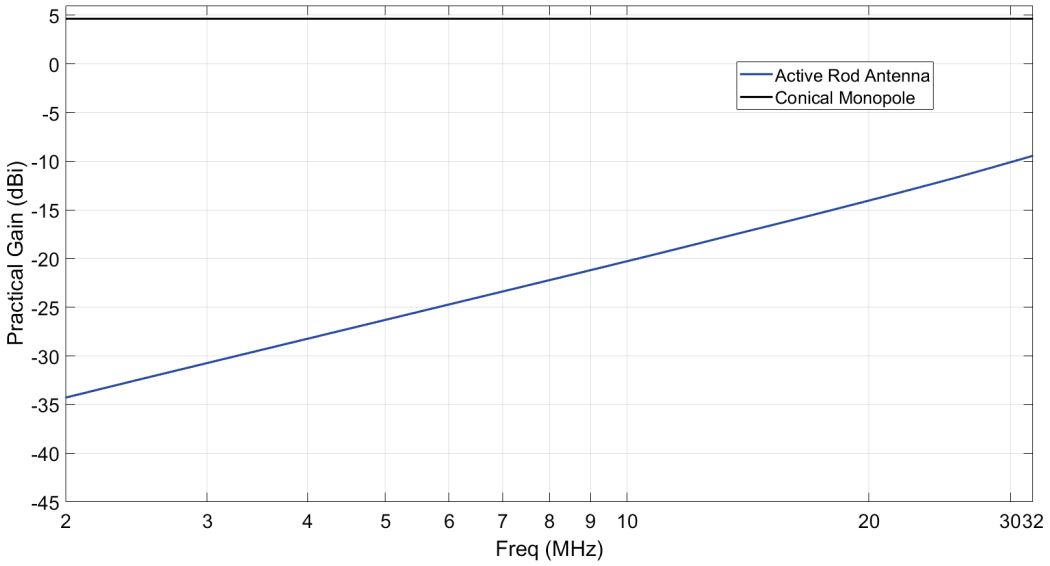

Figure 11. Theoretical practical gains for active portable rod and conical monopole antennas on ground plane.

2.1.2 Transmission line

In addition to cable, the transmission line includes components such as the PR antenna bias unit (that powers the impedance matching circuit), BITF multicoupler (that splits and amplifies the signal so it can be used by multiple receivers), band pass filter (BPF), and a common mode noise rejection (CMNR) filter. Figure 12 shows block diagrams of the portable, MACOPS, and BITF transmission lines.

A 3.8 to 32 MHz BPF was used in all measurements to prevent receiver overload from atmospheric noise, a nearby 2.9 MHz radar, VHF radios, and FM radio stations. The CMNR filter removes effects of cable outer shield currents induced by strong signals. The MACOPS and BITF systems had bulkhead connectors for joining outdoor and indoor cables.

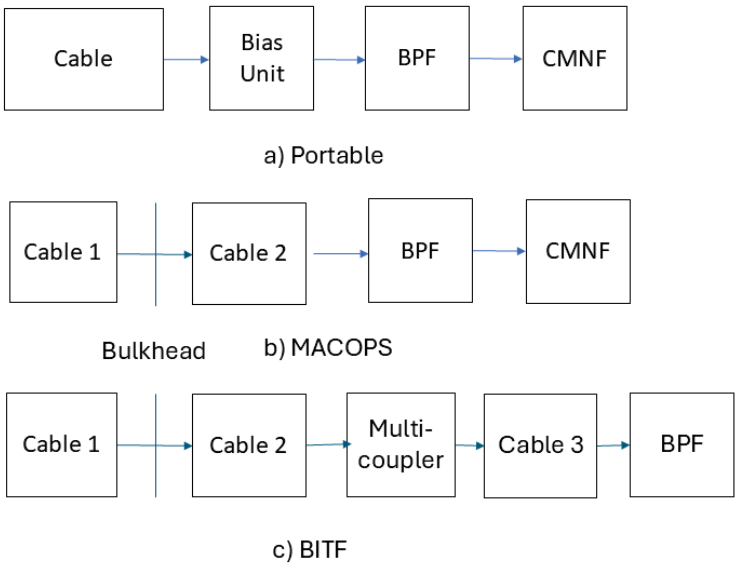

Figure 12. Transmission lines for the portable, MACOPS, and BITF systems.

2.1.3 Receiver

The receiver is a software defined radio (SDR) controlled by off-the-shelf spectrum measurement software. The receiver operates from 9 kHz to 8 GHz over 12 frequency bands. We use the lowest 9 kHz to 50 MHz frequency band which includes the HF radio band of interest. The receiver signal processing is composed of cascaded filters, amplifiers, variable attenuators, and an analog to digital converter (ADC). The first two amplifiers in the cascade, collectively referred to as the low noise amplifier (LNA), are not protected by the variable attenuators that protect the ADC from power above its dynamic range. Receiver settings are summarized in Table 6.

The fundamental measurement data product is a PSD, $P_{meas}(f)$, created by the SDR from a number of wideband signals that have been transformed to the frequency domain and mean squared averaged. Mathematically

$$P_{meas}(f) = \frac{1}{N}\sum_{n=1}^{N}|X_n(f)|^2$$

where $X(f)$ is the Fourier transformed product of the signal, $x(t)$, and a window function, $w(t)$

$$X(f) = \mathcal{F}\{x(t)w(t)\}\,.$$

The PSD size is determined by

$$N_{psd} = N_{fft}\frac{f_{span}}{f_s} \tag{1}$$

Where N_{fft} is the number of FFT data points, f_s is the receiver sample rate in S/s, and f_{span} is the receiver frequency span in Hz.

Receiver automatic gain control (AGC) is turned off because it can introduce an unknown amount of noise into the measurement. Signal compression flagging is used to identify data that exceeds the ADC dynamic range causing "overload" which manifests itself as higher noise floors and harmonic and intermodulation distortion. The entire PSD is flagged if just one of the time domain samples used to create it caused overload.

Table 6. Receiver signal processing settings.

Parmeter	Value
Sample rate	62.5 MS/s
FFT size	16,384
FFT period	262 μs
FFT frequency resolution	3.817 kHz
FFT window	Blackman Harris
FFT window equivalent noise normalized BW	2.0
FFT resolution BW	7.647 kHz
PSD range	2 MHz–32 MHz
PSD span	30 MHz
PSD size	7864
PSD detection algorithm	RMS
RMS averages	100
RMS averaging period	26.2 ms
PSD collection period	1 min
PSD collection rate	1 PSD/min
AGC	Off or Manual
Signal compression flagging	On
Attenuation	0–35 dB, Typically 0–20 dB

2.2 Noise Figure Data Processing

Data processing converts measured PSD referenced to the receiver input to a noise figure referenced to the terminals of a lossless antenna. Processing steps for a single location are conceptually outlined in Table 7 and described mathematically in Appendix B.

Table 7. Noise measurement processing steps.

Step	Determine
1	Measurement system internal noise figure
2	External noise power from measured noise power
3	Electric field strength from external noise power
4	Noise figure from electric field strength
5	Remove PSD with overload
6	Noise figure statistics (minimum, median, mean, and maximum)
7	ATC channel power time series

Step	Determine
8	ATC channel median noise figure
9	SFTR channel power time series

With the exception of receiver noise figure or as otherwise noted, all measurement system component parameters needed for noise measurement processing were derived from theory or manufacturers' specifications. This approach was driven by the difficulties associated with measuring the gain of the PR antenna at HF band frequencies. In lieu of this measurement, we approximated the ground plane the PR antenna specifications were measured with. In addition it was not possible to obtain BITF CM transmission line gain and noise figure measurements. Component specifications are provided in Appendix C. Measurement system noise figures are provided in Appendix D.

Finally, it is important to note that only "external noise" power is derived from the measured power. No attempt is made to remove atmospheric or galactic noise power so only MMN power remains. This is particularly important when discussing noise measured in quiet rural areas where atmospheric and galactic noise powers can be comparable to MMN power.

2.3 Result Display

When possible each measurement location is documented with the following plots:

- Measured PSD time series i.e. spectrogram or "waterfall" plot. This figure is only provided for long duration measurements.
- Measured PSD maximum, mean, median, and minimum statistics at each frequency.
- Median noise figure spectrum. These results do not apply to frequencies where intentional signals are present.
- ATC channel measured power time series
- SFTR channel measured power time series
- ATC channel noise figure time series
- ATC channel hourly noise figure statistics
- ATC channel noise figure CCDF

Measured power is the power digitized by the receiver. No corrections for losses or gains before the receiver input have been applied. In the event of receiver overload, the data is not displayed. This creates white horizontal lines in PSD time series and gaps in time series. We use the 9.032 MHz ATC channel because it was identified by the radio operators as the primary channel. For reference purposes, the ITU MMN median noise figures are plotted along with noise figure results. Also, the internally generated noise power limit is represented as a dashed red line.

3. Table Mountain Radio Quiet Zone

The system was subjected to extensive characterization measurements prior to being used in Antarctica. The characterization measurements were conducted at the ITS TMRQZ outside Boulder, CO, U.S.A., which provided an ideal setting for testing noise measurement sensitivity. Figure 13 shows the area of TMRQZ where measurements were conducted. Standard frequency and time reference (SFTR) signals transmitted from WWV transmitters 65 km (40 mi) from Fort Collins, CO, U.S.A., were used as reference signals.

Figure 13. TMRQZ outside Boulder, CO, U.S.A. Equipment was operated within the building shown. The antenna was approximately 61 m (200 ft) to the right of the building. (Credit: Robert Achatz)

Figure 14 is a PSD time series plot of data collected over a 24-hour period beginning November 6, 2024, 15:55 local time at the top and ending November 7, 2024, at 15:56 on the bottom. These dates are near the October 15, 2024, solar maximum. The sunset, sunrise, and solar noon are 16:54, 6:34, and 11:44, respectively, over this 24-hour period.

The vertical streaks are signals and horizontal white lines are PSDs removed because of receiver overload. Diurnal ionosphere effects are highlighted by the lowest power darker blue areas. There is also likely to be less nearby MMN during the night when humans are less active.

Figure 15 is the corresponding measured power statistics plot that condenses the PSD time series into maximum, mean, median, and minimum powers at each frequency. The internally generated noise power is represented by the dashed red line.

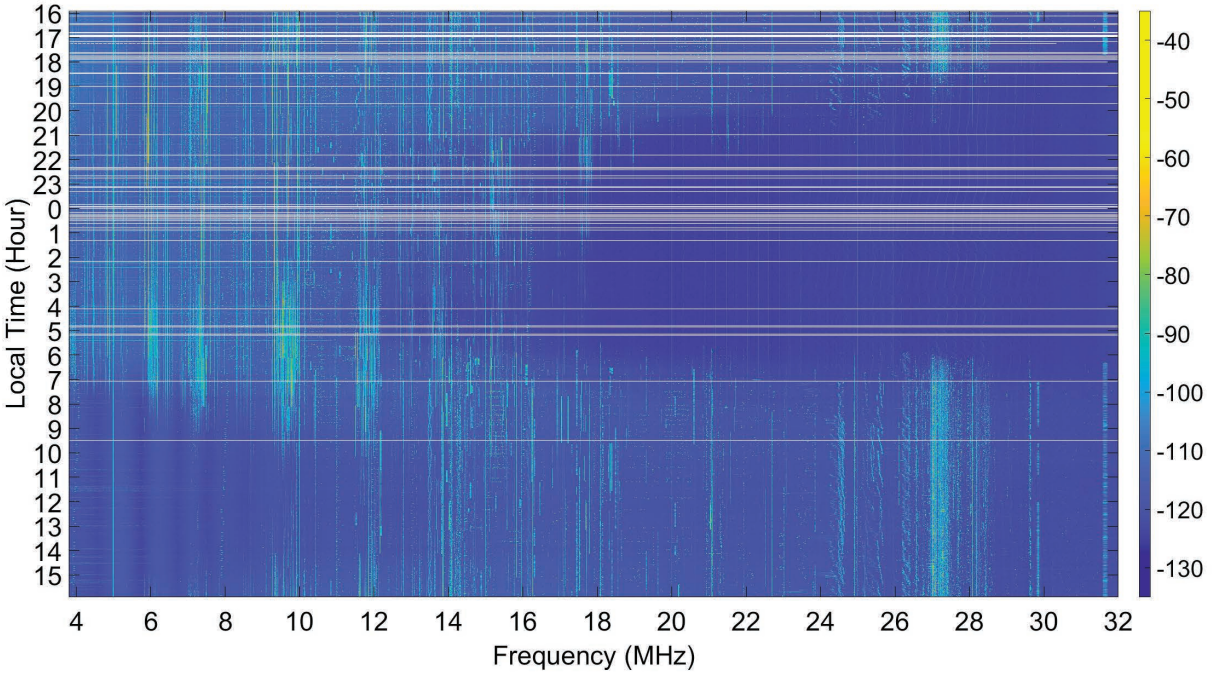

Figure 14. 24-hour TMRQZ PSD time series. Colors represent measured power in dBm. White horizontal lines represent PSDs removed because of receiver overload.

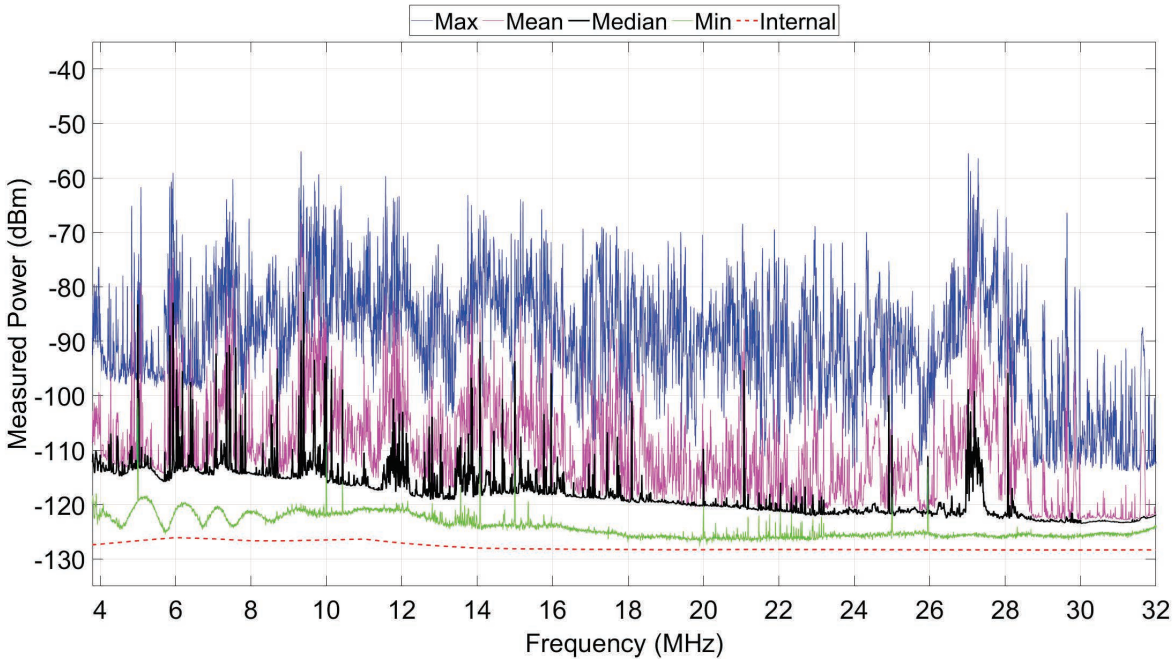

Figure 15. 24-hour TMRQZ PSD statistics.

Figures 16 and 17 condense data to noon hour PSD statistics and median noise figure spectrum. Figures 18 and 19 do the same for the midnight hour. The hourly median noise figure is the metric used by HF radio engineers.

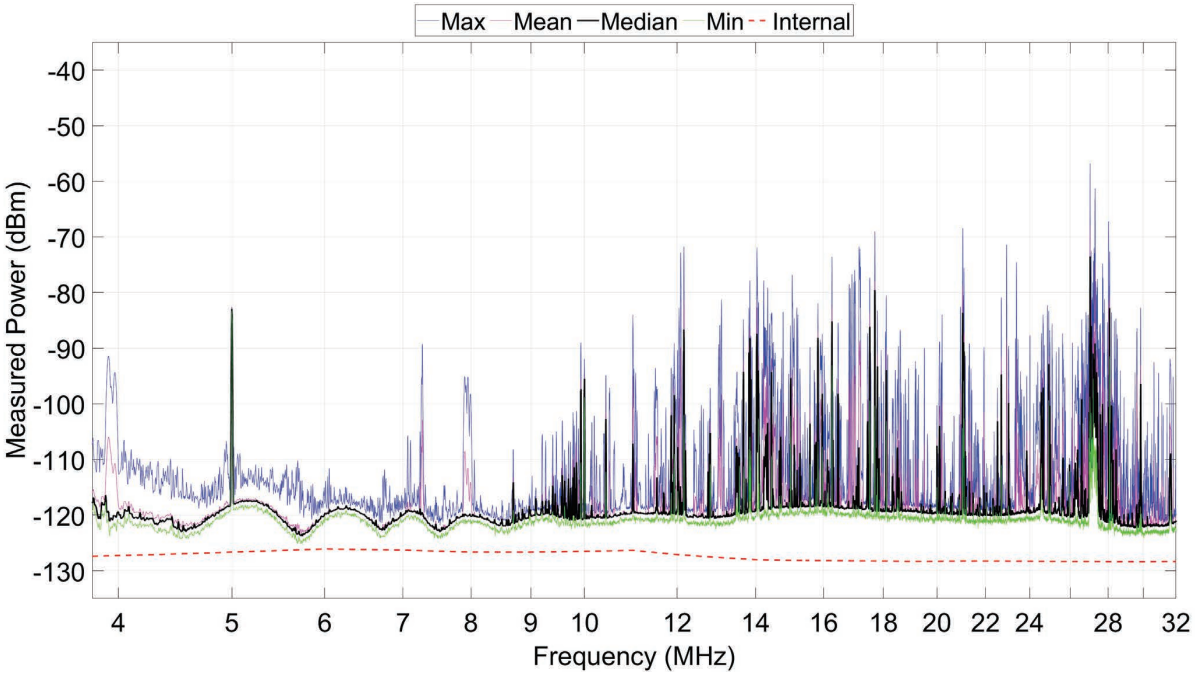

Figure 16. Noon hour TMRQZ PSD statistics.

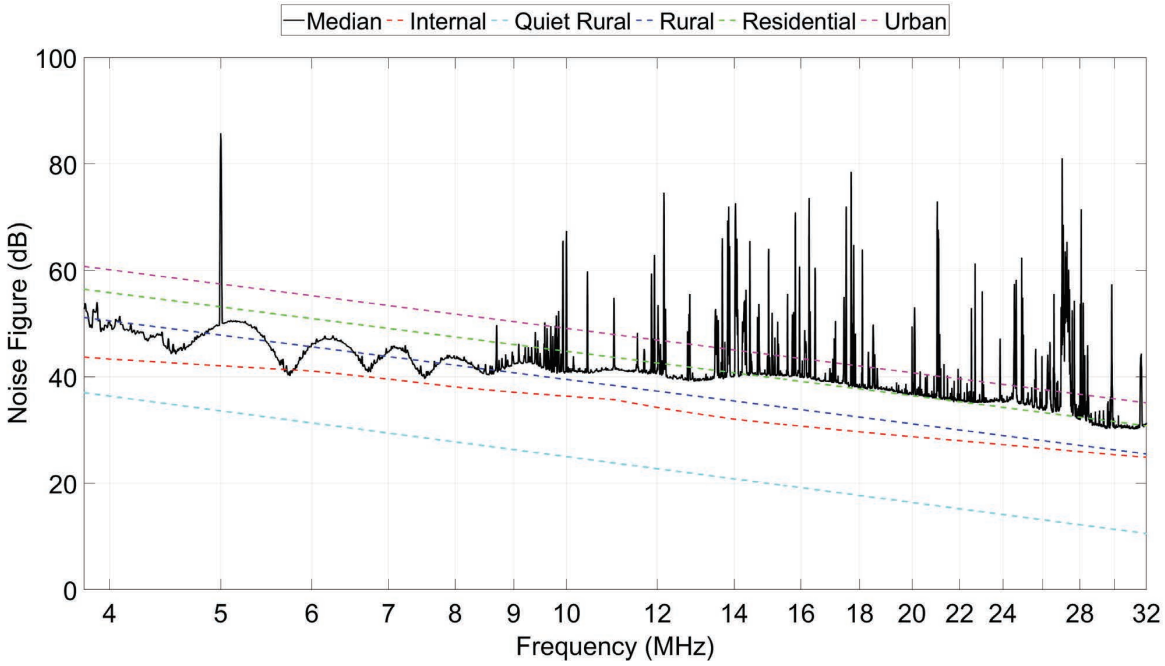

Figure 17. Noon hour TMRQZ median noise figure spectrum.

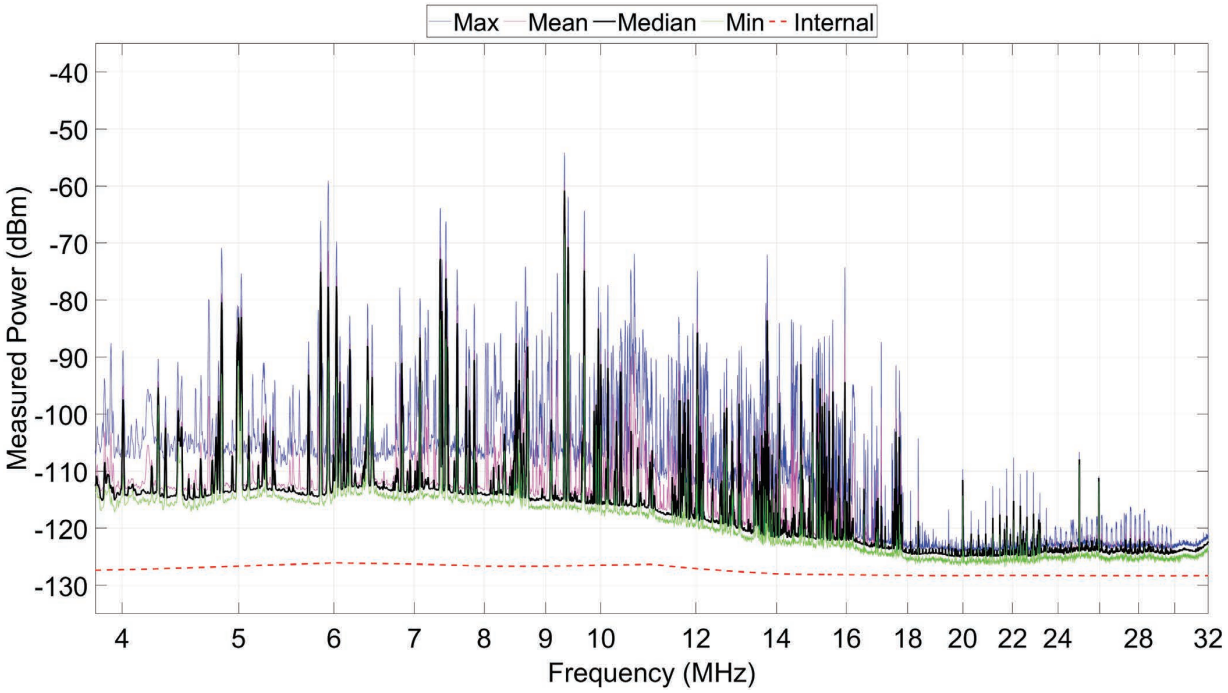

Figure 18. Midnight hour TMRQZ PSD statistics.

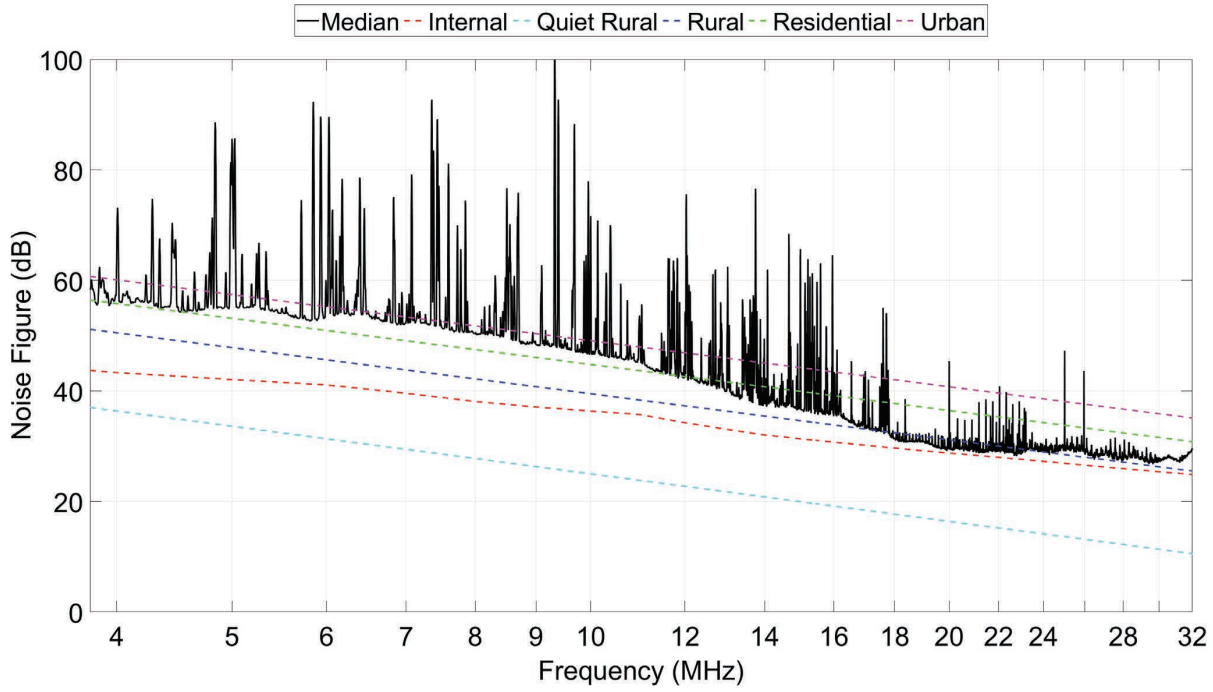

Figure 19. Midnight hour TMRQZ median noise figure spectrum.

Figures 20 and 21 show the 9.032 MHz ATC and 10.0 MHz SFTR channel measured power time series. The 10 MHz SFTR channel is also assumed to have a ground path component from the WWV transmitter 65 km away. Both show diurnal skywave behavior, although the 10 MHz SFTR channel has considerably more variability. The 9.032 MHz channel has nighttime powers as high as -85 dBm from 17:00 to 7:00, indicative of ATC channel use. The

smoothly decreasing power between 17:00 and 18:00 suggests a receding aircraft. Noise is nominally -115 dBm in the night and -120 dBm during the day. The SFTR signal nighttime powers as high as -75 dBm are well above the ATC channel noise powers.

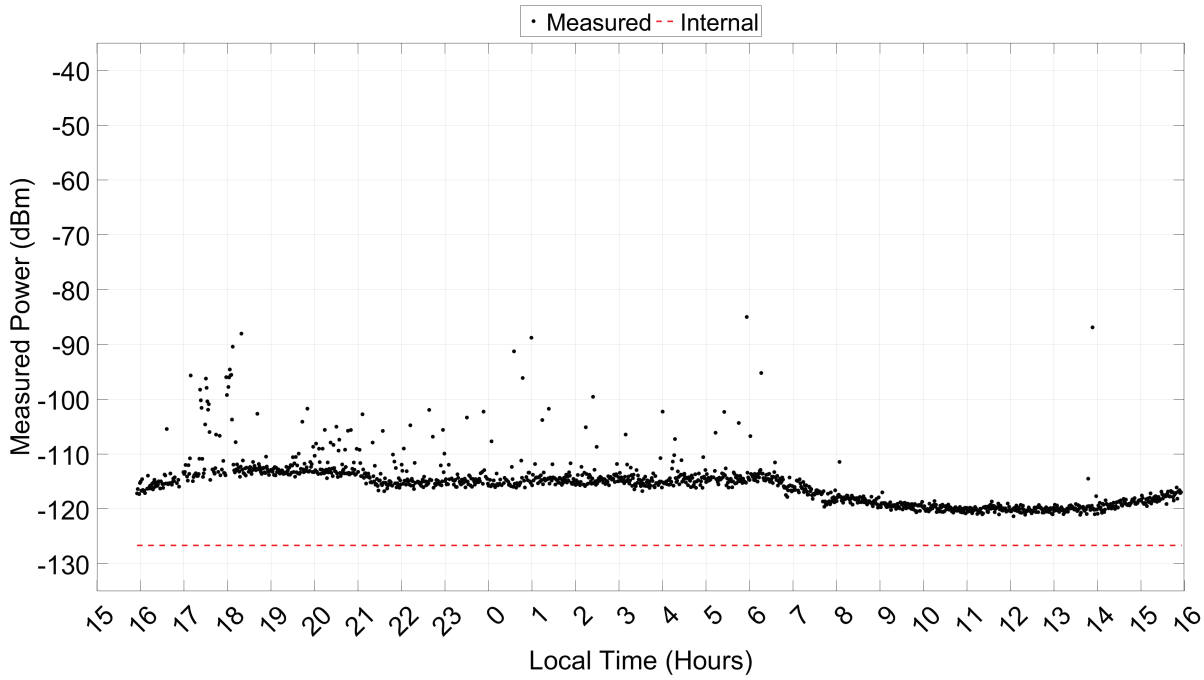

Figure 20. 24-hour TMRQZ 9.032 MHz measured power.

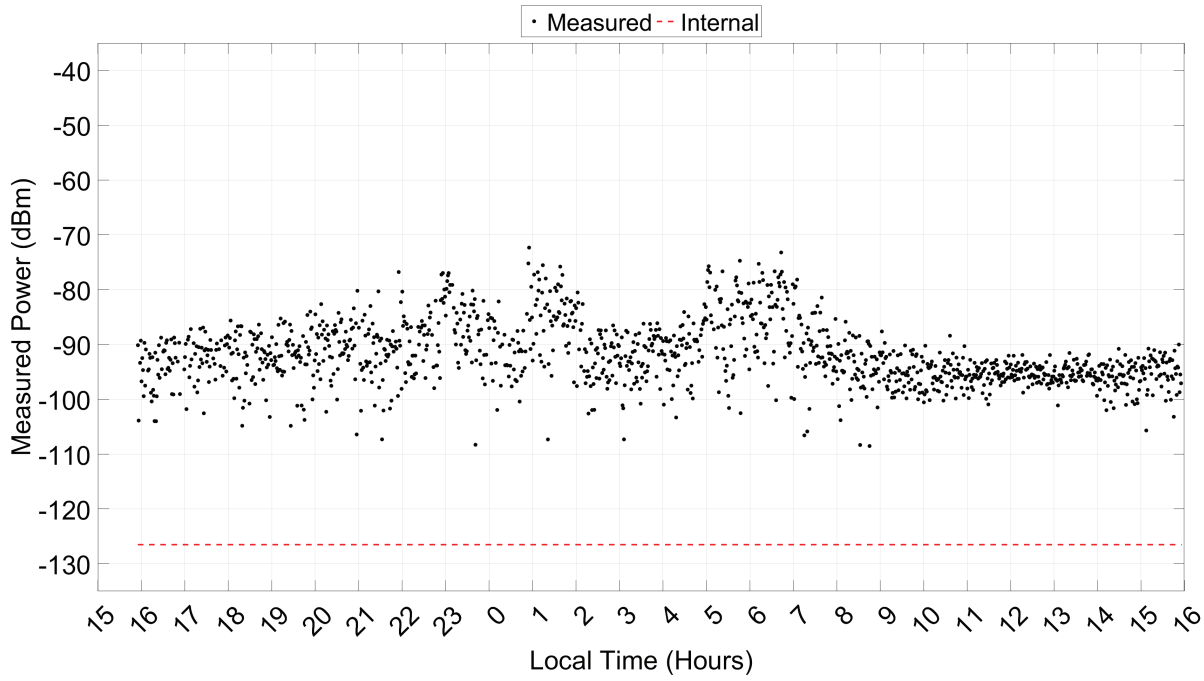

Figure 21. 24-hour TMRQZ 10.0 MHz SFTR signal measured power.

Figures 22 and 23 show noise figure time series and corresponding hourly statistics. The hourly median is seen to vary between rural and urban but spends most hours near

residential. Figure 24 is the complementary cumulative distribution function (CCDF) of all noise figures. Inflection points at the 1st, 8th, and 60th percentiles highlight cumulative statistical effects of the ATC signal, D-layer absorption, and human activity. Median noise figures for all ATC channels are provided in Table 8.

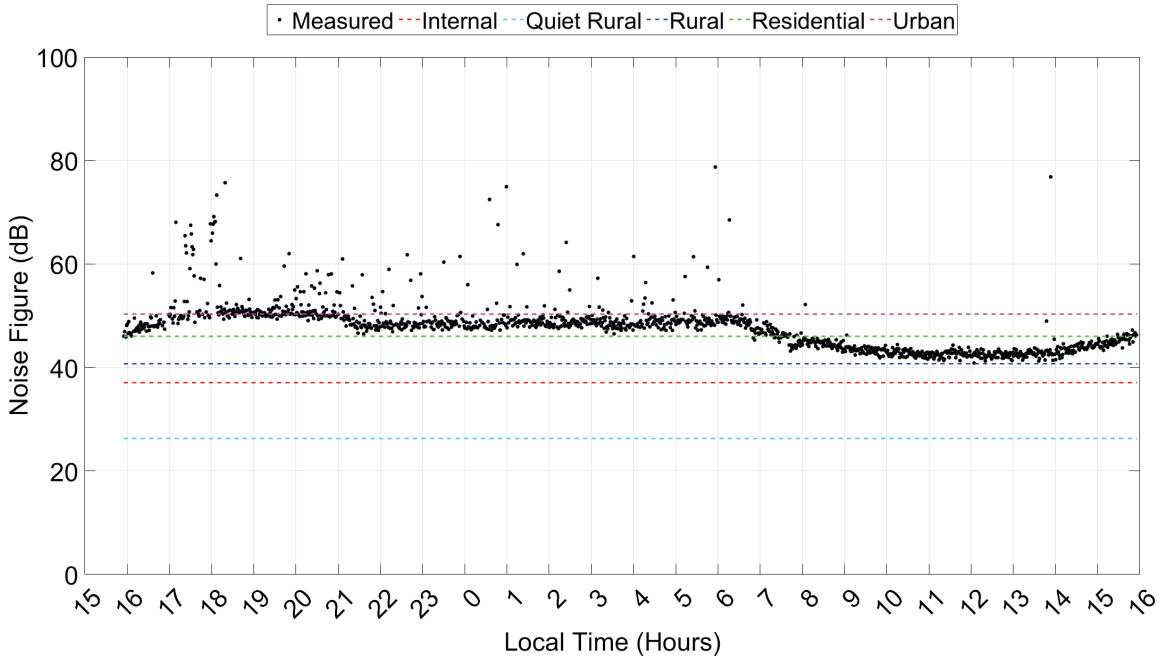

Figure 22. 24-hour TMRQZ 9.032 MHz ATC channel noise figure time series.

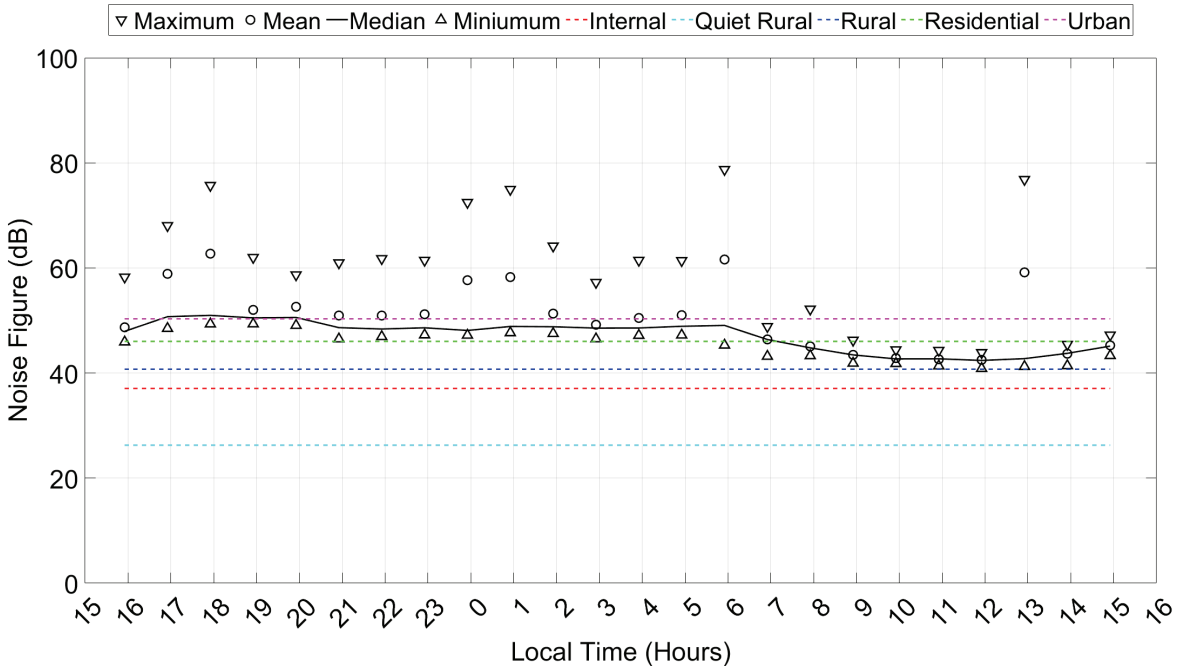

Figure 23. 24-hour TMRQZ 9.032 MHz ATC channel hourly median noise figures.

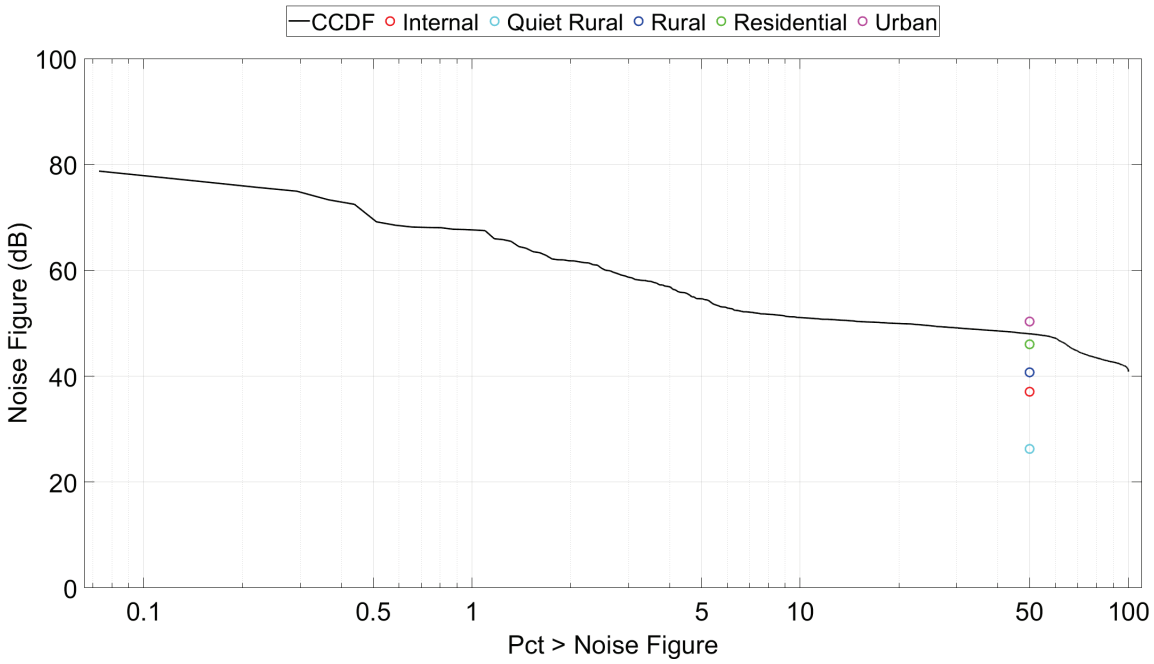

Figure 24. 24-hour TMRQZ 9.032 MHz ATC channel noise figure CCDF.

Noon hour median noise figures that hover around rural at the lower frequencies and midnight hour median noise figures that hover around rural at the higher frequencies demonstrate the system is capable of measuring rural noise figures in Antarctica. Because these measurements were performed with a slightly less sensitive active PR antenna model, the R&S HE016, and longer 61 m (200 ft) transmission line than was used in Antarctica we expect the Antarctica system to be able to measure even lower noise figures.

Table 8. TMRQZ median noise figures.

ATC Channel Frequency (MHz)	Median NF (dB)
4.718	54.8
5.726	51.5
6.708	51.5
9.032	48.0
11.256	44.4
13.251	40.8
18.0	38.3

4. Prior Studies

Table 9 summarizes relevant prior studies. The Stanford University (SU) study [1] measured noise at 19 locations, including the BITF. The U.S. Navy (USN) [13] focused on the BITF location. Finally, the ITS has conducted studies since 2022 either remotely with measurement systems in Antarctica controlled from its offices in Boulder, Colorado, or in-person. The most consequential measurement, performed remotely in November 2023, is highlighted here.

Table 9. Relevant prior studies.

Year	Org.	Loc.	Antenna	Mount	BW (kHz)	Results
1970	SU	MS BITF	Passive PR	Raised	5	Field strength
1997	USN	BITF	CM	Ground plane	3	Power
1997	USN/HP	BITF	Active PR	Raised	10	Field strength
1997	USN	BITF	Active PR	Raised	10	Field strength
2024	ITS	T-Site BITF	CM	Ground plane	7.6	Noise figure

4.1 Stanford University

The purpose of the SU study was to identify radio quiet areas within 100 km of MS where radio noise sensitive experiments could be conducted. The study used a field strength meter connected to a rod antenna mounted on a tripod. A PCA event was reported during the measurement period.

Figure 25 shows noise figures calculated with our processing method from the reported field strengths. The locations shown are in the vicinity of those of this current ITS study. Additional information regarding these measurements is provided in Appendix E. The MS locations were found to be much noisier than urban areas—a surprising result, given the low MS population. With few exceptions, BITF was found to be much quieter than MS.

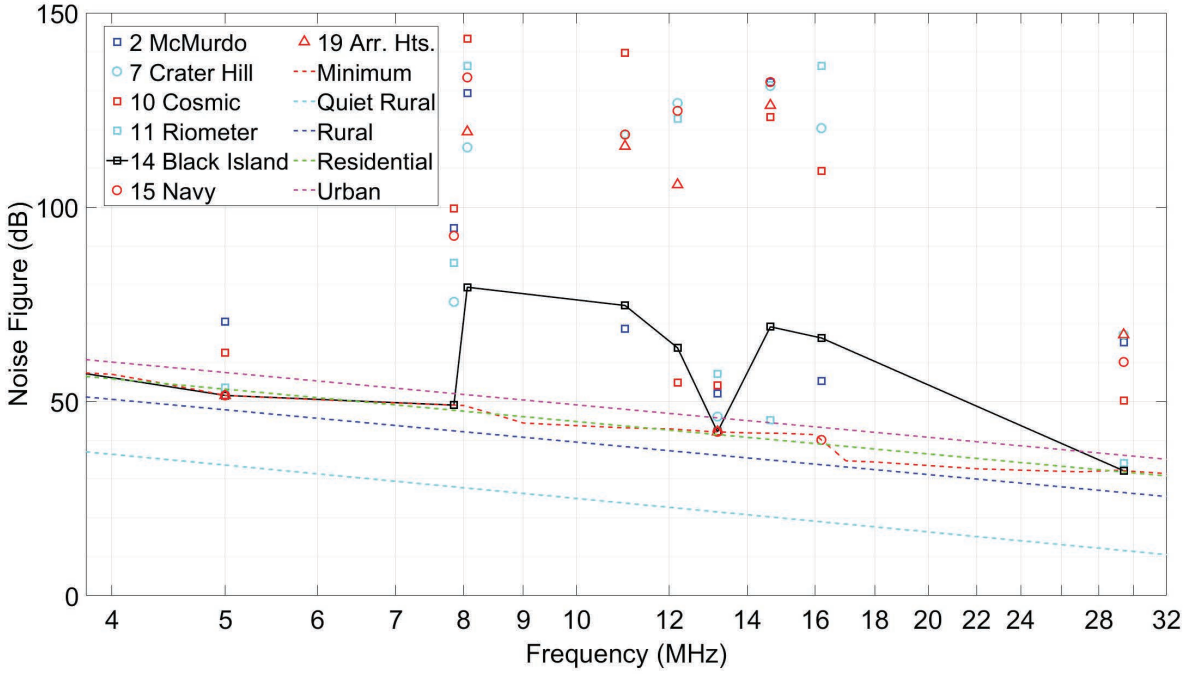

Figure 25. Comprehensive SU results.

4.2 U.S. Navy

Figure 26 shows results digitized from three figures in the USN study. The CM1AVG3K line is for the CM antenna and digitized from the figure of the same name. The NMAVG10K line is for the active PR antenna and digitized from the figure of the same name. The HP 1982 line is once again for the active PR antenna but digitized from the figure entitled "#16". This HP 1982 measurement differs from the NMAVG10K measurement in that its setup emulates the unspecified conditions of an earlier measurement made by Mr. Gary Lewandowcki (sic) of Hewlett Packard (HP) in 1982.

The USN study results did not include receiver noise figure or transmission line loss, so internal noise power was not removed. CM1AVG3K and NMAVG10K were acquired with normal wind turbine and rectifier operation. All PR measurements were performed with the antenna raised off the ground in some way and there was no mention of a radial ground plane. The HP 1982 results spanned urban-to-rural noise environments from the bottom to the top of the band. The NMAVG10K results were 20 dB higher in spite of using a similar antenna. The CM1AVG3K results indicated a quiet rural noise environment at the low end of the band and an urban noise environment at the high.

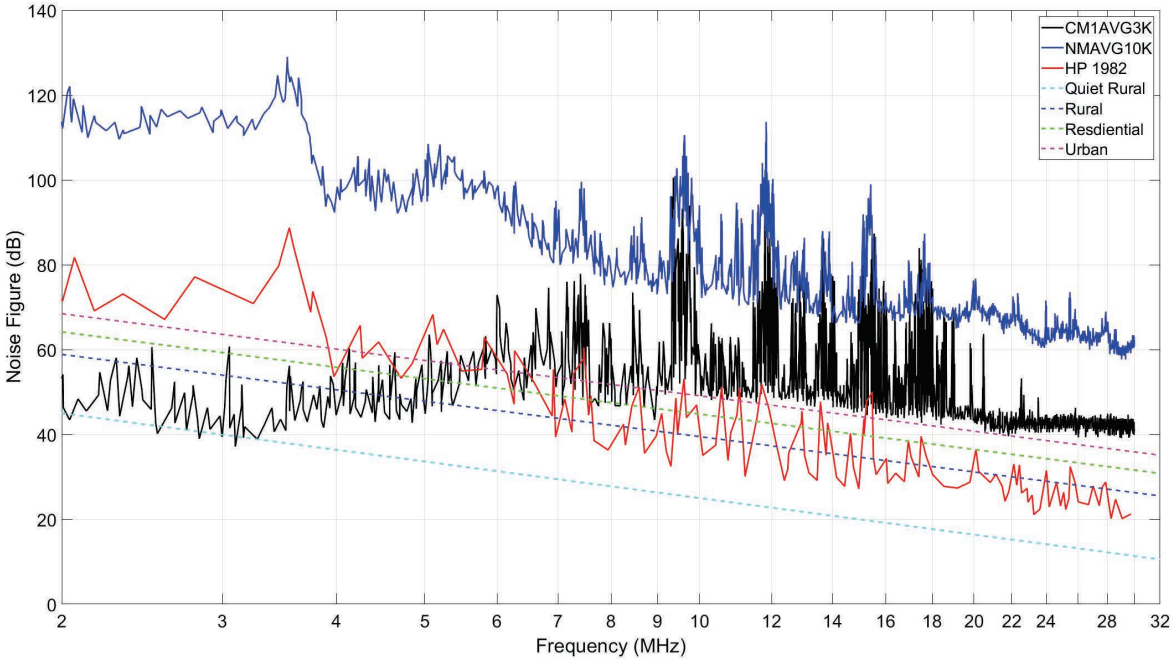

Figure 26. USN Black Island results.

4.3 ITS

ITS conducted remote measurements with the BITF CM and identical T-Site CM-5. As shown in Figures 27 and 28, noise figure was generally much higher at T-Site than at the BITF. At the lower frequencies T-Site is about 20 dB higher. At 8.5 MHz the difference is as great as 30 dB. The measurements merge above 25 MHz. Additional details and power time series for all ATC channel frequencies are provided in Appendix F.

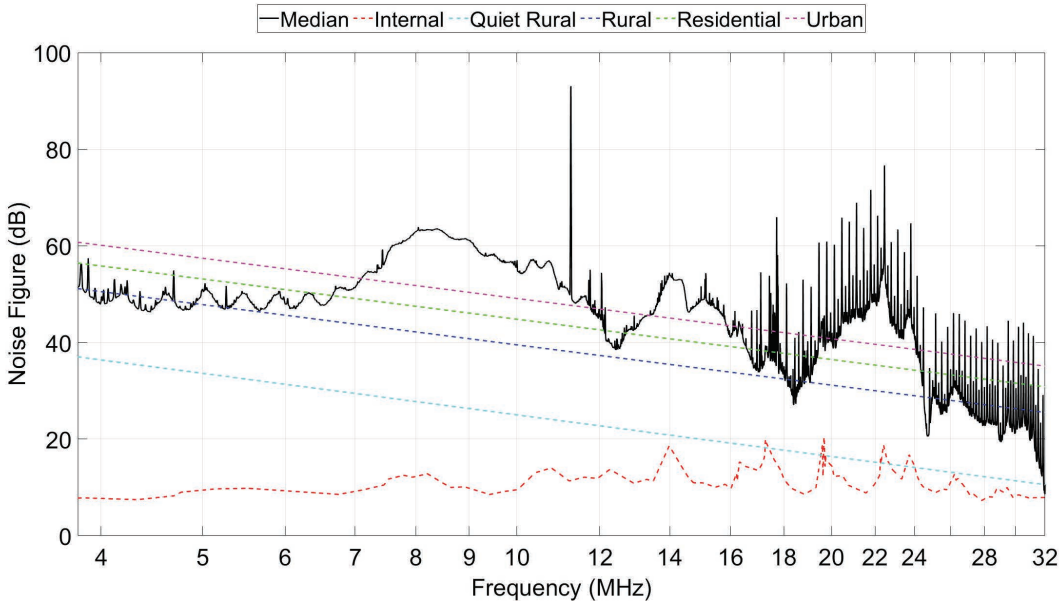

Figure 27. Noise figure spectral density for T-Site CM-5 antenna.

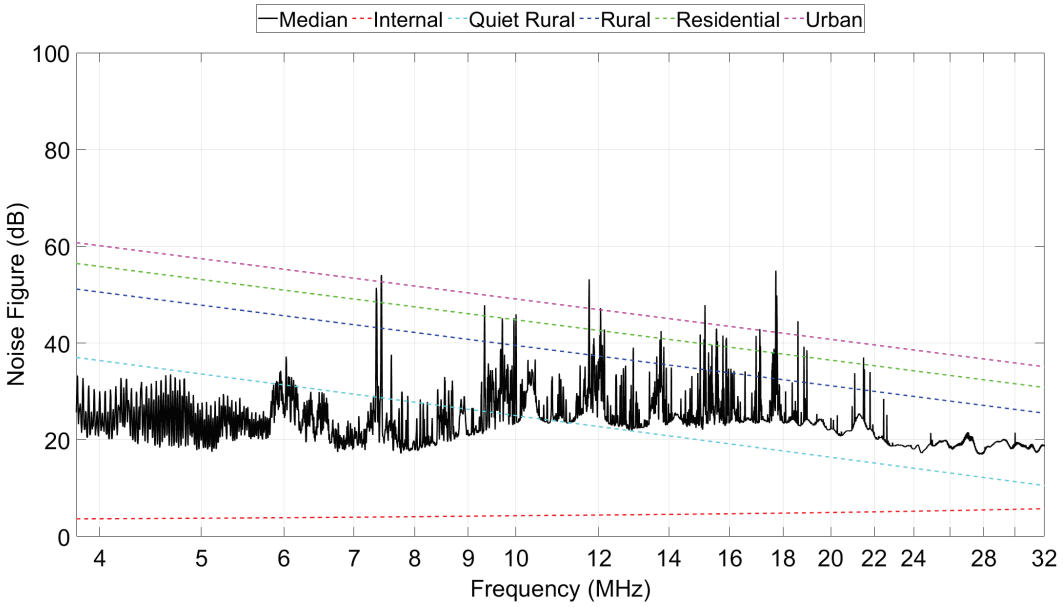

Figure 28. Noise figure spectral density for BITF CM antenna.

5. Data Collection

5.1 Location

MS is a collection of buildings with a footprint of approximately 1 sq. km surrounded on one side by bluffs and on the other by the Ross Sea and ice shelf. Figure 29 identifies all MS measurement locations in an aerial photo. T-Site and SuperDARN locations have powerful HF transmitters that can potentially cause receiver overload. Figures 30 and 31 are photos of the location setting. Figure 2 previously identified the BITF antenna in another aerial photo.

Table 10 summarizes the locations and antennas for all measurements. Locations are categorized as remote, in-town, and on-bluff. The BITF is the only remote location. In-town locations have more buildings and electrical devices than on-bluff locations. All measurement locations had buildings to shield the receiver and computer from inclement weather and provide power.

Table 10. Measurement locations.

Location	Also Known As	Building	Antenna	Category
BITF	Black Island Telecommunication Facility	56	CM	Remote
MACOPS	McMurdo Communications & Operations	165	CM	In-town
T-Site	Transmitter Site	221	PR	On-bluff
MTRS-2	NASA Radome MTRS-2 McMurdo TDRS Relay System	69	PR	On-bluff
MGS	RADARSAT NASA Ground Station McMurdo Ground Station	71	PR	On-bluff
HS	Ham Shack IMP-8 Shelter	67	PR	In-town
AH	Arrival Heights Clean Air Facility	197	PR	On-bluff

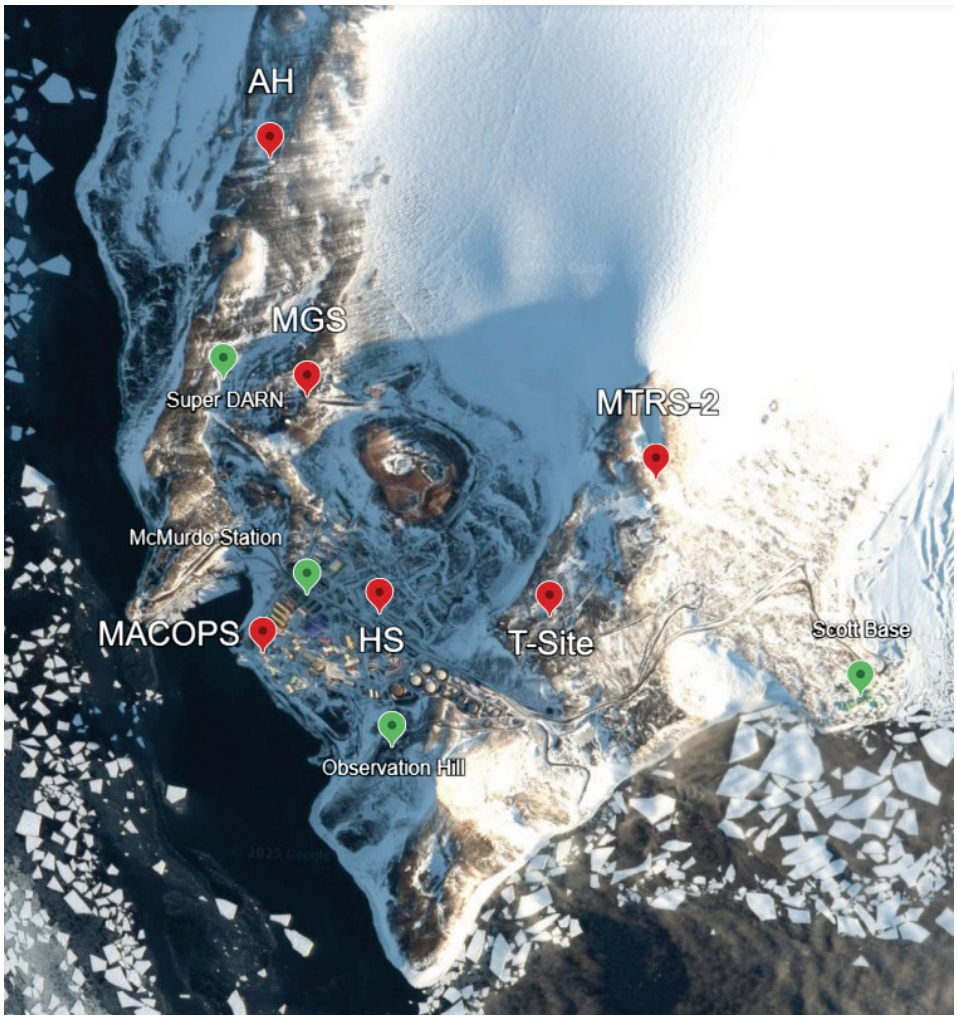

Figure 29. MS measurement (red) and landmark (green) locations. (McMurdo Area, Ross Island, Antarctica, Google Maps, 2025)

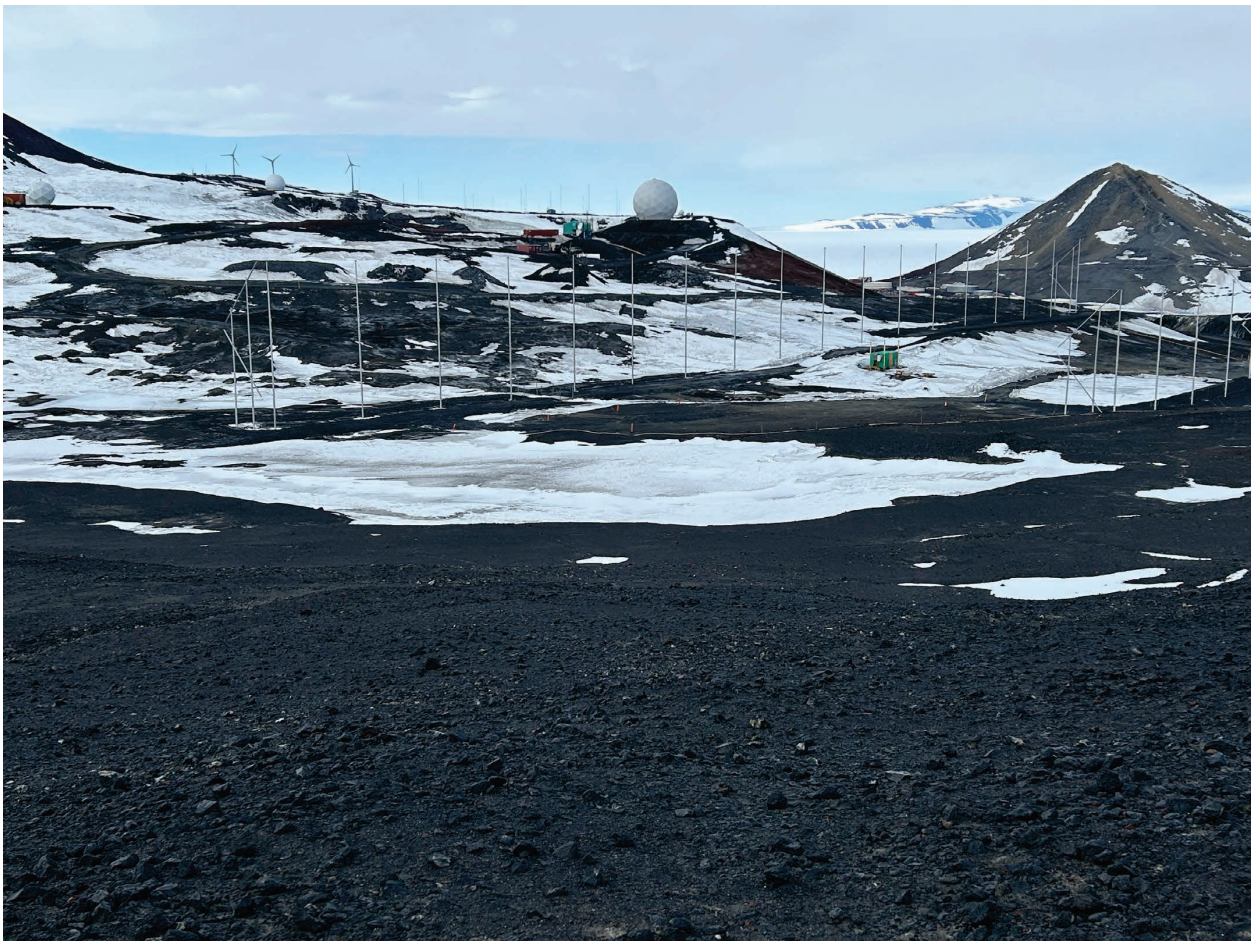

Figure 30. Photo overlooking SuperDARN HF radar antenna consisting of a line of vertical poles in foreground. MTRS-2 is near the wind turbines at upper left, T-Site is between wind turbines and large white radome. MGS is near the green building to the lower left of the large white radome. Observation Hill is in the upper-right corner. (Credit: Robert J. Achatz.)

Figure 31. Photo overlooking MS from Observation Hill. MS is the collection of buildings beneath the bluffs. MACOPS is in MS by the ice edge. HS is in the center of MS. T-Site and MTRS-2 are on bluff to the right. MGS and AH are on bluff to the left. (Credit: Robert J. Achatz.)

5.2 Conditions

Data was collected near the October 15, 2024, solar maximum. Daylength was 24 hours during the measurement period with solar noon occurring at approximately 13:45 hrs. Minimal D-layer absorption was verified by NOAA DRAP at solar noon where the highest frequency experiencing 1 dB absorption was approximately 5 MHz.

5.3 Procedure

The PR antenna data collection procedure consisted of the following steps. The CM antenna data collection procedure excludes the second and third steps.

1) Transport equipment to the measurement location
2) Set up the antenna and radial ground plane
3) Set up the transmission line from the antenna to the building sheltering the receiver and laptop
4) Set up the receiver and laptop
5) Initialize receiver settings
6) Perform calibrations (if needed)
7) Initiate measurement

8) Collect measurement data

9) Terminate measurement

10) Store measurement data for later processing

11) Break down the system for transport to next location

5.4 Inventory

Data collection times and duration are summarized in Table 11. The number of PSD analyzed is less than the number of PSD collected because analysis does not include PSD with overload.

Table 11. Data collection local times and duration.

	Location	Start Month/Day hr:min	End Month/Day hr:min	Duration hr:min	PSD Collected	PSD Analyzed
1	BITF	12/14 21:19	12/15 22:16	24:57	1499	1297
2	MACOPS	12/08 11:46	12/08 15:23	03:36	218	103
3	T-Site	12/09 15:49	12/10 10:07	18:18	1100	857
4	MTRS-2	12/10 12:15	12/11 12:19	24:04	1446	1378
5	MGS	12/11 15:23	12/12 15:24	24:01	1443	372
6	Ham Shack	12/13 08:52	12/13 09:51	00:59	59	21
7	Arrival Heights	12/13 15:21	12/13 15:51	00:30	31	31

6. Spectrum Survey Results

The Spectrum XXI spectrum engineering tool used by NTIA shows 151 spectrum allocations in Antarctica. The majority of allocations are for systems that use single-sideband (SSB) amplitude modulation with a suppressed carrier, designated as a J3E emission, with bandwidths on the order of 3 kHz typical of analog voice telephone equipment. The systems provide ATC, air-to-ground, ship-to-shore, field party voice communications, international distress beacons, and computer and scientific instrument data networking.

The histogram in Figure 32 shows allocation in terms of the number of allocations/MHz and the allocation cumulative distribution function (CDF) in terms of the number of allocations at or below a frequency. The histogram shows the most (16) allocations at 5 and 11 MHz. The CDF shows 90 percent of allocations are between 2 and 15 MHz.

Table 12 shows the number of allocations by transmitter location (Spectrum XXI field 401) in descending order. The majority of allocations, 69.5 percent, are for the entire Antarctica continent, which would include MS. If we add these to the allocations for MS, we see that 84 percent of the allocations could potentially be observed in MS.

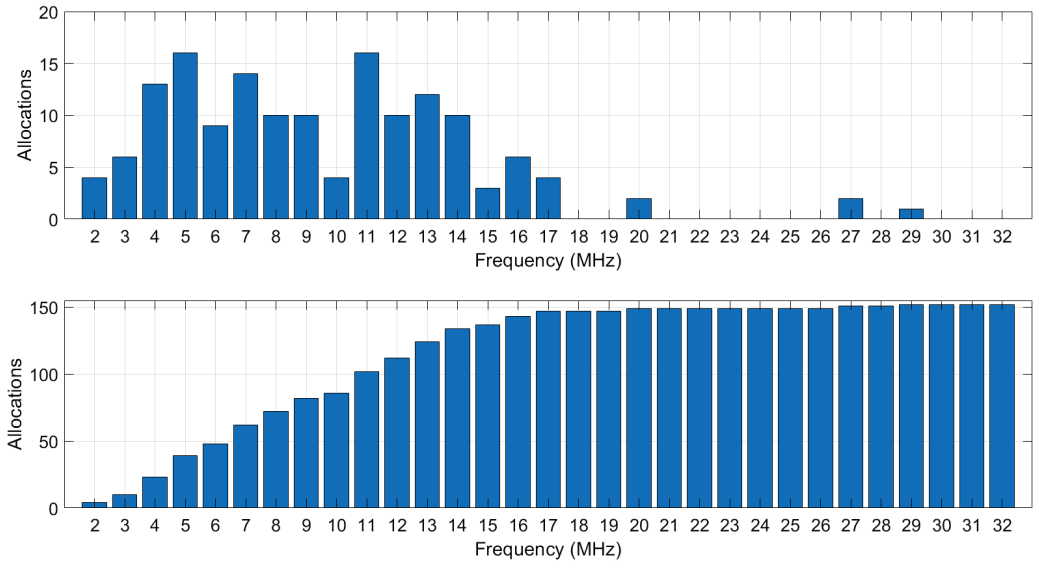

Figure 32. Spectrum XXI allocation histogram (top) and cumulative distribution (bottom).

Table 12. Spectrum XXI allocations by transmitter location.

Transmitter Location	Allocations	Percent
Antarctica Continent	105	69.5
McMurdo Station	22	14.5
South Pole Skiway	9	6.0
Ships	8	5.3
Palmer Station	3	2.0

Transmitter Location	Allocations	Percent
Aircraft	1	<1
WAIS Divide Skiway	1	<1
South Pole Station	1	<1
Thwaites Glacier Field Camp	1	<1

Spectrum survey measurement results consist of a set of 1440 PSDs collected once a minute over 24 hours at a location. PSD power is the power measured at the receiver input. Effects of measurement system noise, antenna gain, or transmission line loss are not compensated for so power is relative to the measurement system characteristics.

Spectrum survey results are displayed as PSD time series plots and PSD statistics. The statistics plot is useful for discerning signal center frequencies and bandwidths while the PSD time series shows how often a signal was captured. The probability that a signal is captured depends on its intermittency.

We use both plots to identify signals that persist over much of the 24-hour measurement period. Persistent signals have high median and mean powers in the statistics plot and vertical bands in the PSD time series.

Figures 33 and 34 are the 24-hour PSD time series for the BITF and MTRS-2 locations. Figures 35 and 36 are the corresponding statistics plots. As expected, most signals occupy the lower HF band. Effects of increased daytime D-layer absorption and decreased nighttime critical frequencies like that seen at the TMRQZ is not observed.

Differences in signal populations are evident. As an example, the SuperDARN radar was much less prominent at the BITF than at MS MTRS-2, where it was found to occupy spectrum around 10.3 MHz the entire day.

The MTRS-2 signals have lower maximum power because the PR antenna gain is much lower than the BITF CM antenna gain. The MTRS-2 results also have low level intermodulation causing the faint vertical stripes which are not evident in the BITF CM results. The MACOPS CM PSD, shown later in Figure 45, shows that the intermodulation persists at MS regardless of antenna.

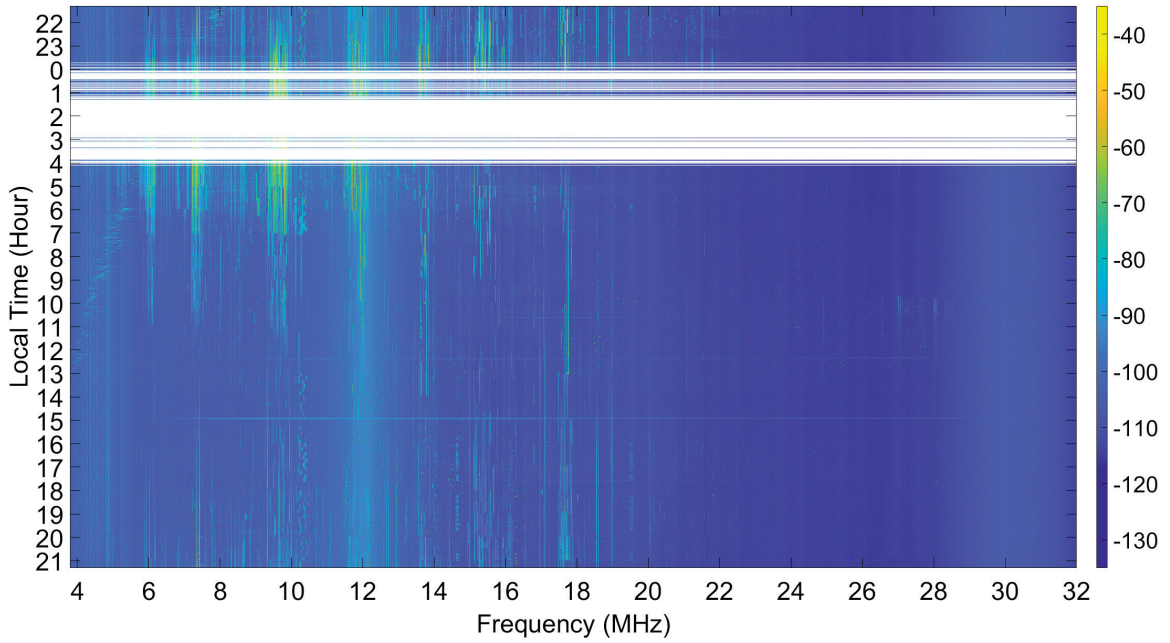

Figure 33. 24-hour. BITF PSD time series. Colors represent measured power in dBm corresponding to scale on right. White horizontal lines represent PSDs with overload.

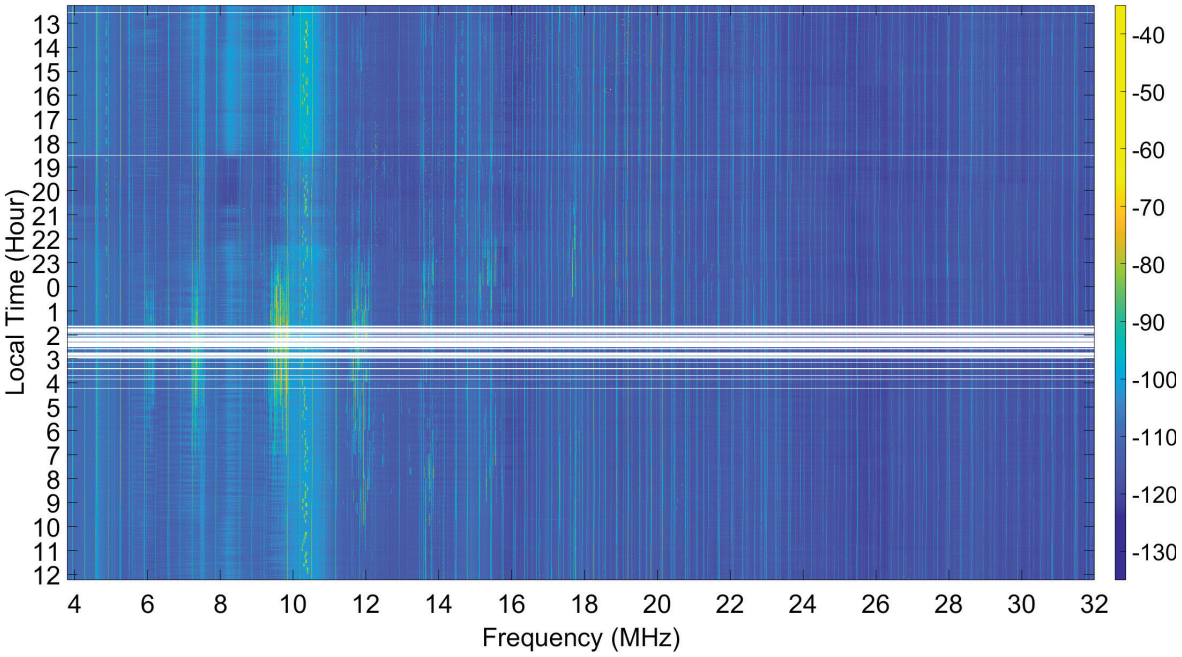

Figure 34. 24-hour MTRS-2 PSD time series. Colors represent measured power in dBm corresponding to scale on right. White horizontal lines represent PSDs with overload.

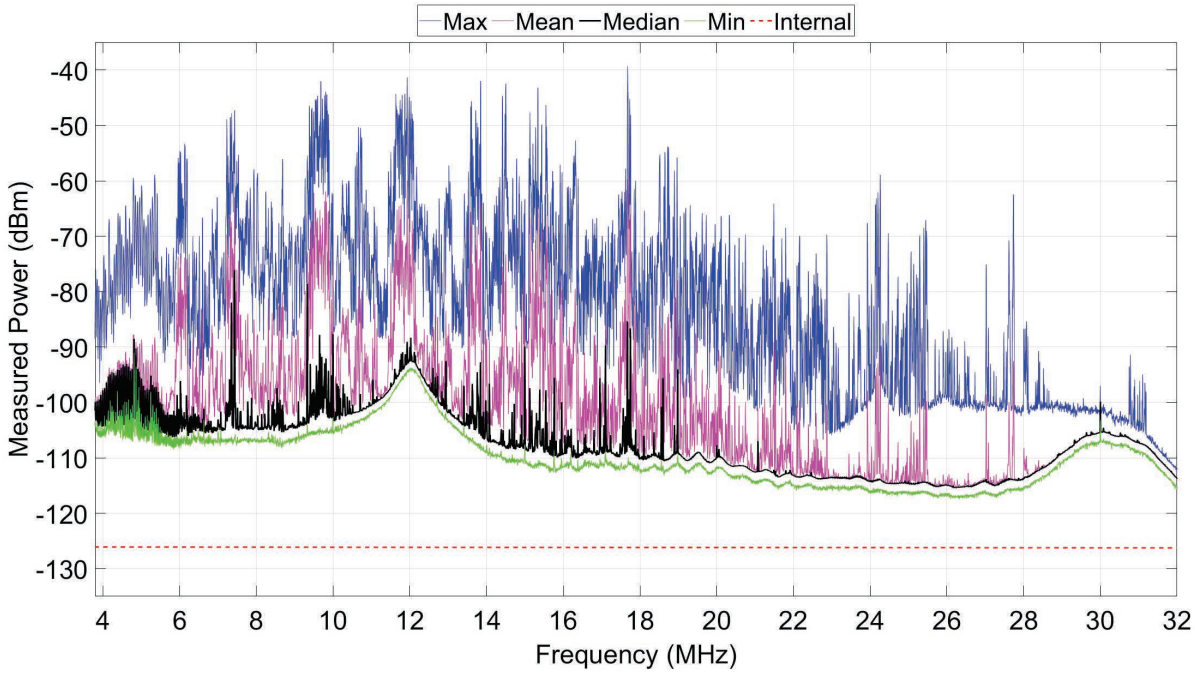

Figure 35. BITF PSD statistics.

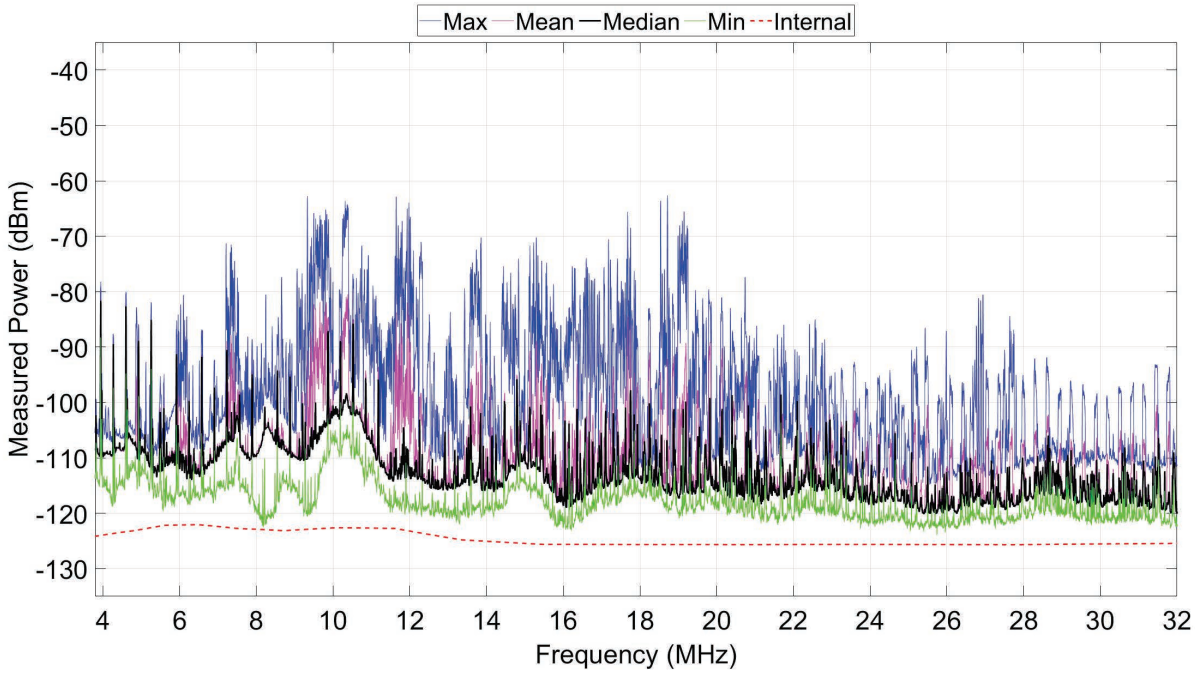

Figure 36. MTRS-2 PSD statistics.

7. Noise Measurement Results

7.1 BITF

The BITF measurement was conducted over a 24-hour period with the BITF "Out of Service" CM antenna and transmission line leading to Building 56 where the receiver and computer were located.

PSD time series and statistics were shown previously on a linear frequency scale in Section 6 Figures 33 and 35, respectively. Figures 37 and 38 show the PSD statistics and corresponding noise figure spectra, respectively, on a log frequency scale. Cause of "bumps" at 4.5, 12, and 30 MHz is unknown. Neglecting the bumps, the noise is approximately quiet rural, as one might expect of a remote Antarctica facility. Median noise figures for all ATC channels are provided in Appendix G.

Figures 39 and 40 show the 9.032 MHz ATC and 10.0 MHz SFTR channel measured power time series. The 9.032 MHz ATC channel power samples are relatively constant except for the time period 23:30 to 06:30 when the channel is being used. While in use the SNR ranges from 25 to 35 dB. Overload, not necessarily by this signal, creates sample sparseness from 00:00 to 04:30. The 10.0 MHz SFTR channel varies over 35 dB in a sinusoidal manner presumably imposed by the ionosphere.

Figures 41 and 42 show the noise at 9.032 MHz is quiet rural. The CCDF in Figure 43 has linear inflection points at the 5th and 20th percentiles caused by usage. Still the CCDF median corresponds closely to the Figure 42 hourly medians when the ATC channel was not being used.

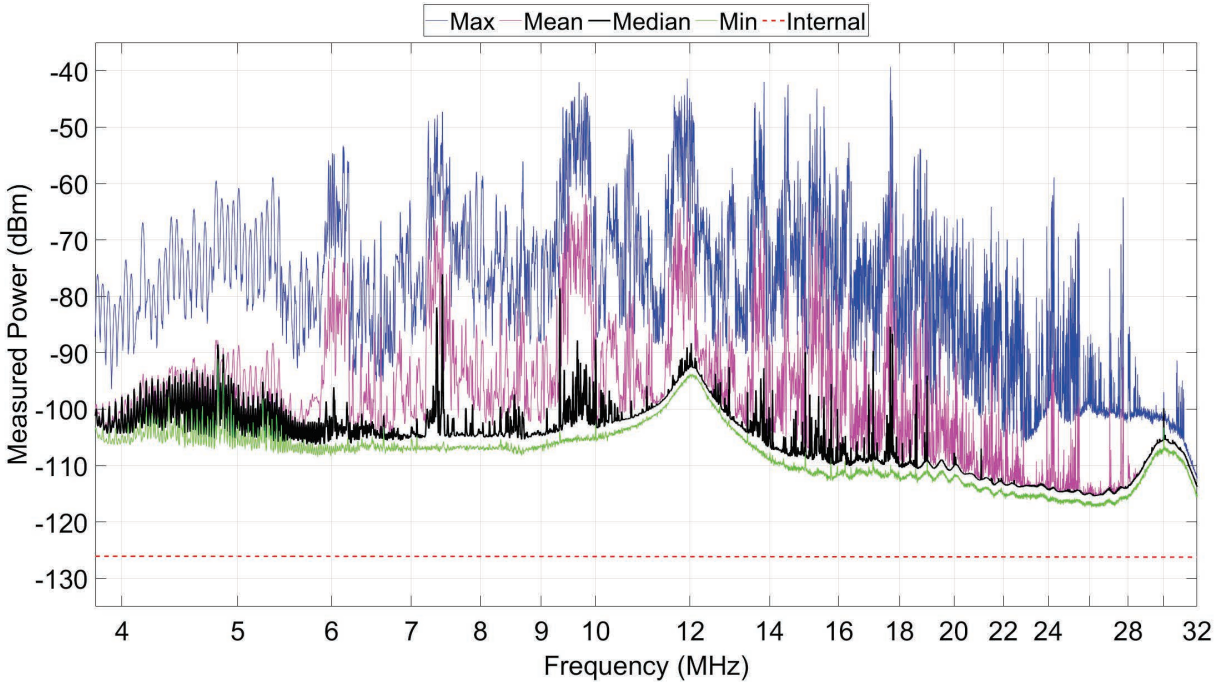

Figure 37. BITF PSD statistics.

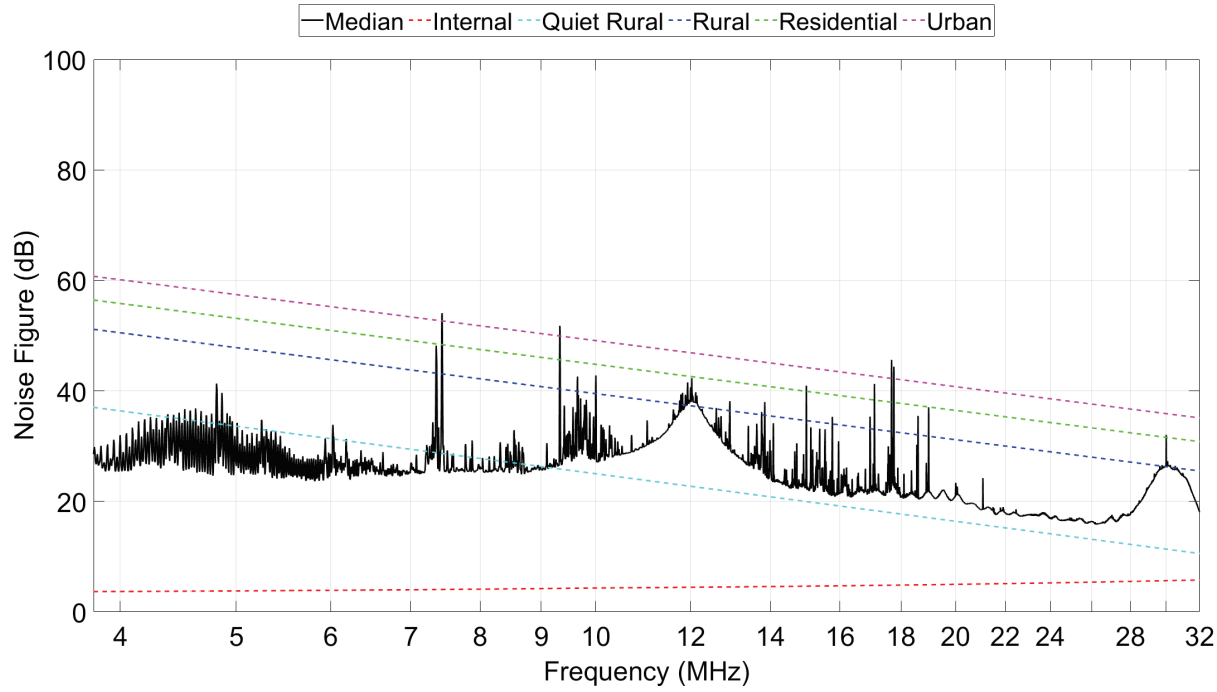

Figure 38. BITF median noise figure spectrum.

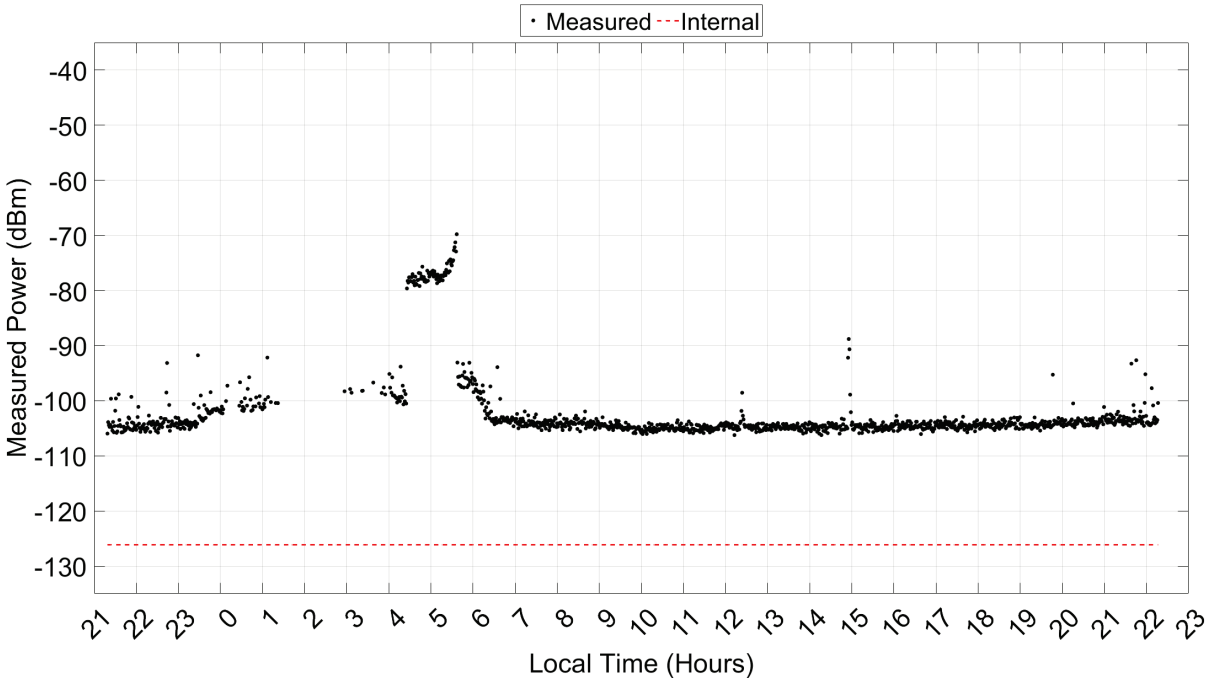

Figure 39. BITF 9.032 MHz ATC channel measured power time series. Gaps in time series represent measurements removed because of receiver overload.

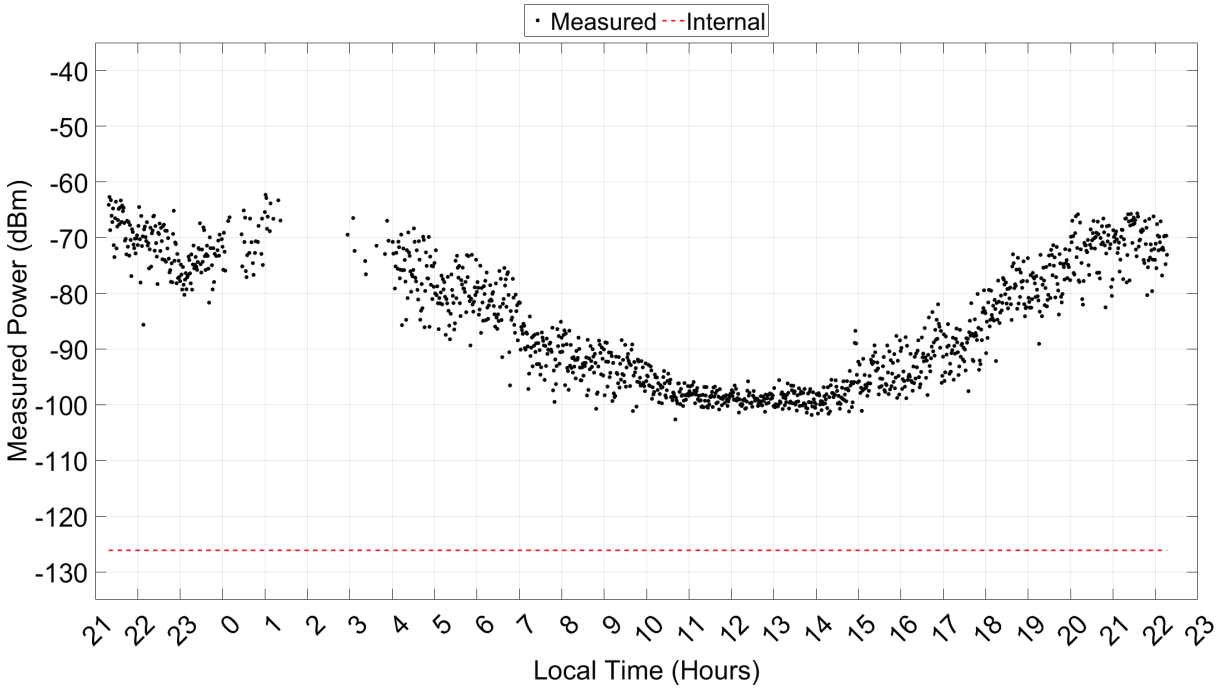

Figure 40. BITF 10.0 MHz SFTR channel measured power time series. Gaps in time series represent measurements removed because of receiver overload.

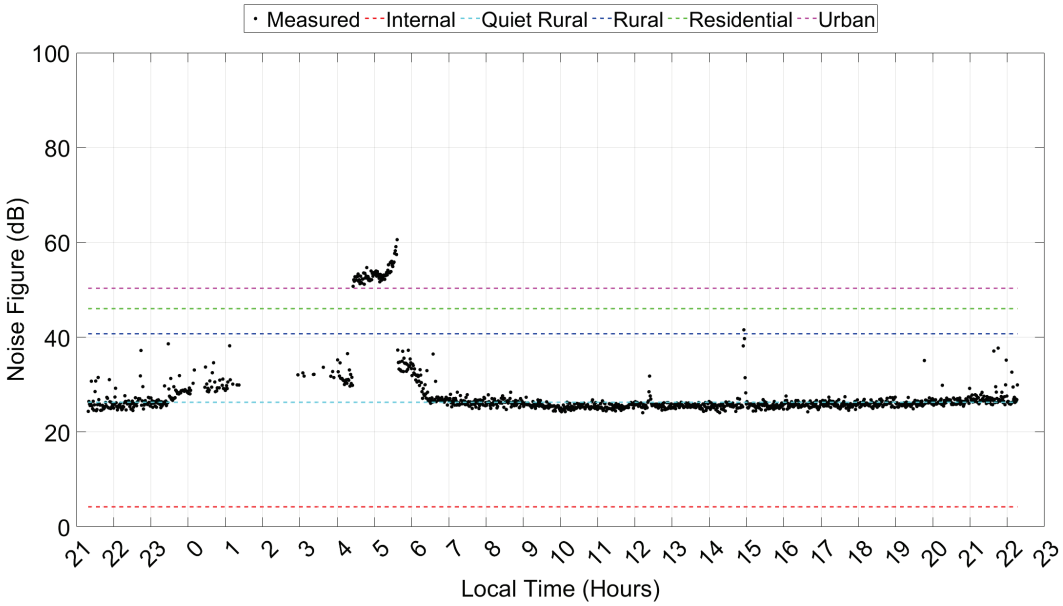

Figure 41. BITF 9.032 MHz ATC channel noise figure time series.

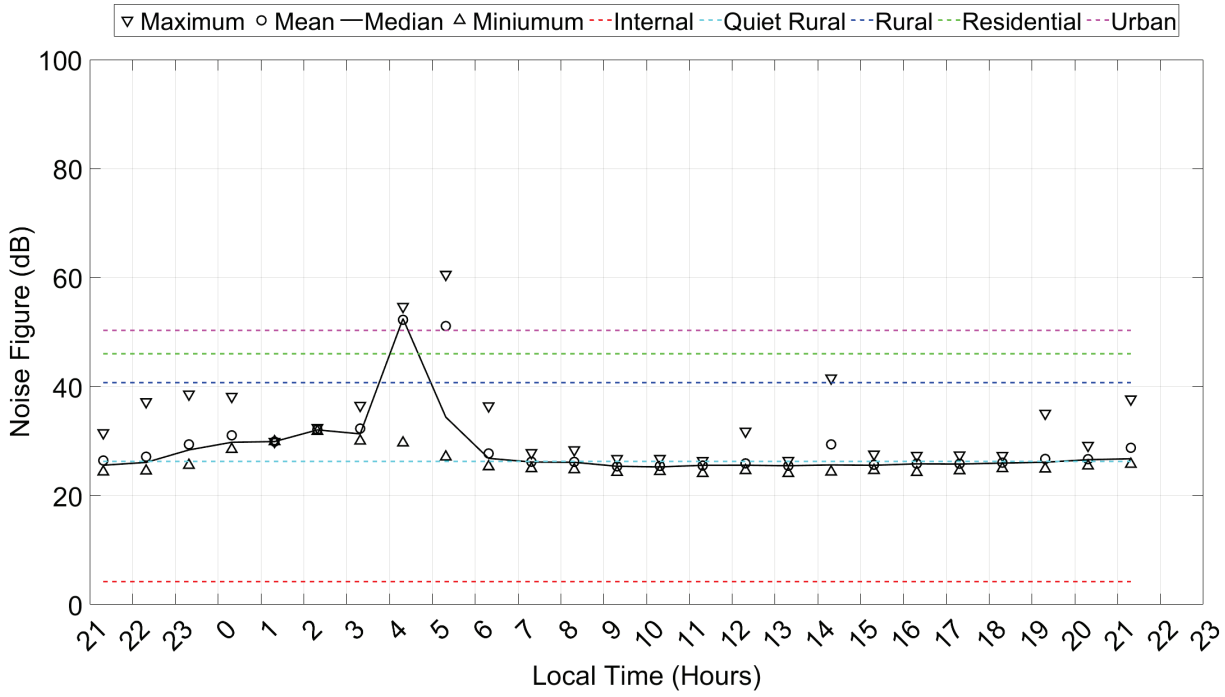

Figure 42. BITF 9.032 MHz ATC channel noise figure hourly statistics.

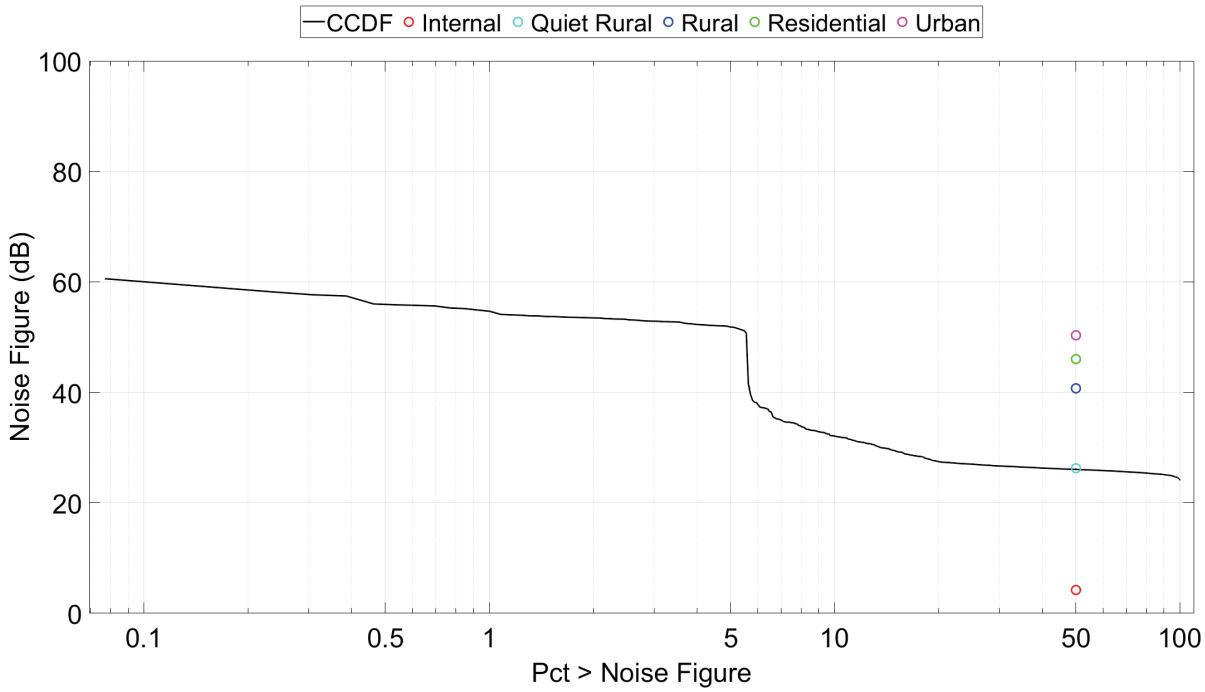

Figure 43. BITF 9.032 MHz ATC channel noise figure CCDF.

7.2 MACOPS

The MACOPS measurement was conducted with the "backup" CM antenna shown in Figure 44 and transmission line leading to the McMurdo operations center (MACOPS) in Building 165. The SuperDARN radar, a persistent cause of overload, was turned off during this measurement.

Figure 44. MS backup CM antenna. (Credit: Adam Hicks)

Figures 45 and 46 show the median power and noise figure spectra, respectively. The causes of the spikes and 8.5 MHz spectral bump are unknown. Neglecting these, the noise is approximately rural. Median noise figures for all ATC channels are provided in Appendix G.

Figures 47 and 48 show the 9.032 MHz ATC and 10.0 MHz SFTR channel measured power time series. Measurements from 11:45 to approximately 13:30 are not shown because of overload. The 9.032 MHz ATC channel powers are relatively constant. The 10.0 MHz SFTR powers are also relatively constant and approximately the same as those measured at the BITF for the same time of day.

Figures 49 and 50 show that the noise at 9.032 MHz is residential. The deviation from rural is due to the spectral bump. The CCDF in Figure 51 has no inflection points associated with channel use and its median corresponds to the hourly medians in Figure 50.

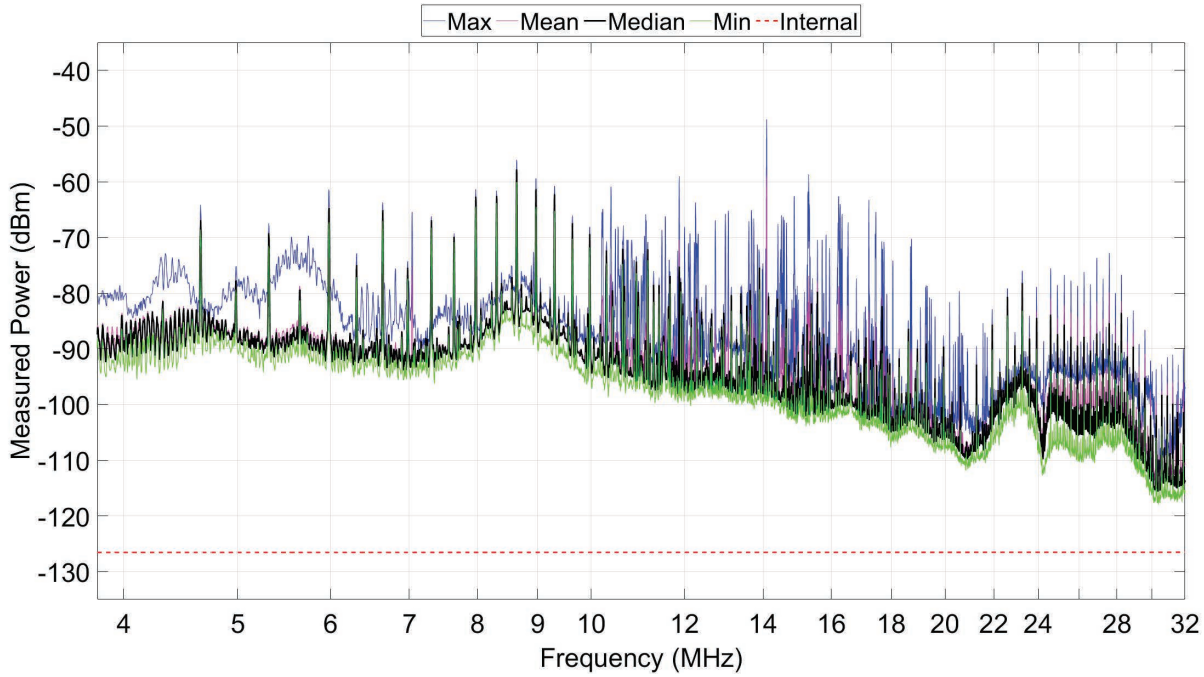

Figure 45. MACOPS PSD statistics.

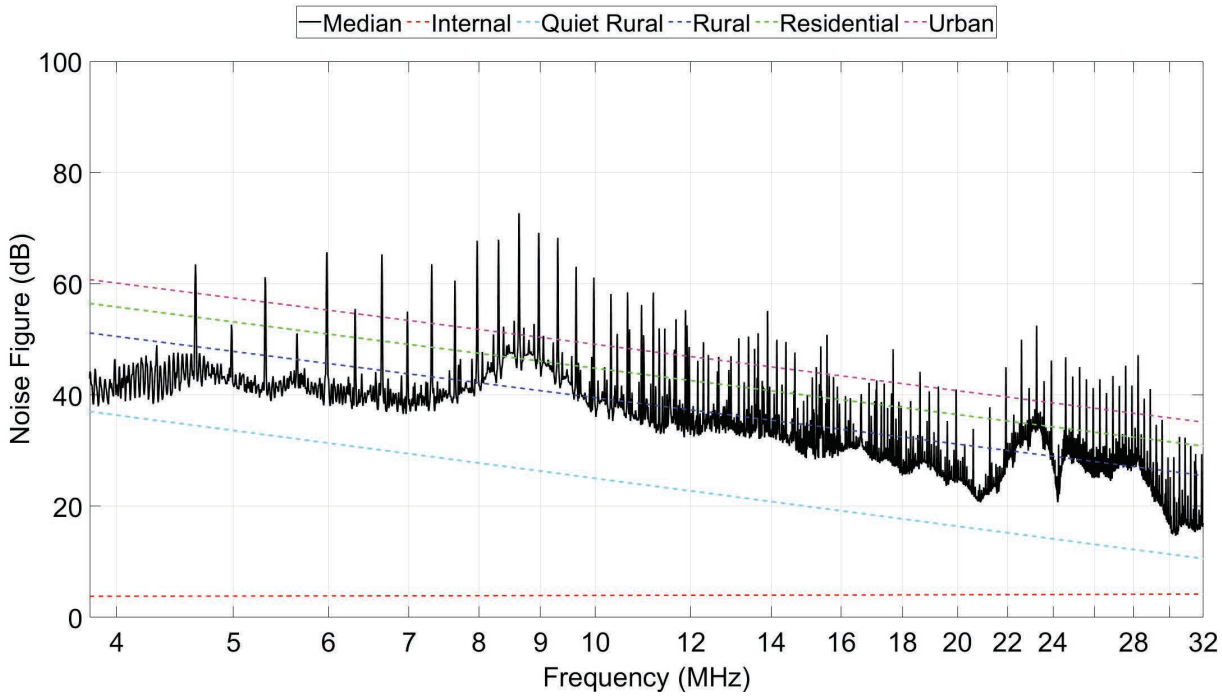

Figure 46. MACOPS median noise figure spectrum.

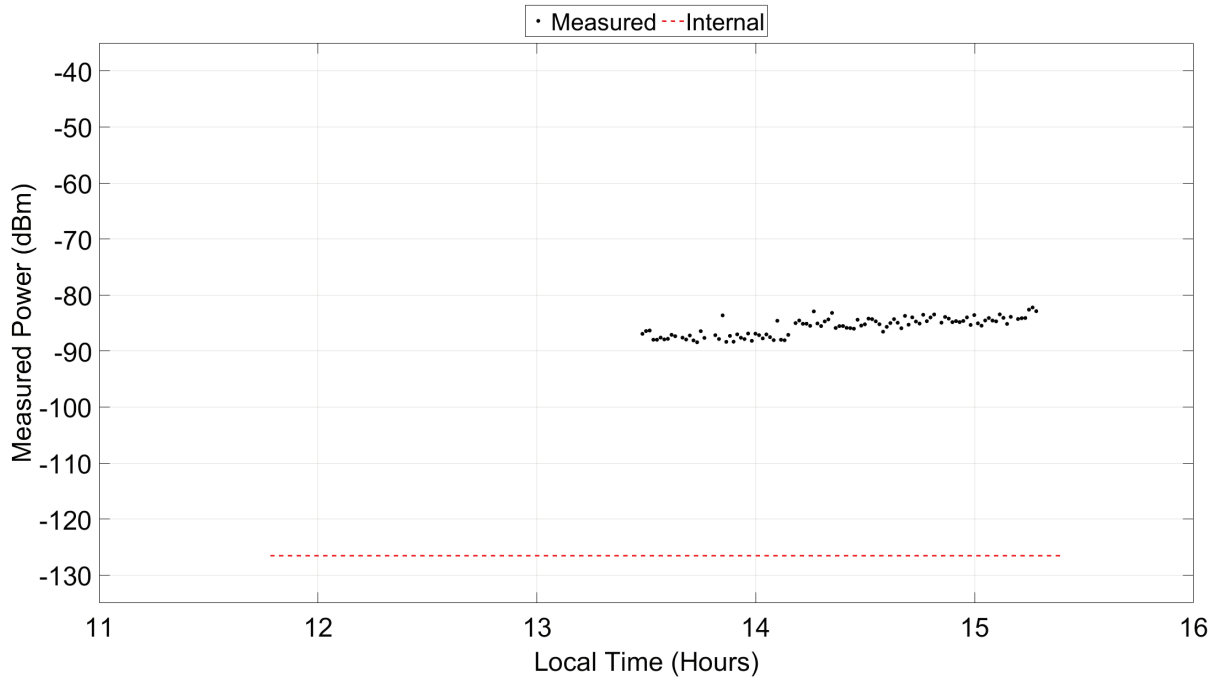

Figure 47. MACOPS 9.032 MHz ATC channel measured power time series. Gap in time series from 11:45 to 13:30 represents measurements removed because of receiver overload.

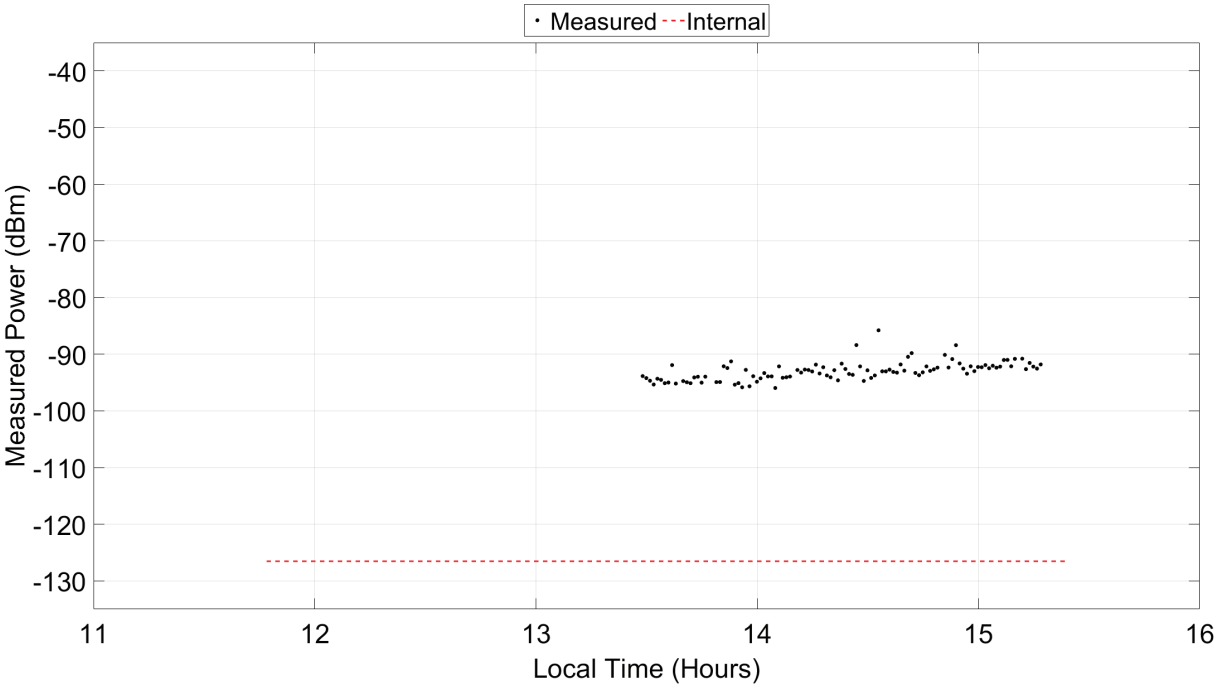

Figure 48. MACOPS 10.0 MHz SFTR channel measured power time series. Gap in time series from 11:45 to 13:30 represents measurements removed because of receiver overload.

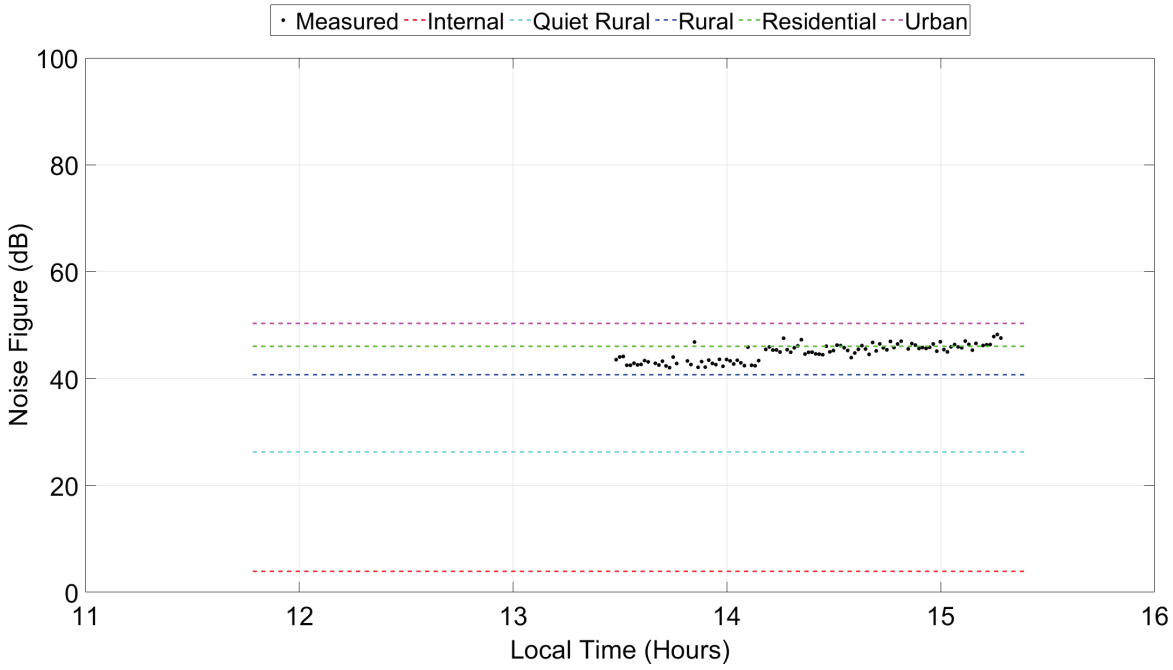

Figure 49 MACOPS 9.032 MHz ATC channel noise figure time series

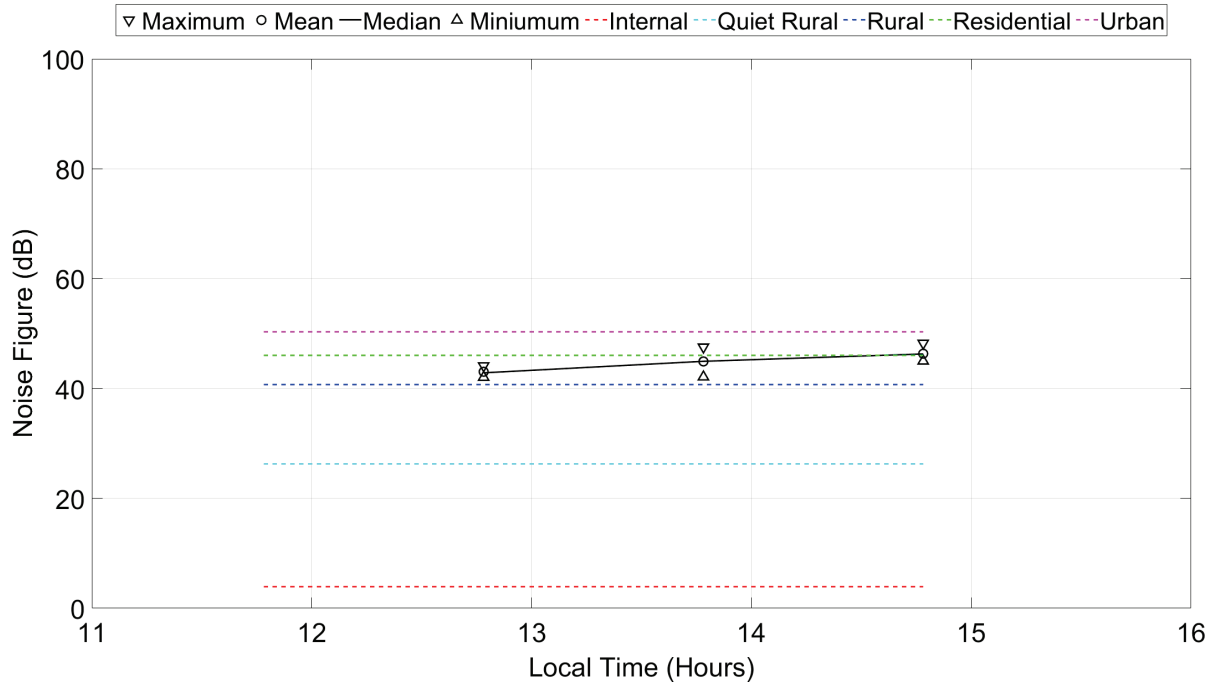

Figure 50. MACOPS 9.032 MHz ATC channel noise figure hourly statistics.

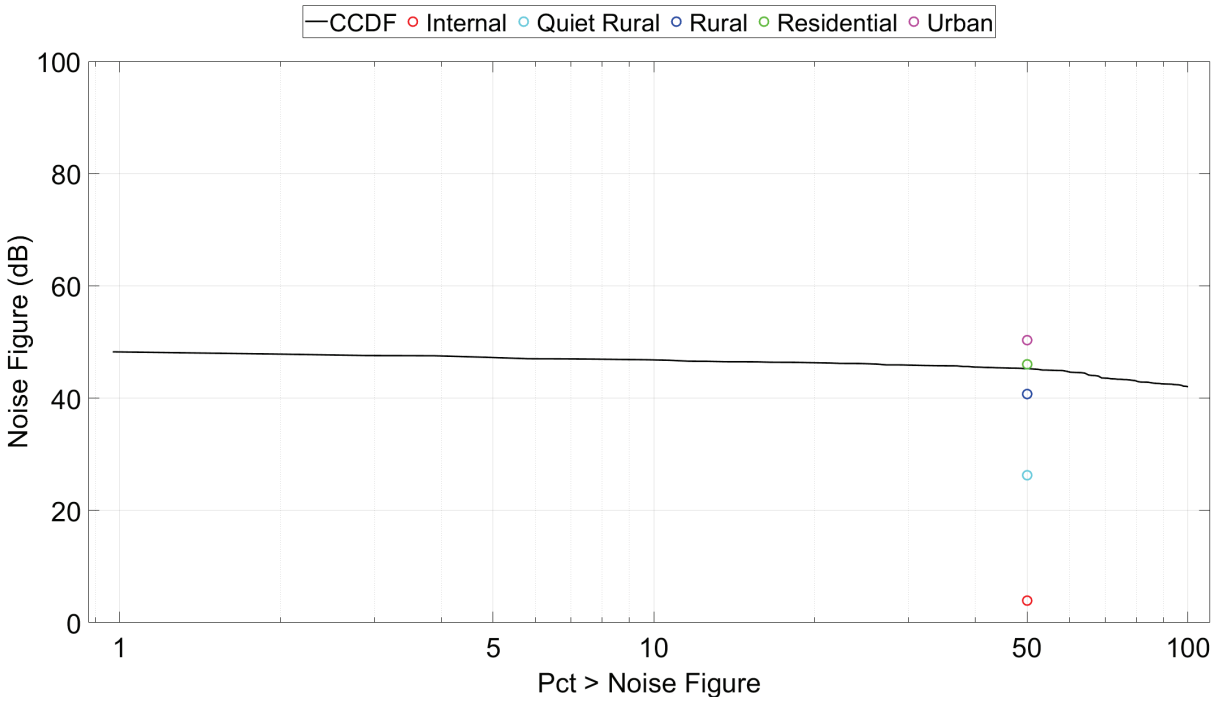

Figure 51. MACOPS 9.032 MHz ATC channel noise figure CCDF.

7.3 T-Site

T-Site, an abbreviation for transmitter site, hosts a number of transmit antennas for the HF, VHF, and microwave bands as shown in Figure 52. Even the local FM broadcast band antennas are located at T-Site. T-Site measurements used the PR antenna and radial ground plane as shown in Figure 10. Measurement equipment was set up in Building 221, which shelters a large amount of communications equipment.

Figure 52. Transmit antennas at T-Site. (Credit: Robert Achatz)

Strong signals observed at 4 and 6 MHz cautioned us from measuring across the entire HF band so we measured with a 9-15 MHz BPF placed between the PR antenna and the receiver.

Figures 53 and 54 show the median power and noise figure spectra, respectively, over the 9-15 MHz bandpass filter bandwidth. Median noise figures for the ATC channels in this bandwidth are provided in Appendix G. The noise ranges from urban at the lower frequencies to rural at the higher.

Figures 55 and 56 show the 9.032 MHz ATC and 10.0 MHz SFTR channel measured power time series. The 9.032 MHz ATC channel power is a relatively constant -108 dBm with no significant lapses caused by overload. The 10.0 MHz SFTR channel power varies a few dB about -90 dBm or 18 dB higher than the 9.032 MHz ATC channel noise power.

Figures 57 and 58 show the noise at 9.032 MHz is almost urban. The CCDF in Figure 59 has no inflection points associated with channel use and its median corresponds to the hourly medians in Figure 58.

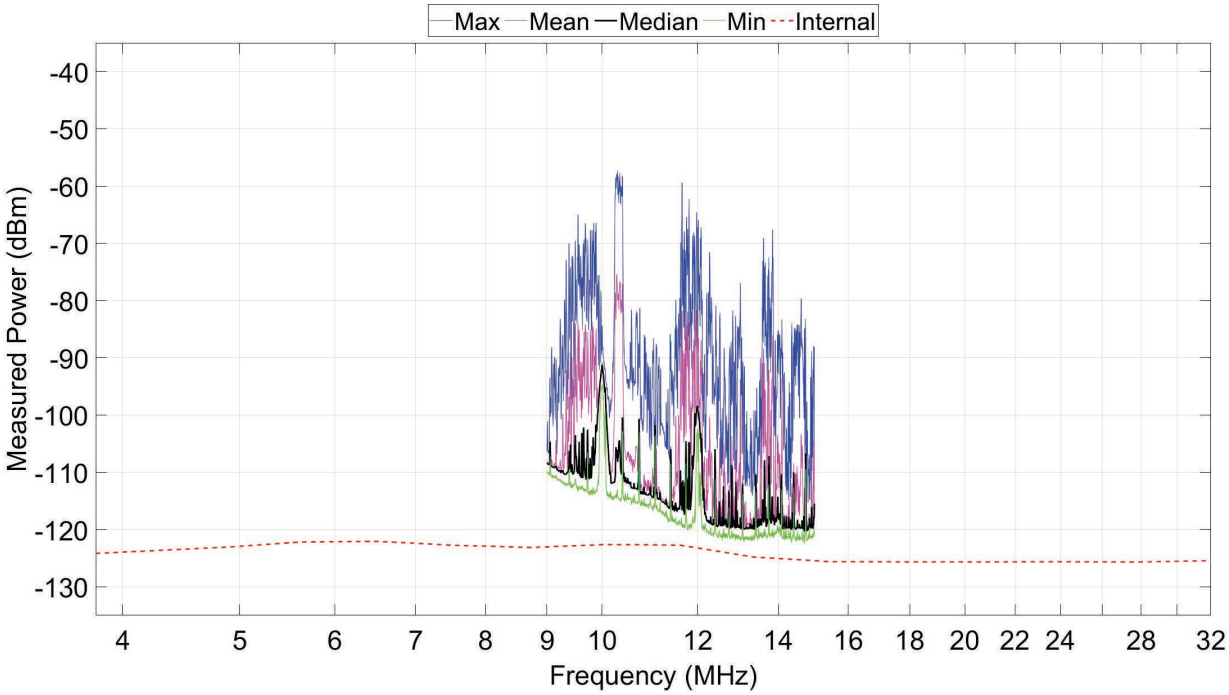

Figure 53. T-Site PSD statistics.

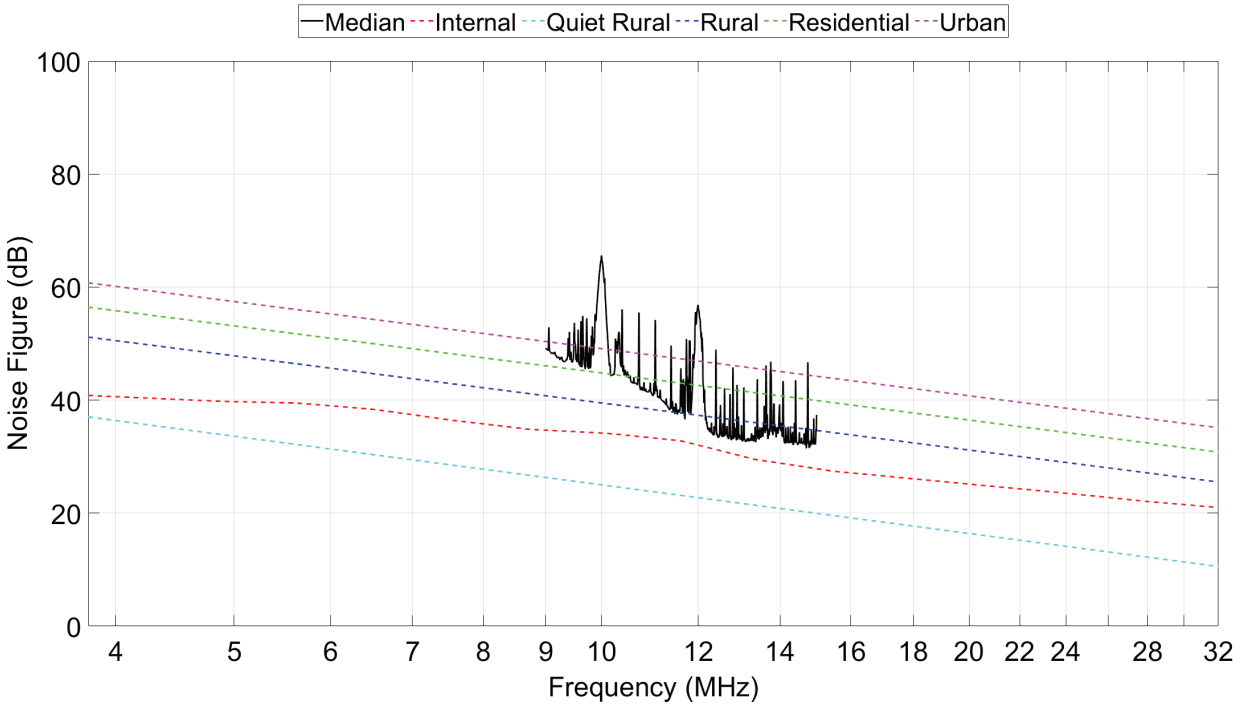

Figure 54. T-Site noise figure spectrum.

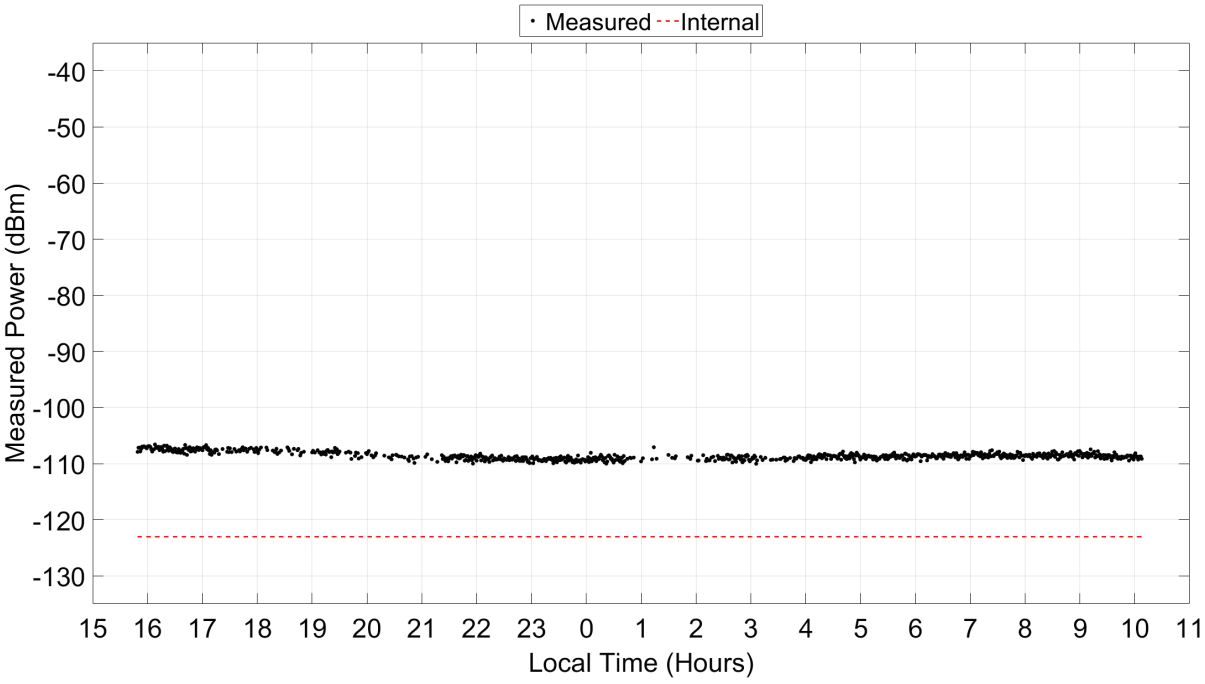

Figure 55. T-Site 9.032 MHz ATC channel measured power time series. Gaps in time series represent measurements removed because of receiver overload.

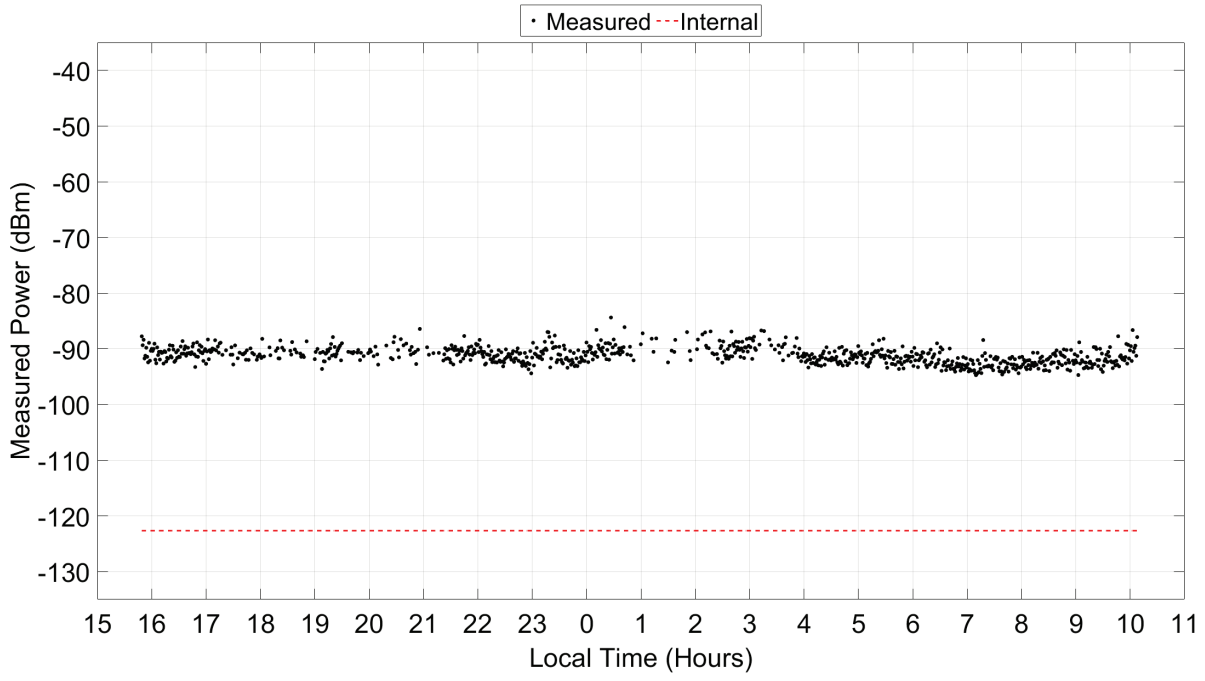

Figure 56. T-Site 10.0 MHz SFTR channel measured power time series. Gaps in time series represent measurements removed because of receiver overload.

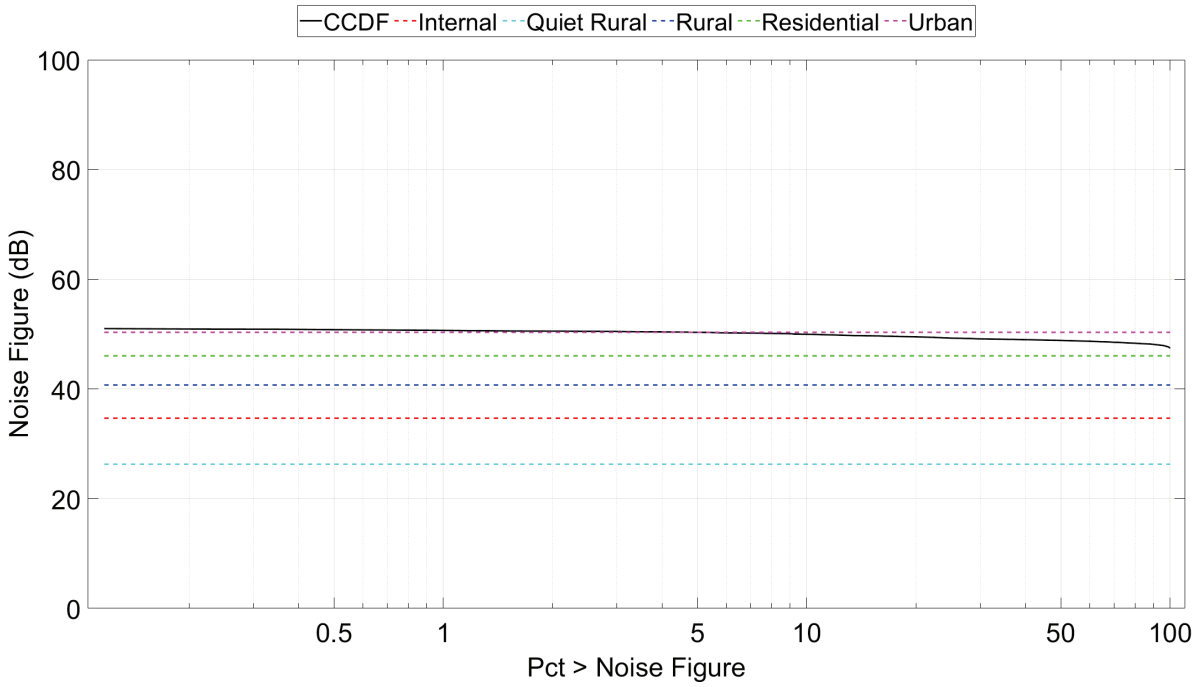

Figure 57. T-Site 9.032 MHz ATC channel noise figure time series.

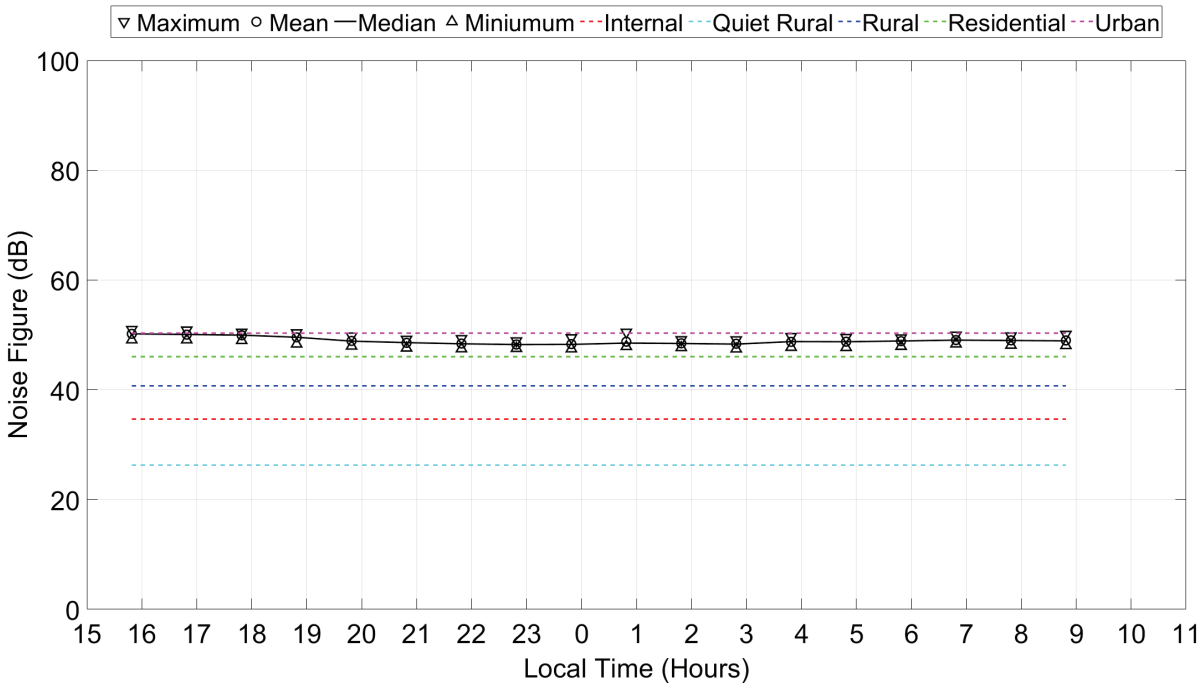

Figure 58. T-Site 9.032 MHz ATC channel noise figure hourly statistics.

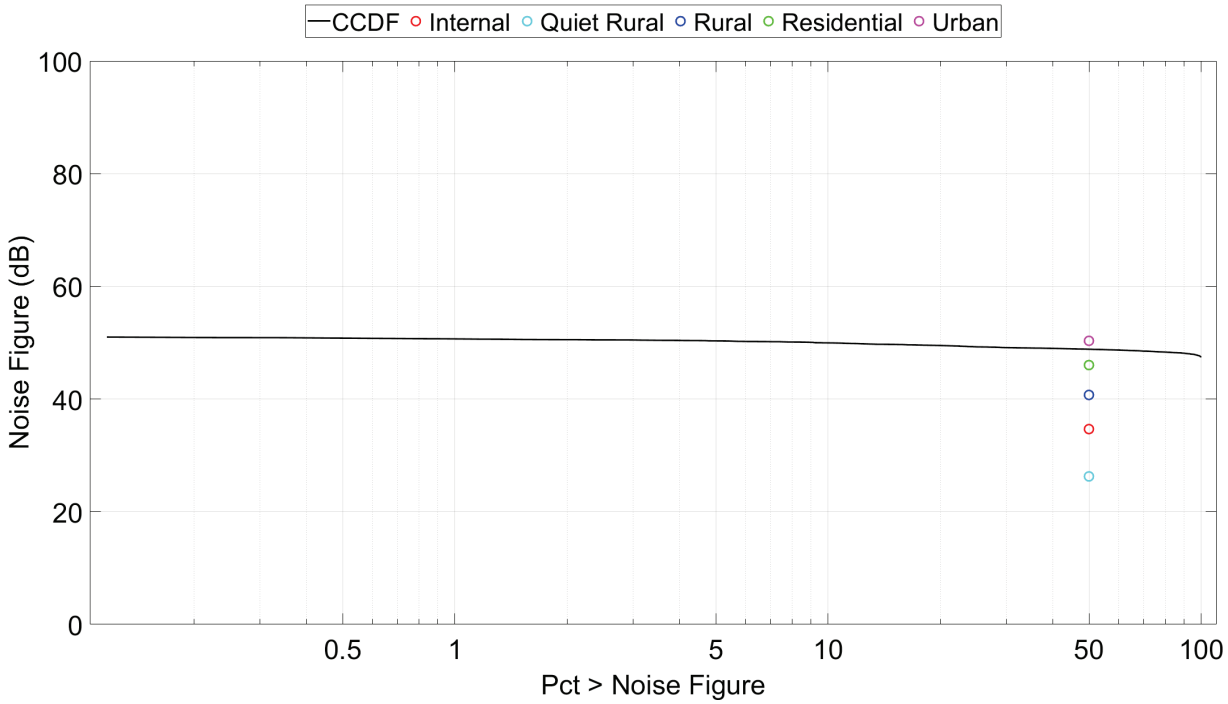

Figure 59. T-Site 9.032 MHz ATC channel noise figure CCDF.

7.4 MTRS-2

MTRS-2 is located on the bluff above MS near a group of wind power generators as shown in Figure 60. Equipment was set up in Building 69 underneath a radome painted red and white like a "beach ball".

Figure 60. Setting up radial ground plane at MTRS-2 with three wind generators in background. (Credit: Robert Achatz)

PSD time series and statistics were shown previously on a linear frequency scale in Section 6 Figures 34 and 36, respectively. Figures 61 and 62 show the measured power statistics and noise figure spectra, respectively, on a log frequency scale. Median noise figures for all ATC channels are provided in Appendix G. The causes of the spikes are unknown. The spectral bump around 10.3 MHz may be related to SuperDARN. Neglecting this, the noise is approximately residential.

Figures 63 and 64 show the 9.032 MHz ATC and 10.0 MHz SFTR channel measured power time series. The 9.032 MHz ATC channel power has some variability. Notable periods are a 3 dB drop between 18:00 and 22:00 and brief high signal power at 23:00. The 10.0 MHz SFTR channel shows ionospheric effects from 18:00 to 06:00 and peaks at midnight approximately 25 dB below that measured by the BITF CM as expected by the differences in antenna gains. The other hours are limited by MMN.

Figures 65 and 66 show the noise at 9.032 MHz is residential. The CCDF in Figure 67 has no inflection points associated with channel use and its median corresponds to the hourly medians in Figure 66.

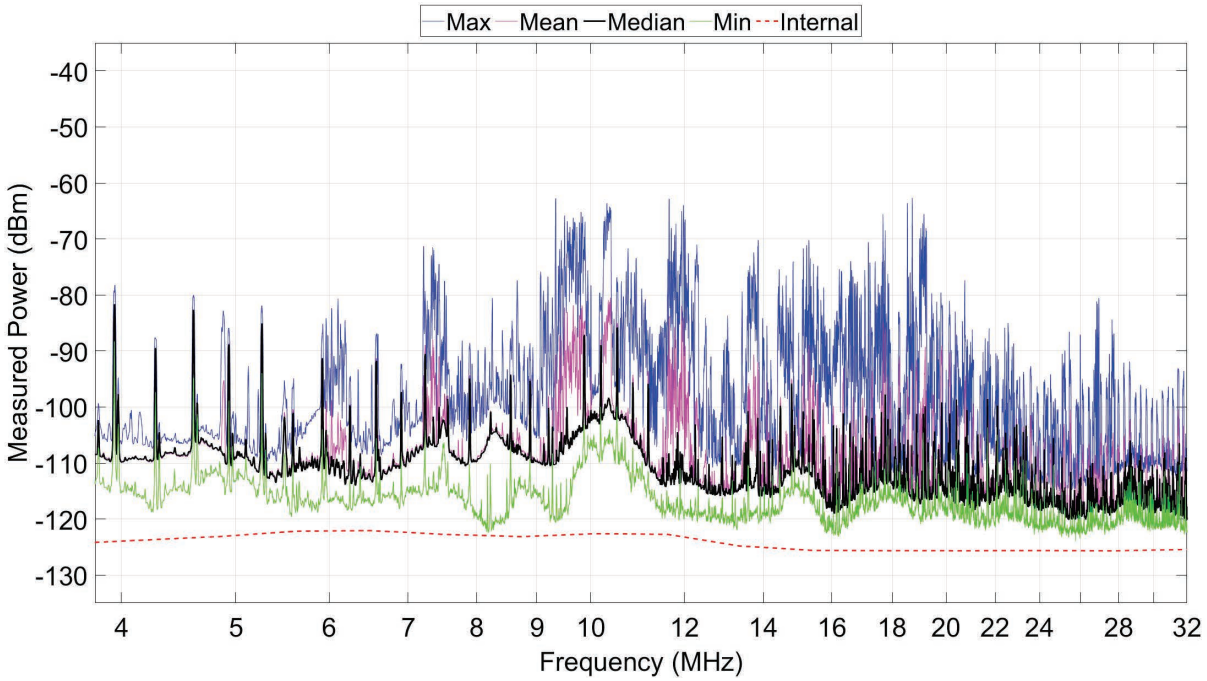

Figure 61. MTRS-2 PSD statistics.

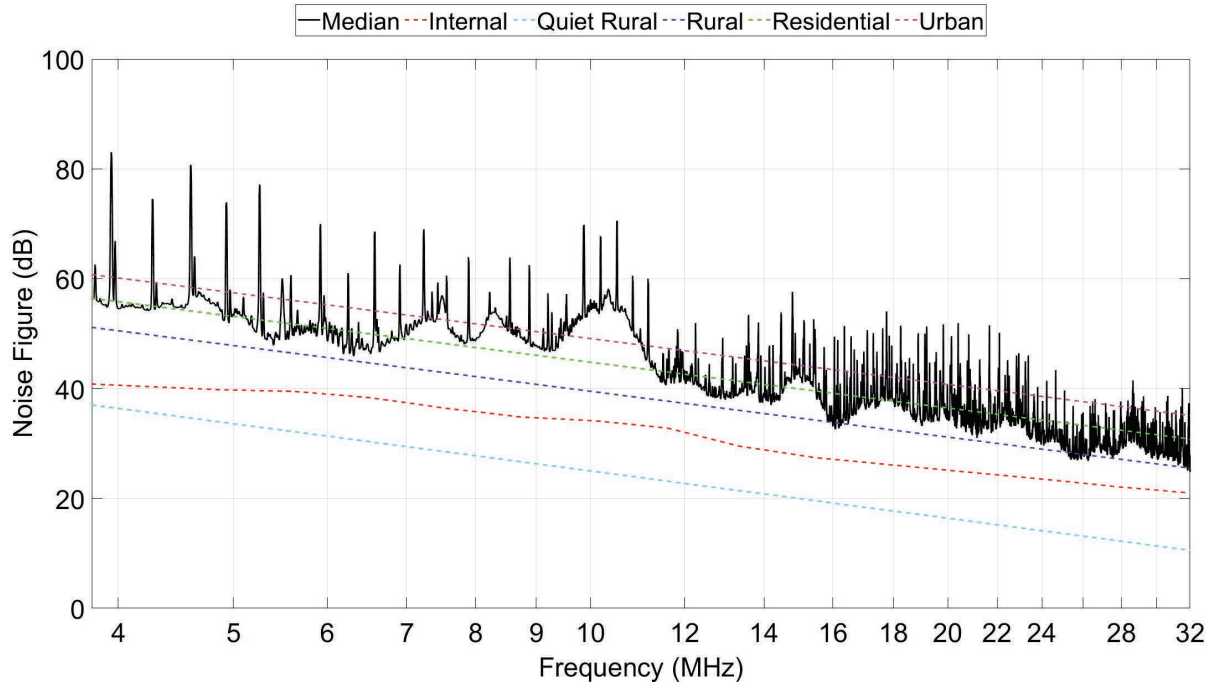

Figure 62. MTRS-2 median noise figure spectrum.

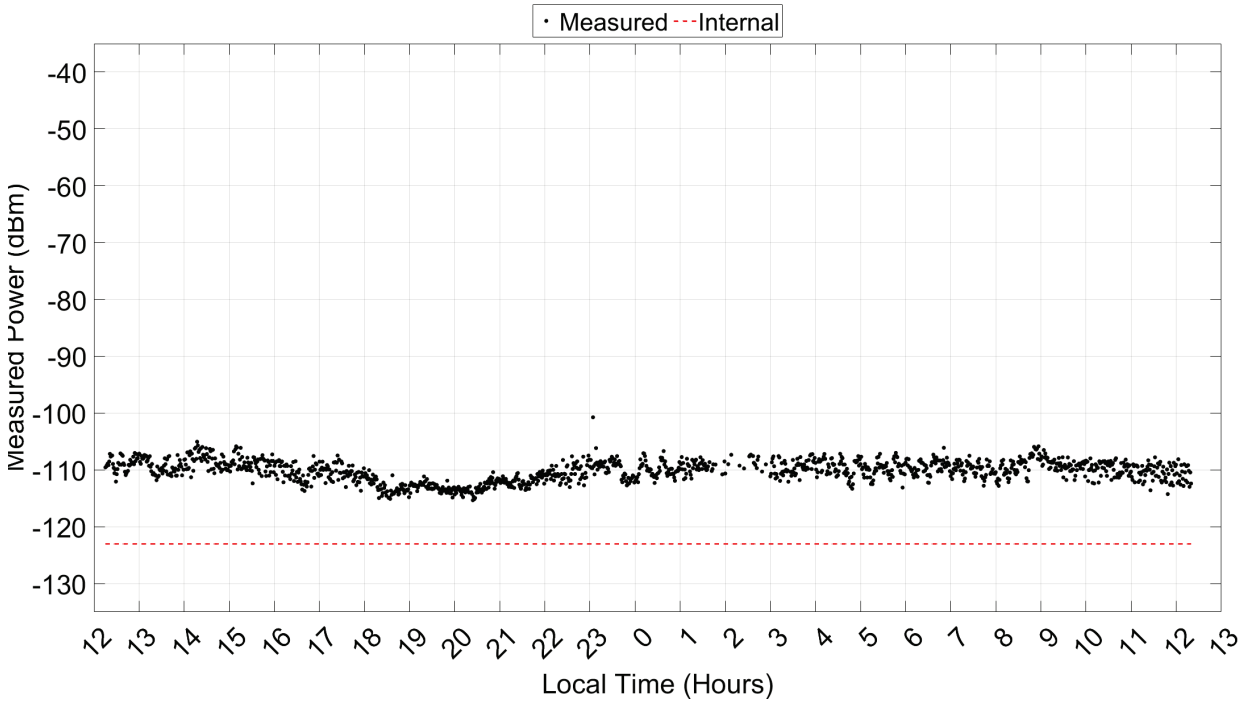

Figure 63. MTRS-2 9.032 MHz ATC channel measured power time series. Gaps in time series represent measurements removed because of receiver overload.

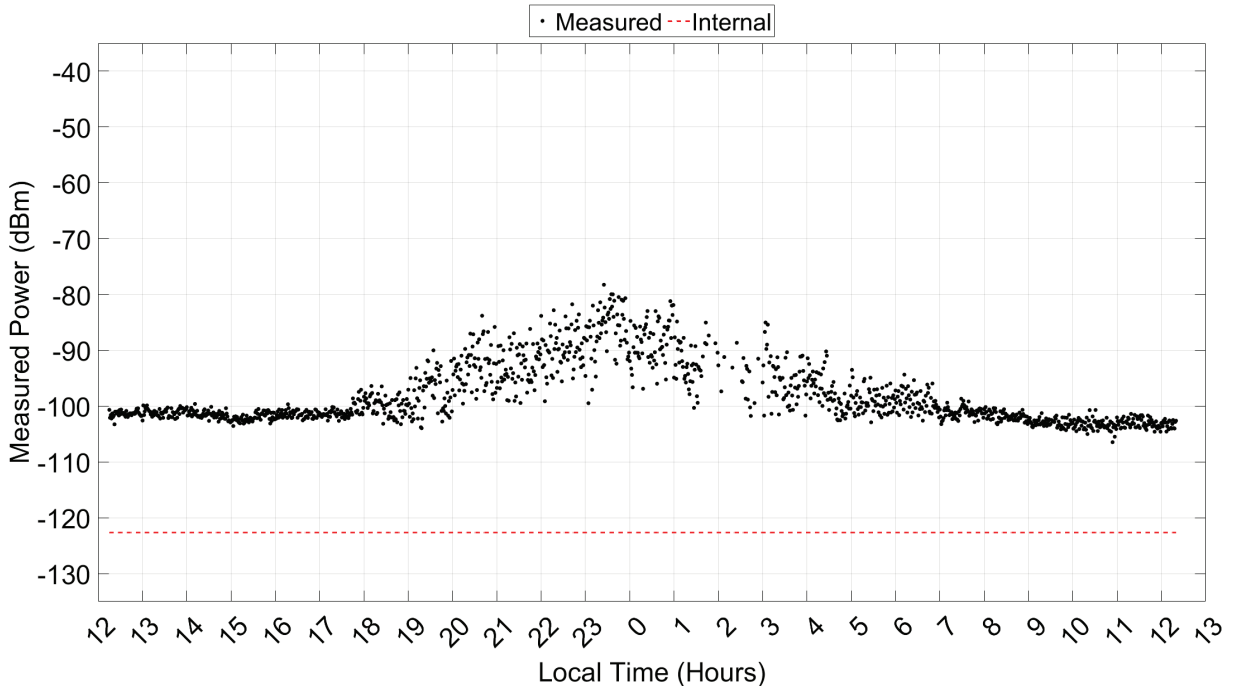

Figure 64. MTRS-2 10.0 MHz SFTR channel measured power time series. Gaps in time series represent measurements removed because of receiver overload.

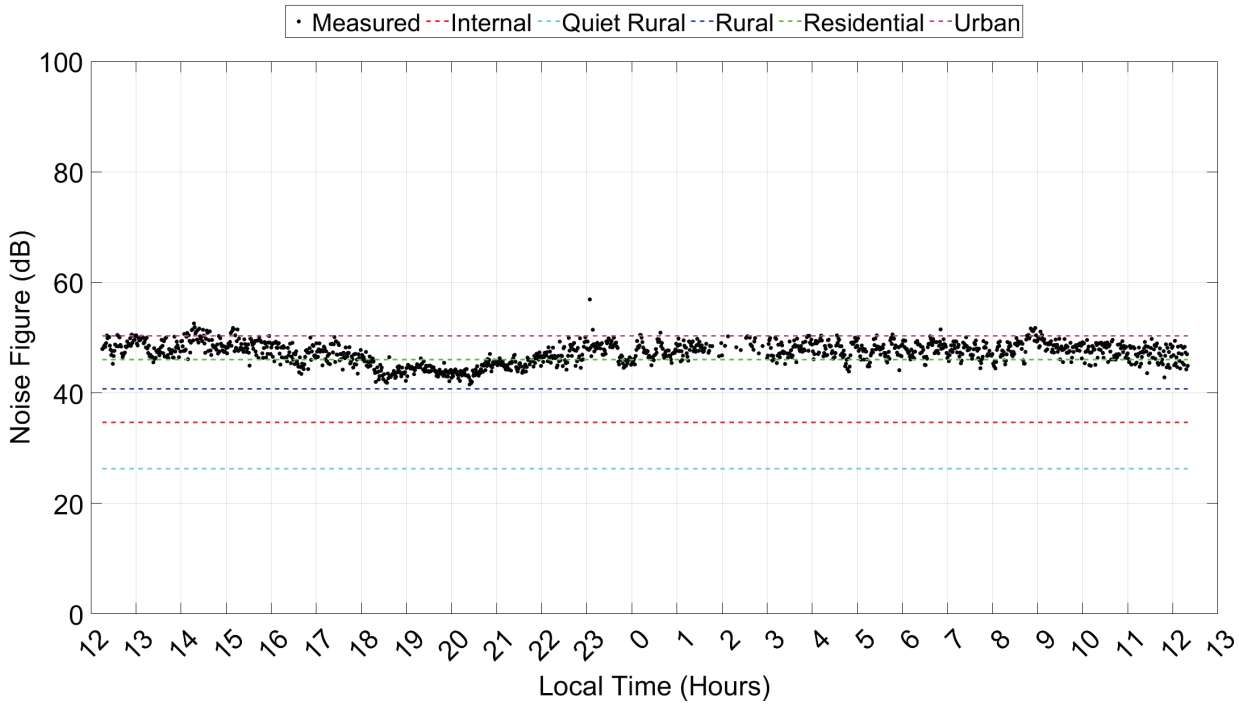

Figure 65. MTRS-2 9.032 MHz ATC channel noise figure time series.

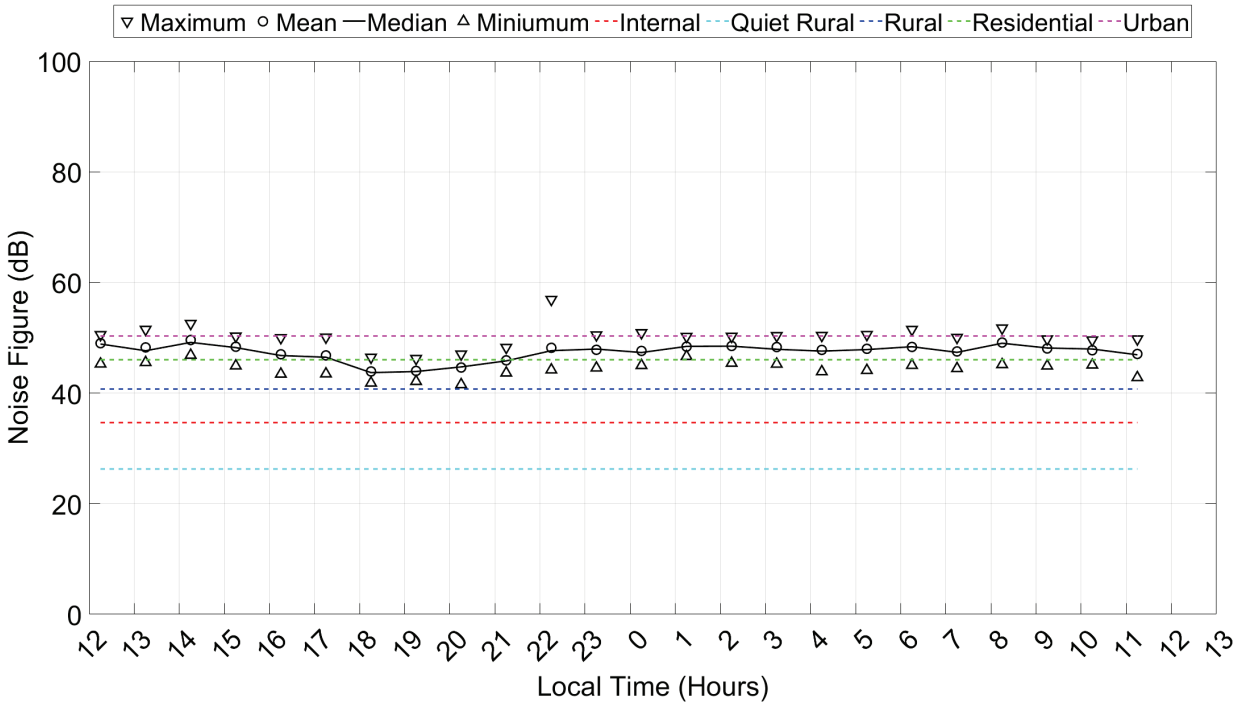

Figure 66. MTRS-2 9.032 MHz ATC channel noise figure hourly statistics.

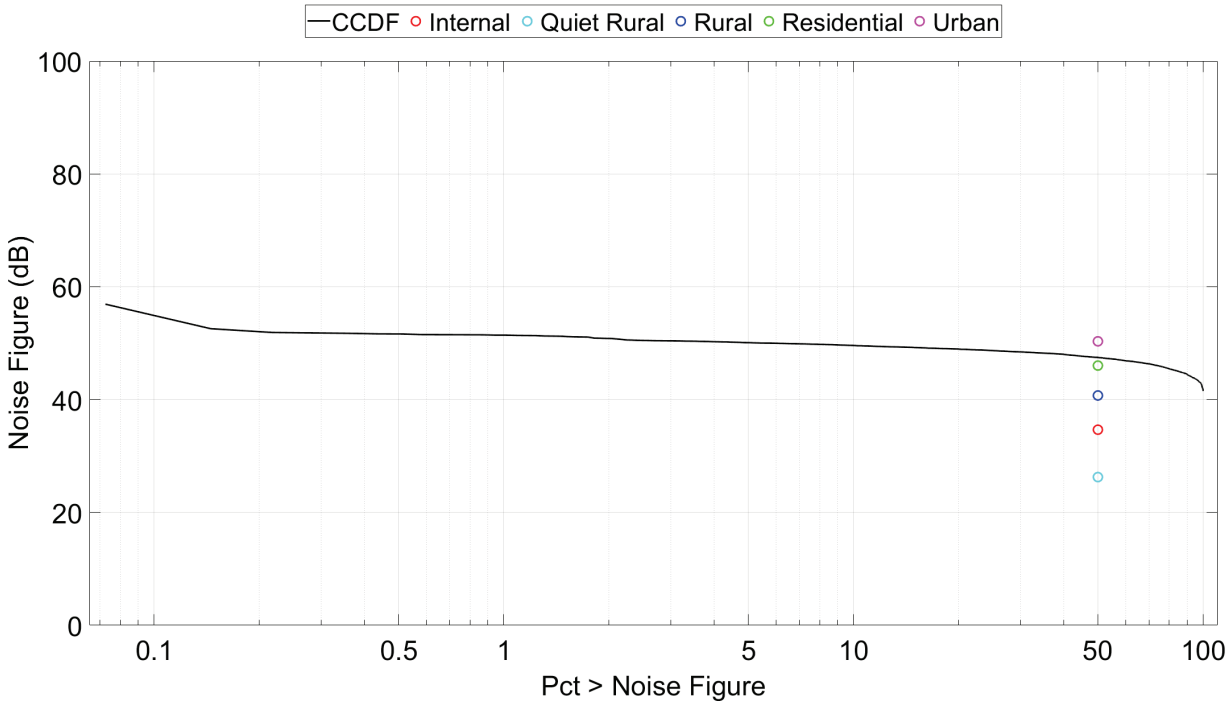

Figure 67. MTRS-2 9.032 MHz ATC channel noise figure CCDF.

7.5 MGS

The MGS is located on the bluff above MS. Measurement equipment was set up in Building 71. Figure 68 shows the building where the equipment was kept and the area just in front of the building where the PR antenna and radial ground plane were set up.

Figure 68. The road leading up to Building 71. (Credit: Robert Achatz)

Figures 69 and 70 show the median power and noise figure spectra, respectively. Median noise figures for all ATC channels are provided in Appendix G. Overall, the noise figure spectrum shows a tendency toward residential, with excursions from rural to urban.

Figures 71 and 72 show the 9.032 MHz ATC and 10.0 MHz SFTR channel measured power time series. The 9.032 MHz ATC channel power has consistent variability across the measurement period. Between 1:00 and 2:30 overload occurred, and ATC channel use is evident at 23:45 and 7:15. The 10.0 MHz SFTR channel power shows ionospheric effects from 18:00 to 06:00 and peaks at midnight approximately 25 dB below that measured by the BITF CM as expected by the differences in antenna gain.

Figures 73 and 74 show the noise at 9.032 MHz is residential. The CCDF in Figure 75 has inflections at the 0.8 and 5th percentiles likely caused by channel use and its median corresponds to many of the hourly medians in Figure 74.

The MGS results are very similar to those of the MTRS-2 location, with the exception that there is more within-the-hour variability.

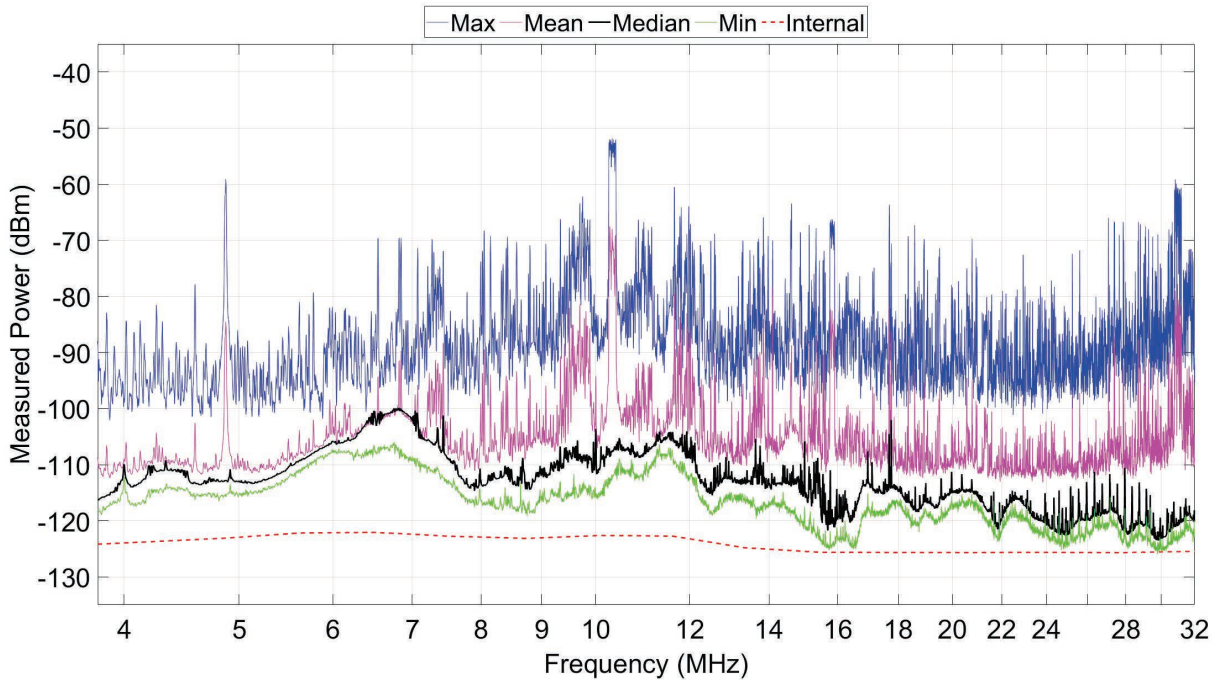

Figure 69. MGS PSD statistics.

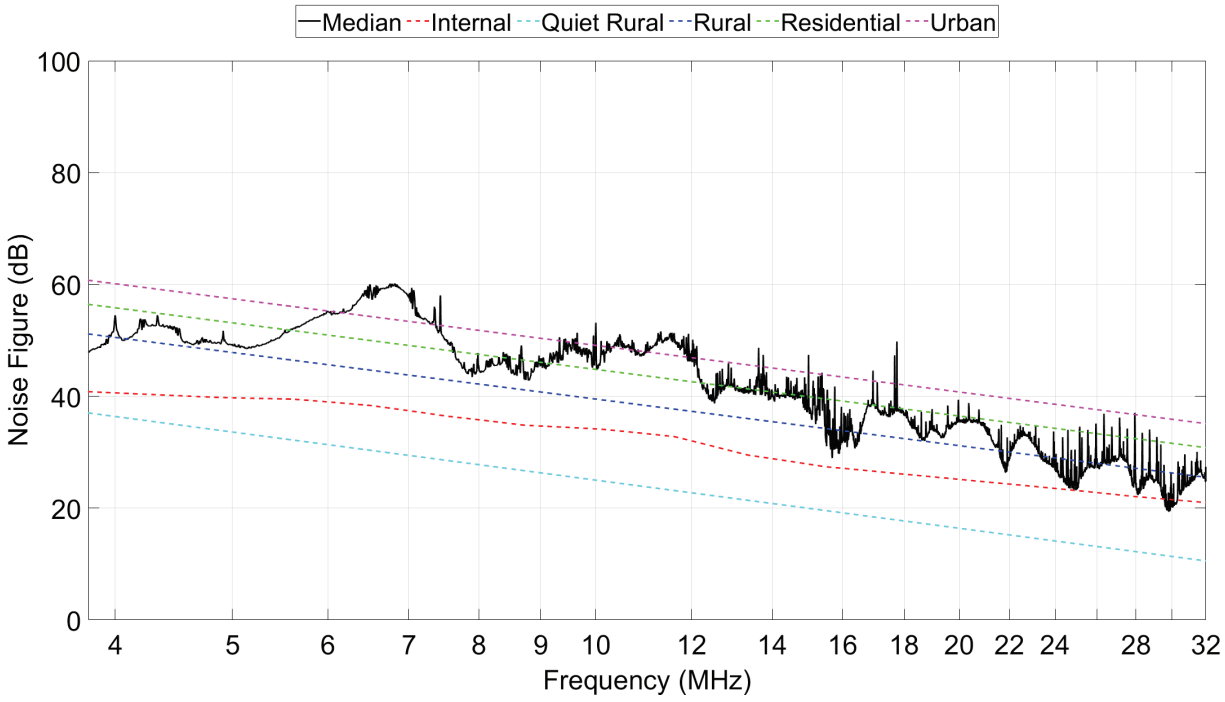

Figure 70. MGS median noise figure spectrum.

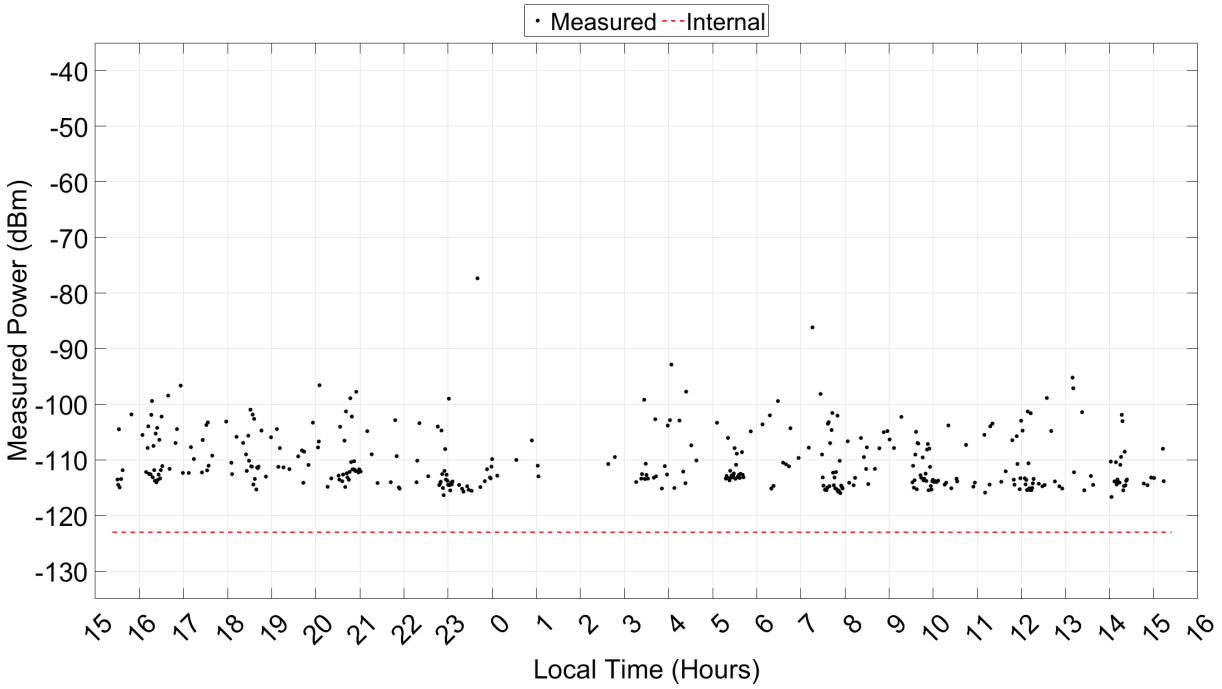

Figure 71. MGS 9.032 MHz ATC channel measured power time series. Gaps in time series represent measurements removed because of receiver overload.

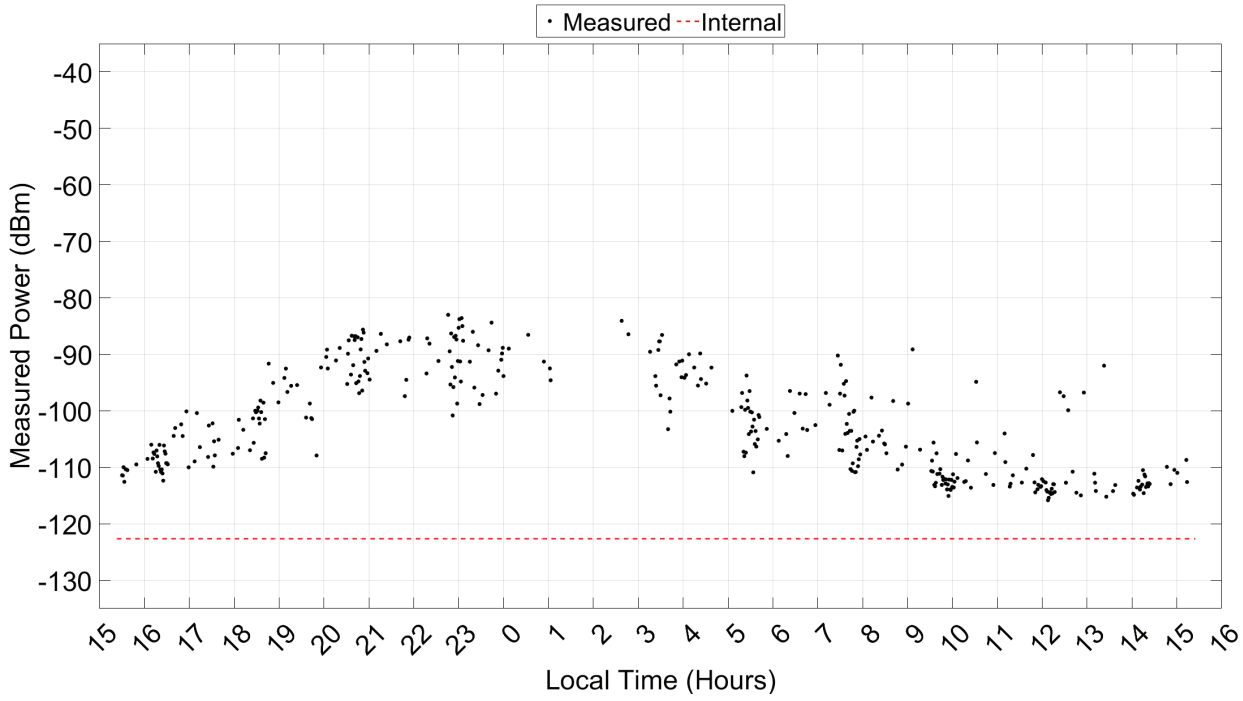

Figure 72. MGS 10.0 MHz SFTR channel measured power time series. Gaps in time series represent measurements removed because of receiver overload.

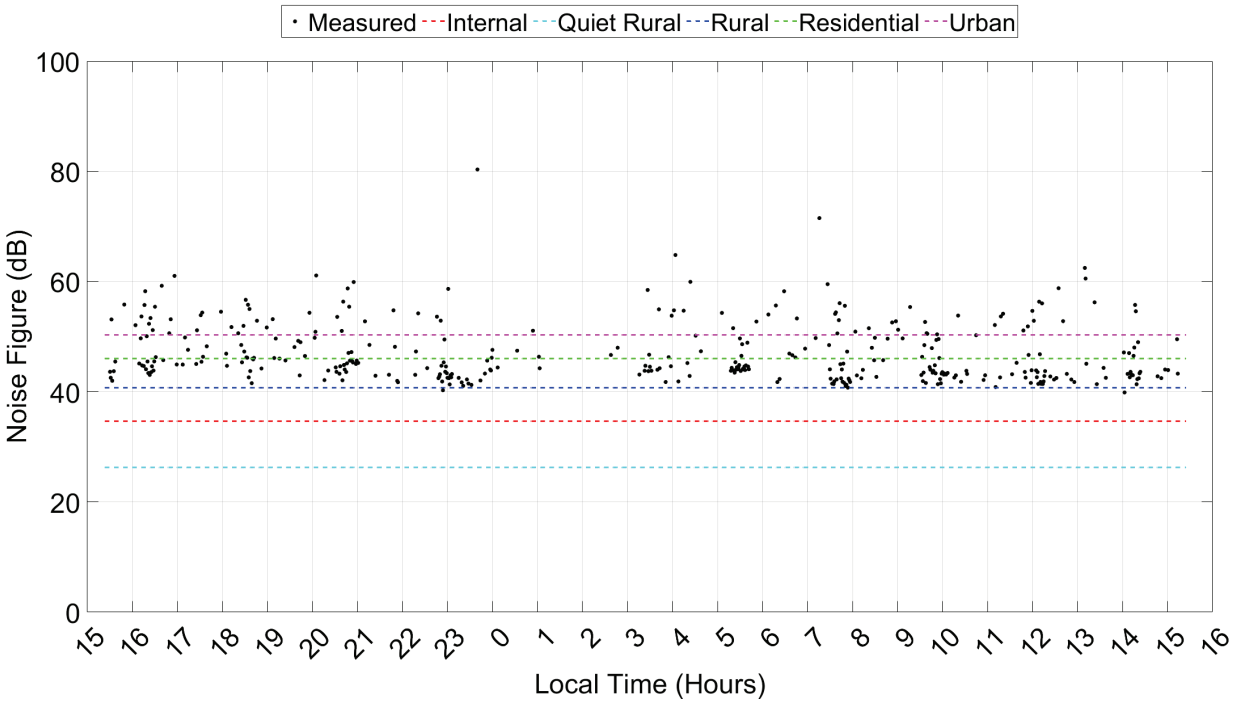

Figure 73. MGS 9.032 MHz ATC channel noise figure time series.

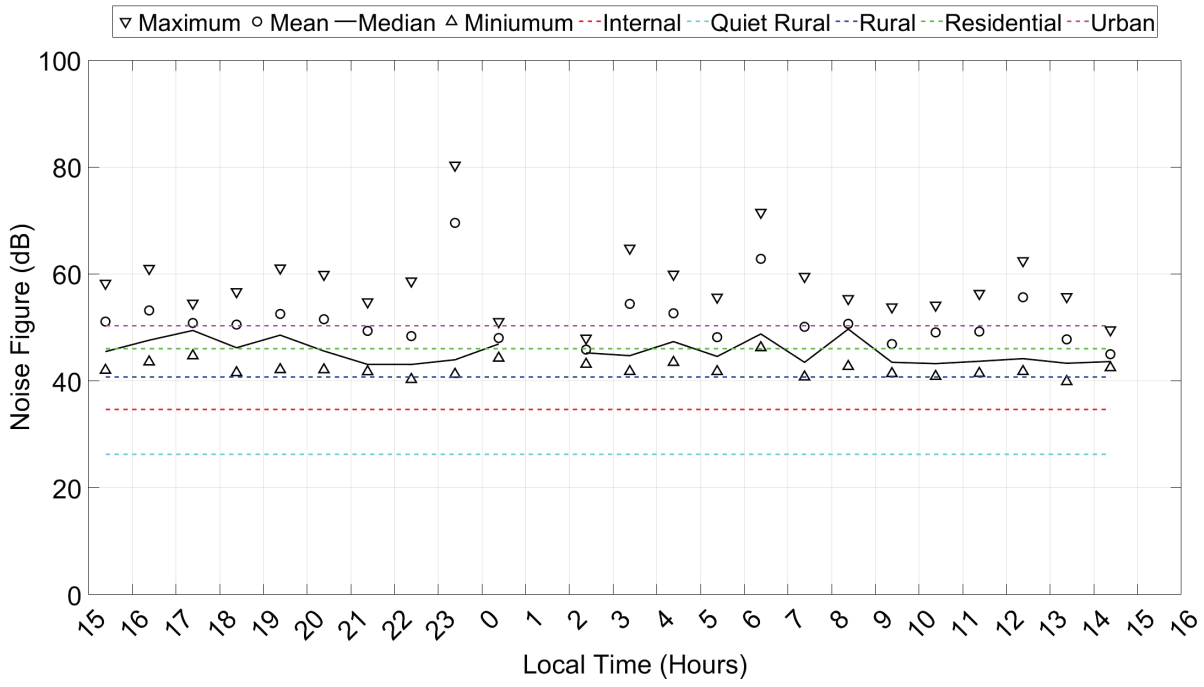

Figure 74. MGS 9.032 MHz ATC channel measured power hourly statistics.

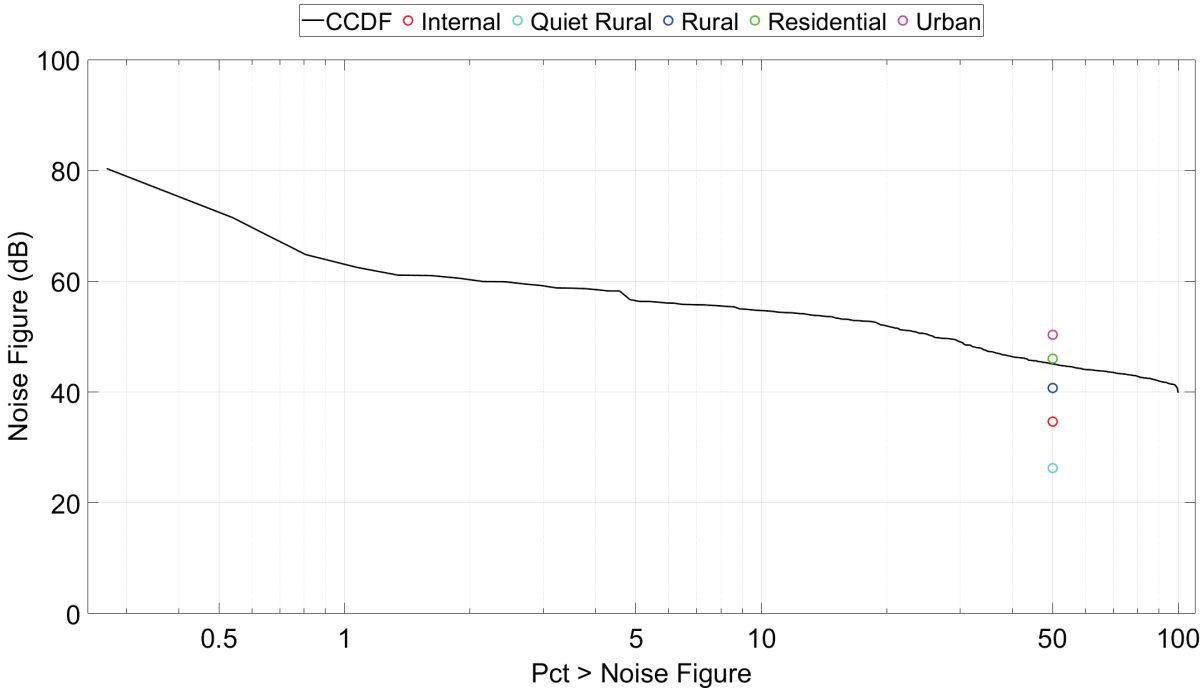

Figure 75. MGS 9.032 MHz ATC channel noise figure CCDF.

7.6 Ham Shack

The Ham Shack location is in town adjacent to a storage yard filled with supplies on pallets and large refrigerated containers. Anecdotally, it was the HF receive site before that site was moved to the BITF. Measurement equipment was set up in a small utility shed as shown in Figure 76.

Figure 76. HS location. Large antenna in background is for the use by HAM radio operators seated in adjacent small brown "Ham shack". White refrigerator container units are to the right of the HAM shack. (Credit: Robert Achatz)

Figures 77 and 78 show the Ham Shack location measured power and noise figure. The measurements were encumbered by a dominant broadband source that included a strong 14.09 MHz discrete signal. Figure 79 shows the broadband source noise figure spectrum and Figure 80 shows the Ham Shack location noise figure spectrum without the broadband source. The broadband source is believed to be the refrigerator container compressor motors.

With the broadband source, the noise is comparable to that found in a residential noise environment. Without the broadband source, the overall noise figure trends towards rural and sometimes as high as residential. Median noise figures for all ATC channels are provided in Appendix G. The measurements were too short in duration to justify a time series analysis.

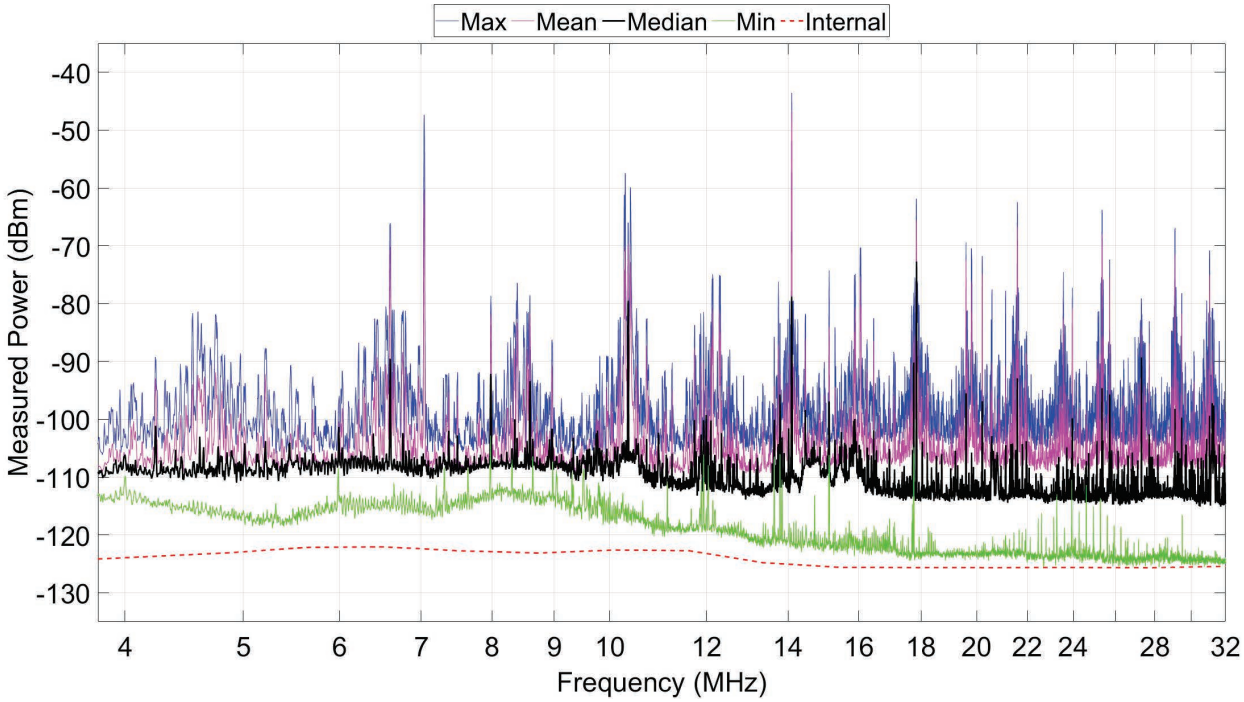

Figure 77. Ham Shack measured PSD.

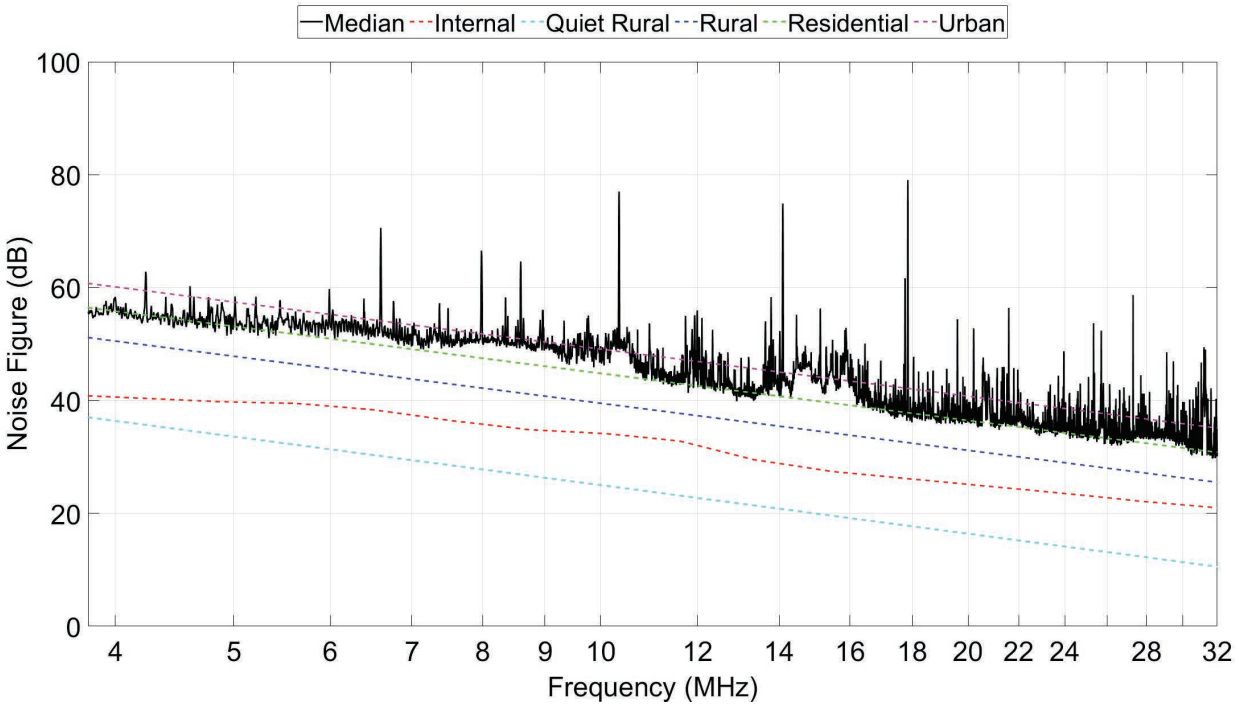

Figure 78. Ham Shack noise figure spectrum.

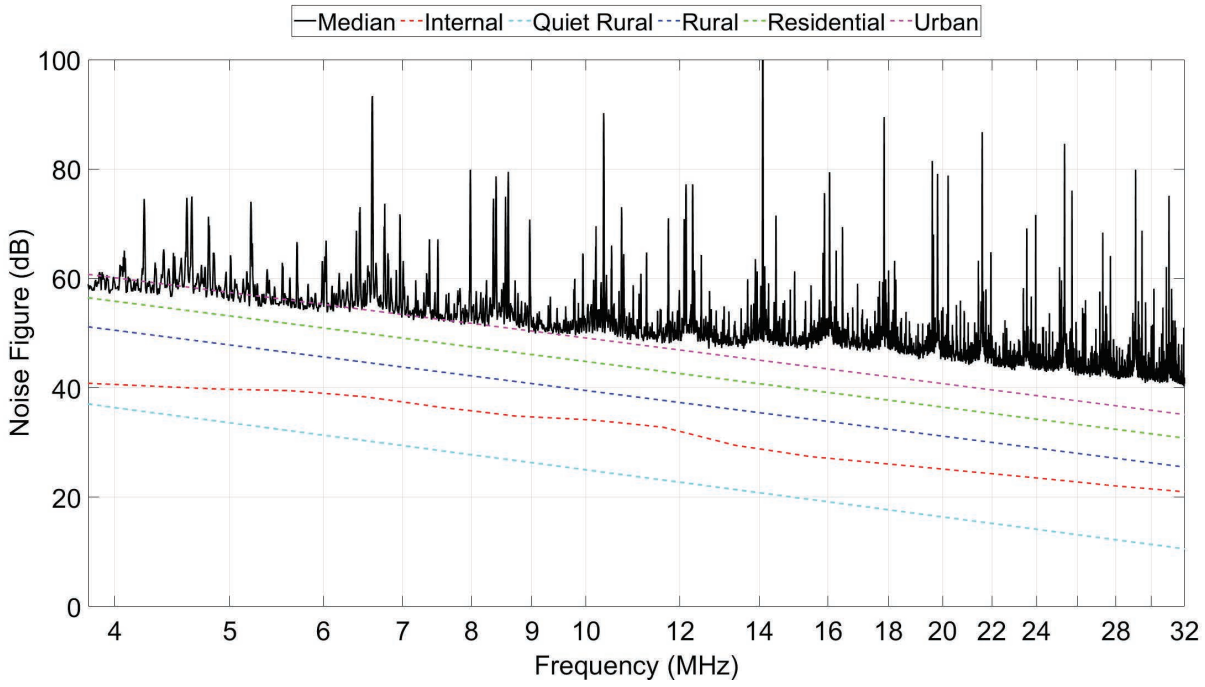

Figure 79. Ham Shack dominant source noise figure spectrum.

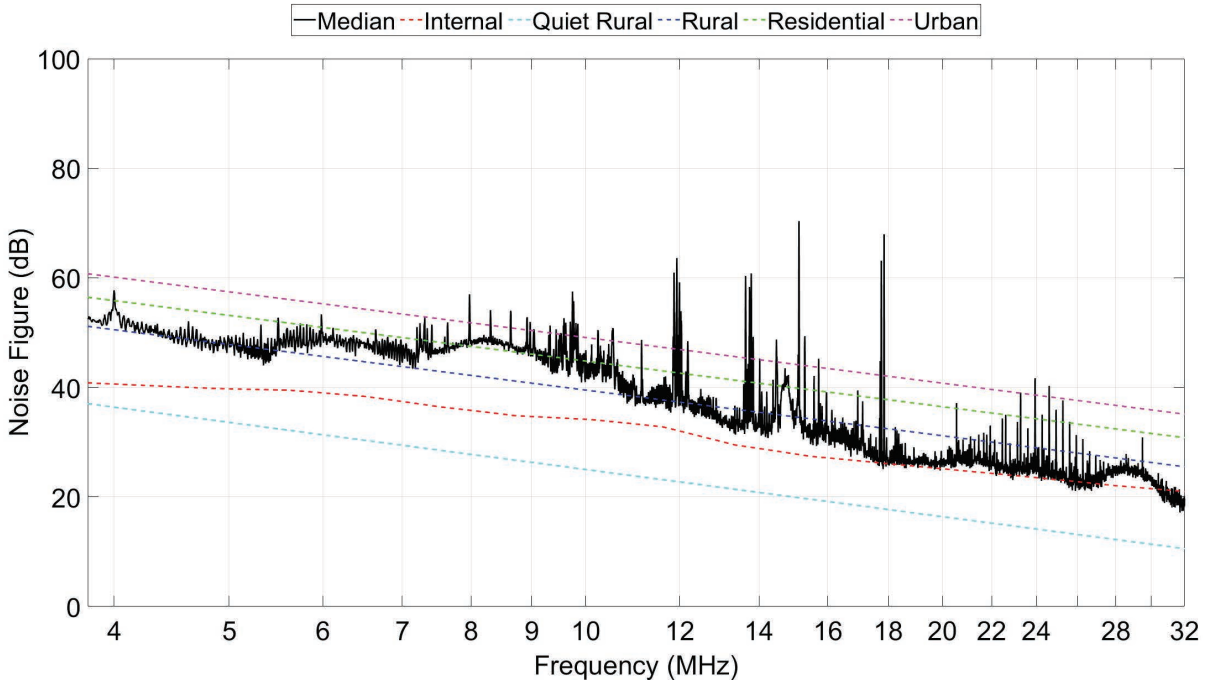

Figure 80. Ham Shack median noise figure spectrum without dominant source.

7.7 Arrival Heights

The Arrival Heights Clear Air Facility is located on the bluff above MS. Measurement equipment was set up in Building 197. A picture of the surrounding area is shown in Figure 81.

Figure 81. View from Arrival Heights location looking towards the green New Zealand laboratory. (Credit: Robert Achatz)

Figures 82 and 83 show the median measured power and noise figure spectra, respectively. The spike at 10.3 MHz is assumed to be the SuperDARN radar. The cause of the spectral bump at 8.5 MHz is unknown, as is the cause of the oscillations below the bump. Median noise figures for all ATC channels are provided in Appendix G.

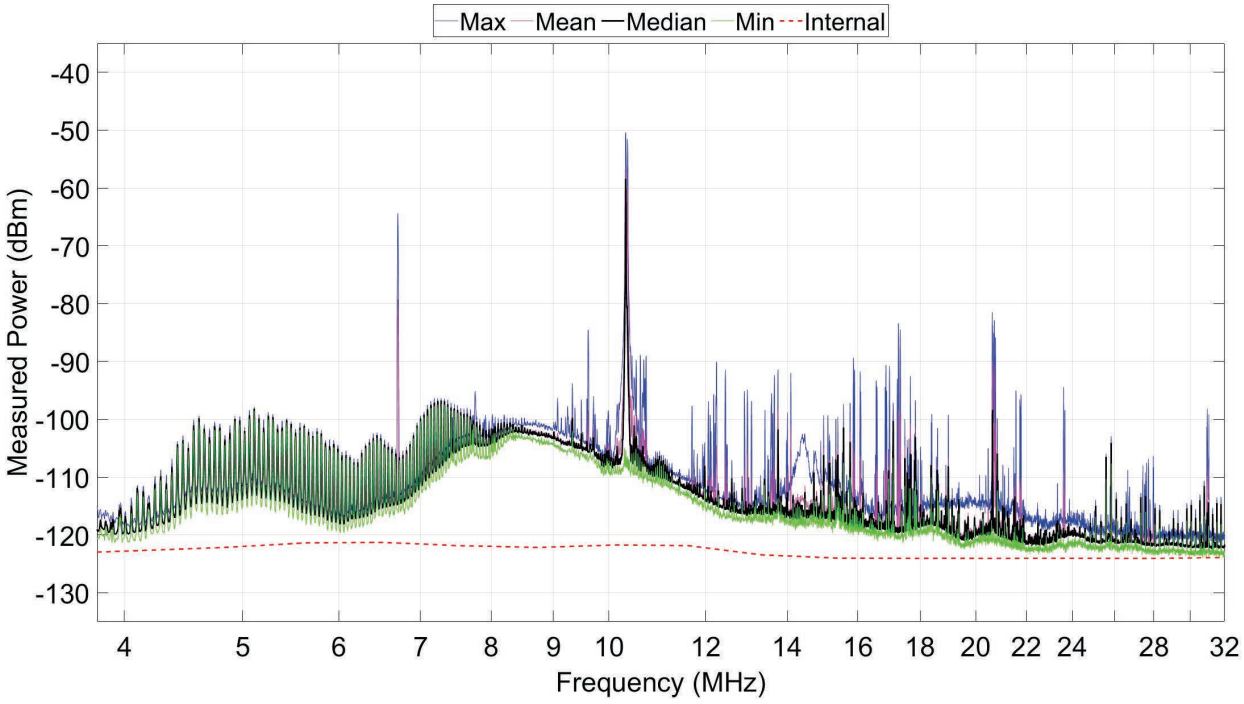

Figure 82. Arrival Heights PSD statistics.

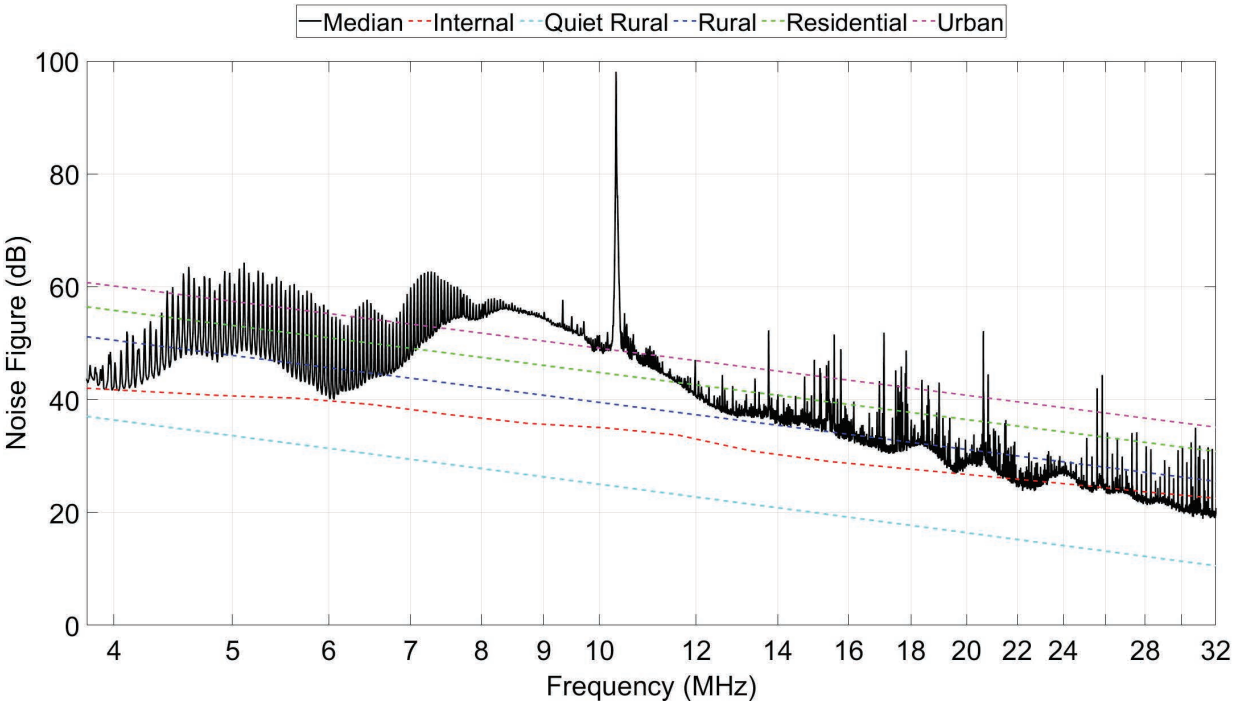

Figure 83. Arrival Heights noise figure spectrum.

8. Discussion

Median noise figures for in-town and on-bluff sites are summarized in Figures 84 and 85, respectively. The two in-town measurements, ranging from rural to residential, show higher noise figures than the BITF measurement. The greatest difference is below 9 MHz when BITF is below quiet rural. Above 9 MHz, where BITF is above quiet rural, the difference diminishes.

On-bluff measurements also show higher noise figures than the BITF measurement. As expected, at any one ATC channel there is considerable location variability. With the exception of 9 and 11.2 MHz, the medians cluster around residential. The 9 and 11.2 MHz ATC channels are higher, with 9 MHz clustering around urban and 11.2 MHz between residential and urban.

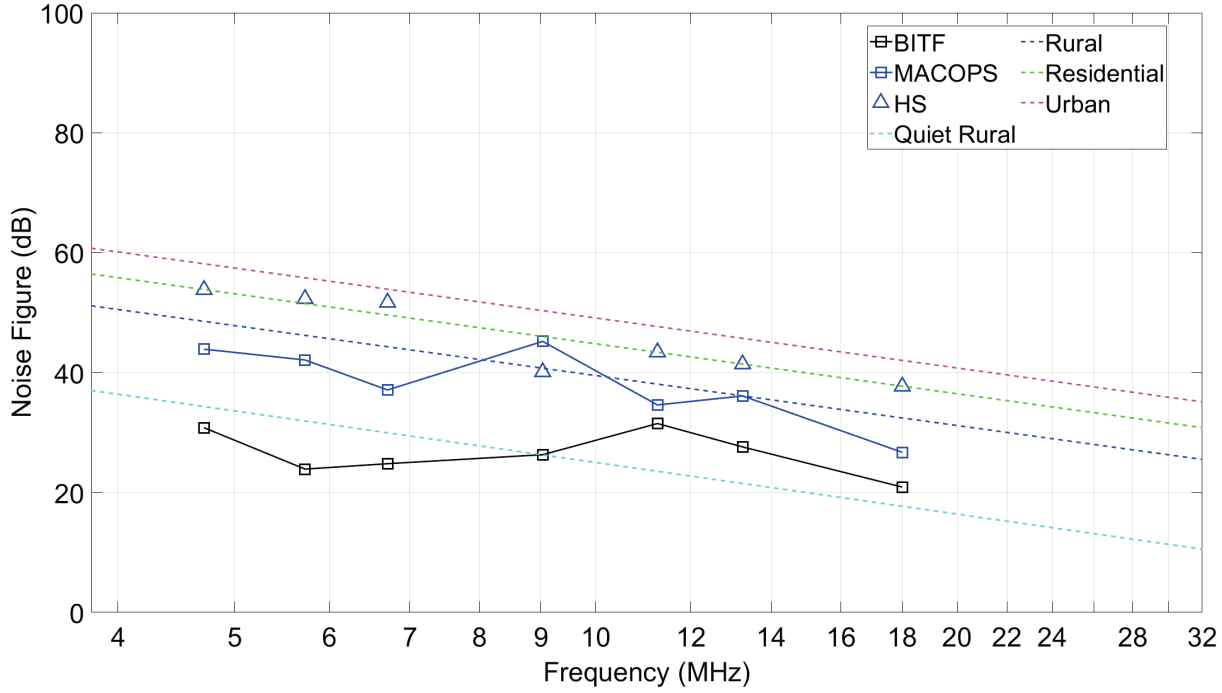

Figure 84. Median noise figures for all ATC channels and in-town sites.

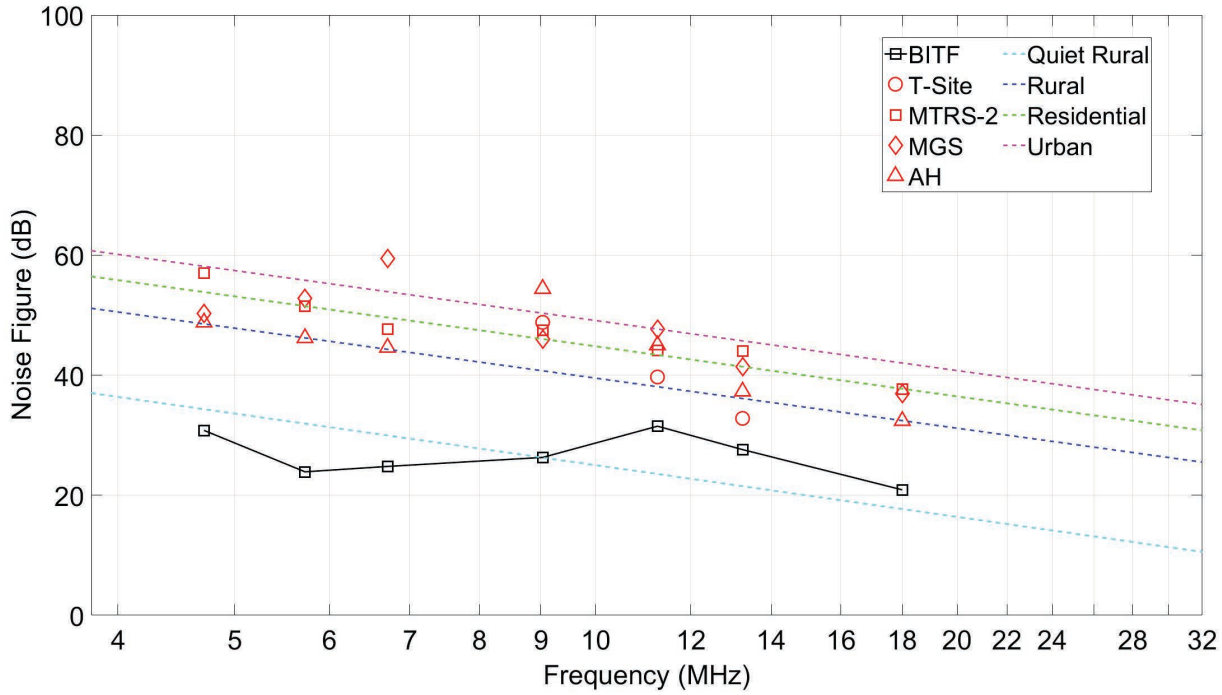

Figure 85. Median noise figures for all ATC channels and on-bluff sites.

Concurrence with previous study results in Section 4 is mixed. Figure 86 compares current results to those of the prior ITS study that used the same type of CM antennas at both locations. In general, the current results (black) corroborate the prior results (magenta). The prior results showed that T-Site (magenta circles) had considerably more noise than the BITF (magenta line). Like the prior T-Site result, the current T-Site PR result (black circles) shows the highest noise at 9 MHz. The 10 dB difference between the T-Site results is most likely caused by the limited number of PR radials, which lowers antenna gain.

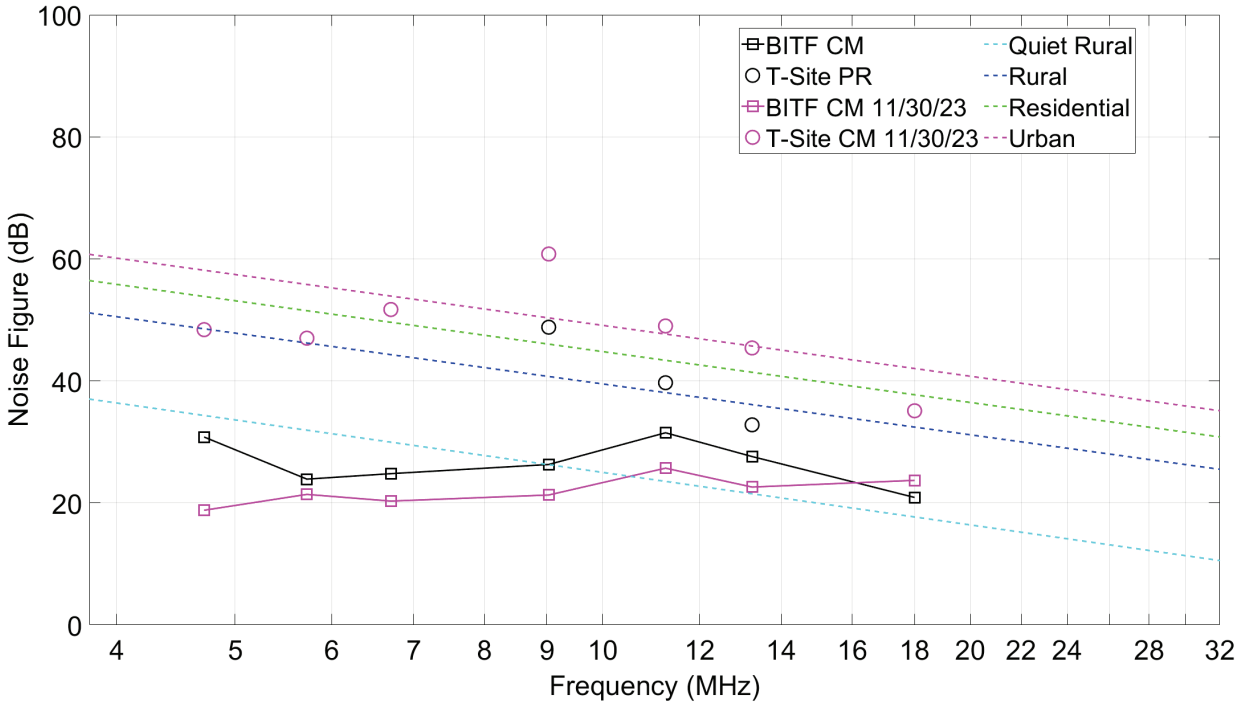

Figure 86. Comparison of current BITF and T-Site measurements to those of a prior study.

Neither of the SU or USN studies found Black Island to be as quiet as our measurements. Also, a large number of prior SU study frequencies around MS have noise figures considerably higher than urban in stark contrast to our ATC channel noise figures which typically ranged from rural to residential.

We found relatively little 9.032 MHz ATC channel noise power variation compared to that of the 10.0 MHz SFTS channel signal power at the MS locations. Since the MS locations are receiving quiet rural skywave noise power comparable to the BITF and because the MS location 9.032 MHz ATC channel noise power is much greater than quiet rural, we assume MS location noise is locally generated.

Curious PSD features such as periodic spectral spikes and bumps with and without spectral oscillations were identified at each location. It is not clear whether these are from the noise environment or introduced by the measurement system.

Measurement data volume was diminished by periods of ATC channel use and receiver overload. ATC channel use was infrequent and is presumed to have little impact on the median noise figure estimate. Overload is presumed to be caused by other signals (not ATC signals) and so is also presumed to have little impact.

Comparison of results obtained with the PR and CM antennas support the reliability of the PR antenna method. First, in-town HS PR measurement noise without the dominant noise source shows good agreement with the in-town MACOPS CM measurement. Second, the current T-Site PR measurement showed higher noise figures, like the prior ITS T-Site CM-5 antenna measurement. Third, maximum 10 MHz SFTR signal measured power was approximately 20 dB greater for the BITF CM than the MTRS-2 and MGS PR measurements, corresponding to the differences in antenna gain.

9. Conclusion

Table 13 provides a subjective assignment of the results into the various ITU noise environments taking into consideration the expected location variability. In-town and on-bluff results both show more noise than BITF. In-town results with rural to residential noise were quieter than on-bluff, with residential to urban. However, as the HS analysis points out, in-town locations are vulnerable to unregulated nearby broadband noise sources.

Table 13. Subjective noise environments.

Frequency (MHz)	BITF	In-Town	On-Bluff
4.718	Quiet Rural	Rural/Residential	Residential
5.726	Quiet Rural	Rural/Residential	Residential
6.708	Quiet Rural	Rural/Residential	Residential
9.032	Quiet Rural	Rural/Residential	Residential/Urban
11.256	Quiet Rural	Rural/Residential	Residential/Urban
13.251	Quiet Rural	Rural/Residential	Residential
18.000	Quiet Rural	Rural/Residential	Residential

Most on-bluff results indicate residential noise. Referring to Table 14, one could expect a 14 dB rise in the noise floor moving the HF receiver from the quiet rural BITF noise environment to the MS residential environment. Of the on-bluff results, the 9.032 MHz ATC channel with residential/urban noise corresponding to a 20–25 dB rise in the noise floor is the most concerning. Figure 39 shows the BITF 9 MHz ATC channel signal to noise ratio (SNR) ranges from 25 to 35 dB. A drop of 20–25 dB would undoubtedly affect ATC channel range and voice quality.

Table 14. Relative noise figure increases from quiet rural environment.

	Rural	Residential	Urban
Quiet rural	14	20	25

A large number of prior SU study frequencies have noise figures considerably higher than our estimates. These differences are too great to attribute to location variability. One explanation for today's lower noise is that there is less HF band use now and therefore less unintentional HF radio system emissions because scientific data is now being transmitted out of Antarctica over satellite radio links. Also, while MS historical photos in Appendix H show the number of buildings has increased, the power grid that serves the buildings has been improved. Automotive ignition systems have also become quieter.

With regard to measurement reliability, we spent considerable resources characterizing the noise measurement system at the TMRQZ to demonstrate that it is capable of measuring rural noise. During this characterization, we discovered the importance of placing the PR antenna on a quarter wavelength radial ground plane, adding a BPF to reject high atmospheric noise power, and using a CMNR filter to combat interference from the cable shield.

Our measurements were conducted with azimuthally omnidirectional antennas. HF noise propagating long distances via the ionosphere has been mitigated with directional antennas [14]. Conceivably, if omnidirectional coverage is not needed, with careful antenna design and placement, locally generated MMN can be mitigated in the same way. The challenge is then to prevent new MS MMN sources from interfering.

Inevitably problems occur during measurement campaigns. The measurement plan was written for two measurement systems so that a sufficient number of locations could be measured to estimate the MS median noise figure accurately. One of the systems was battery powered and capable of operation away from buildings which often contain MMN generating electrical devices. The shipment with the battery powered system did not arrive in McMurdo. Consequently, we were forced to measure fewer locations near buildings. Fewer locations undoubtedly impacted our estimate.

Recommendations for future work include

- On-ice measurements at more in-town, on-bluff, and remote MS locations
- Automated measurements throughout the year to determine ionospheric effects
- Analysis of radio noise instantaneous amplitude statistics
- On-ice investigations into causes of the odd spectral bumps and spikes in this measurement data set

This work focused primarily on the effect of radio noise on ATC communications. Antarctica is a vital hub for international scientific research. In many cases the reliability of the research results depends on knowing what signals and noise are present. Following through with these recommendations will bolster the reliability of research results.

10. References

[1] M.J. Sites and G.F. Stuart, "An Electromagnetic Survey of the Hut Point Peninsula and Adjacent Regions," Radioscience Laboratory, Stanford Electronics Laboratory, Stanford University, Stanford, California, Technical Report 3640-1, October 1971. (Prepared for The Office of Polar Programs, National Science Foundation under NSF Grant GA-19603.)

[2] International Telecommunication Union, Recommendation ITU-R P.372-16 (08/2022), *Radio Noise*, ITU, Geneva, Switzerland, https://www.itu.int/rec/R-REC-P.372/en.

[3] International Telecommunication Union, Recommendation ITU-R SM.1753-2 (09/2012), *Methods of Measurements of Radio Noise,* ITU, Geneva, Switzerland, https://www.itu.int/rec/R-REC-SM.1753/en.

[4] R.D. Hunsucker, H.F. Bates, "Survey of polar an auroral region effects on HF propagation," Radio Science, Vol. 4, No. 4, pp. 347–365, April 1969, https://doi.org/10.1029/RS004i004p00347.

[5] NOAA Space Weather Prediction Center, D-Region Absorption Prediction (D-RAP) Model, https://www.swpc.noaa.gov/communities/radio-communications

[6] International Telecommunication Union, Recommendation ITU-R TF.768-5 (2011-04), *Standard frequencies and time signals*, ITU, Geneva, Switzerland, https://www.itu.int/rec/R-REC-TF.768/en.

[7] E. W. Pappenfus, WB6LOH, "The Conical Monopole Antenna," *QST*, November 1966, 21–24. https://www.worldradiohistory.com/INTERNATIONAL/QST/QST-1966-11.pdf

[8] X.-L. Zhang, H.-T. Gao, and Q.-C. Zhang, "An optimum design of low-profile ultra-wideband HF skeletal wire duo-conical monopole antenna with parasitic grounded poles," *Proceedings of the 2016 IEEE APS Topical Conference on Antennas and Propagation in Wireless Communications*, September 19–23, 2016, Cairns, Queensland, Australia, pp. 264–267. https://doi.org/10.1109/APWC.2016.7738173.

[9] U.L. Rhode, "Active Antennas," *RF Design*, May/June 1981, pp. 38–42.

[10] "R&S®HE010E active rod antenna – Compact monitoring antenna for stationary and mobile applications," Rhode & Schwarz, accessed May 29, 2025, https://www.rohde-schwarz.com/us/products/aerospace-defense-security/omnidirectional-mobile-and-semi-mobile/rs-he010e-active-rod-antenna_63493-54030.html

[11] S.W. Maley, "Radial Wire Ground Systems for Vertical Monopole Antennas," In *Proceedings of Environmental Effects on Antenna Performance*, Volume I, James. R. Wait (Ed.), U.S. Department of Commerce, Environmental Science Services Administration, Institute for Telecommunication Sciences, Boulder, Colorado, July 14–18, 1969, pp 196–200. https://doi.org/10.70220/4v6x7d9c.

[12] J.R. Wait, "Characteristics of Antennas Over Lossy Earth," Chapter 23 in Antenna Theory Part 2, Inter-University Electronics Series, Vol. 7, R.E. Collin and F.J. Zucker eds., McGraw-Hill Book Company, 1969.

[13] Naval Command, Control and Ocean Surveillance Center (U.S.). In-Service Engineering, East Coast Division, *Electromagnetic Radiation Hazard (RADHAZ) Surveys, Electromagnetic Compatibility (EMC) Surveys, and Electromagnetic Interference (EMI) Investigations on the Antarctic Continent*, Naval Command, Control, and Ocean Surveillance Center In-Service Engineering, East Coast Division, 1997. (National Science Foundation Event T-408.)

[14] C.J. Coleman, "The Directional Aspect of Atmospheric Noise and its Impact Upon HF Communication Systems," in *Proc. of the Eighth International Conference on HF Radio Systems and Techniques*, July 10–13, 2000, Guildford, U.K., pp. 363–366, https://doi.org/10.1049/cp:20000203.

Appendix A. ITU Noise Figures

The man-made noise (MMN) power present at a location has wide ramifications for HF radio link engineering since the quality of radio reception is primarily determined by the ratio of signal power to noise power. It is impossible to engineer an HF radio link without some idea of the MMN power.

The MMN environment is characterized by the noise figure, F_a, at the output of a lossless short vertical monopole (SVM) antenna on an infinite and perfectly conducting ground plane. This is a convenient reference point as it is the same point used for characterizing basic transmission propagation loss and the noise power added by the receiving system.

F_a is a dimensionless quantity and generally reported in decibels. This way of characterizing MMN was originally developed by the predecessor to ITS, the Central Radio Propagation Laboratory (CRPL), [A-1] to characterize noise caused by atmospheric lightning, and later applied to MMN by the ITS [A-2]. Both efforts became the foundation for the current ITU radio noise models [A-3].

MMN F_a is a random variable that can change with time and/or location and is characterized by "statistics of statistics". The variability in time is addressed by making many F_a measurements within an hour at a location and reporting the ensemble's upper decile, median, and lower decile hourly statistics, referred to as hourly D_u, F_{am}, and D_l, respectively. Figure A-1 is an example of a distribution of F_a measured while driving through a residential area for an hour.

The location variability is addressed by estimating the median F_{am} of a set of hourly F_{am} from different locations—that is, the hourly F_{am} one can expect at 50 percent of locations. This statistic is referred to as F_{am} without the hourly qualifier. Figure A-2 is an example of a distribution of hourly F_{am}measured at 25 residential locations.

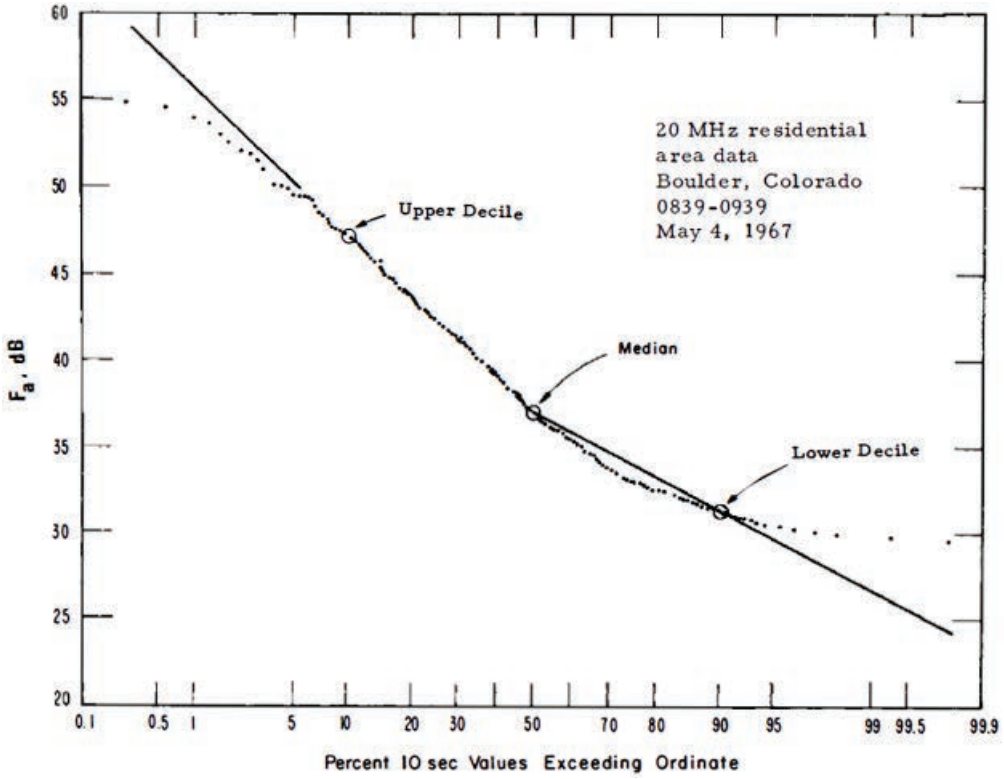

Figure A-1. Distribution of F_a for a give location. (Credit: Figure 3 in [A-2])

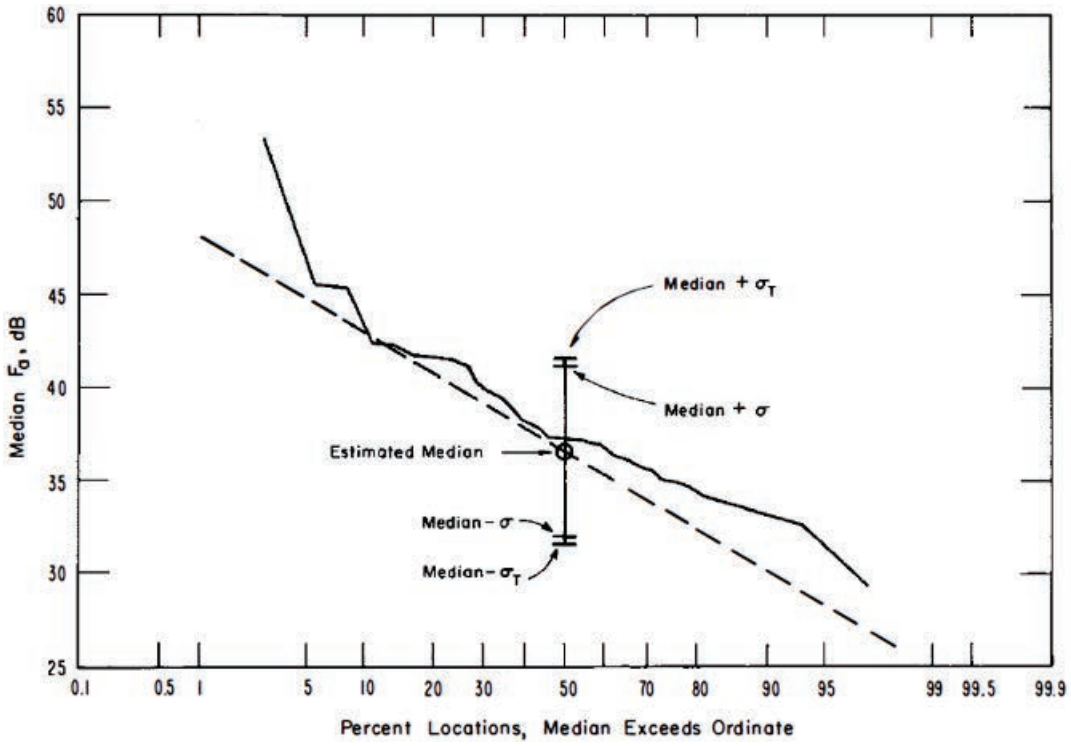

Figure A-2. Distribution of location median F_a. (Credit: Figure 2 in [A-2])

The following equation shows how this F_{am} might be used to compute the received signal to noise ratio (SNR) for an HF radio link where F_{am} is much greater than the equipment or internal noise figure

$$snr = \frac{p_r}{kT_0 b f_{am}} \tag{A-1}$$

where p_r is the signal power received, k is Boltzman's constant, b is signal bandwidth, and all parameters are in linear units. It is important to note that, unlike receiver noise, MMN is often non-Gaussian so the required SNR can differ from that predicted with Gaussian noise.

A.1 References

[A-1] W. Q. Crichlow, D. F. Smith, R. N. Morton, and W. R. Corliss, "Worldwide Radio Noise Levels Expected in the Frequency Band 10 Kilocycles to 100 Megacycles," NBS Circular 557, U.S. Department of Commerce, National Bureau of Standards, August 25, 1955. https://doi.org/10.6028/NBS.CIRC.557

[A-2] A. D. Spaulding, R.T. Disney, "Man-Made Radio Noise – Part I: Estimates for Business, Residential, and Rural Areas," Technical Report OT Report 74-38, U.S. Department of Commerce, Office of Telecommunications, Institute for Telecommunication Sciences, June 1974, https://doi.org/10.70220/p8n359tw.

[A-3] International Telecommunication Union, Recommendation ITU-R P.372-16 (08/2022), *Radio Noise*, ITU, Geneva, Switzerland, https://www.itu.int/rec/R-REC-P.372/en.

Appendix B. Data Processing Algorithms

The measurement system noise factor model, shown in Figure B-1, is composed of external and internal noise components

$$f = f_{ext} + f_{int} - 1 \tag{B-1}$$

where f_{ext} is the external and f_{int} is the internal noise factor. External noise sources include atmospherics, Milky Way galaxy, and electrical devices. The internal noise sources include receiving system active electronic circuits and passive circuit thermal motion.

The internal noise factor is determined by the cascade formula

$$f_{int} = f_c + l_c(f_t - 1) + l_c l_t(f_r - 1) \tag{B-2}$$

where f_c is the antenna (impedance matching) circuit noise factor, l_c is the antenna circuit loss, f_t is the transmission line noise factor, l_t is the transmission line loss, and f_r is the receiver noise factor. This formula is "worst case" in that we assume all components are at room temperature or 290K. Accounting for the effects of cold temperatures on the antenna, matching circuit, and outdoor transmission lines is not deemed necessary for accuracies needed by this study.

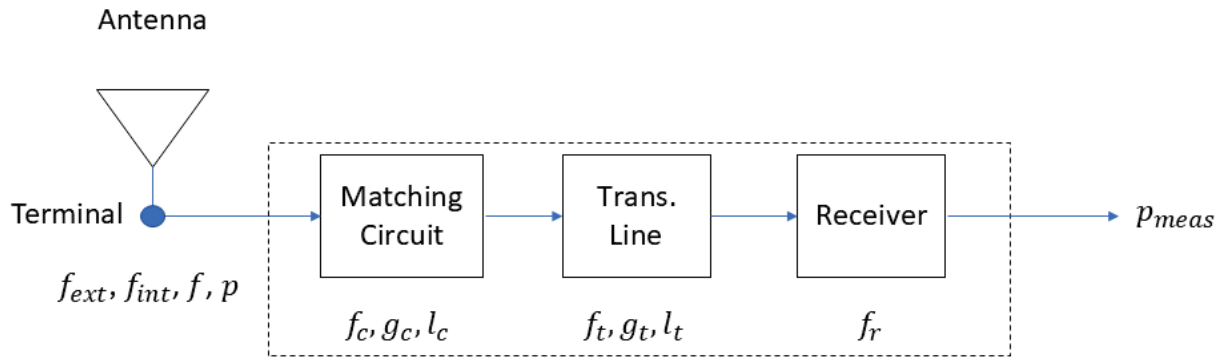

Figure B-1. Measurement system noise factor model. Cascaded components in dotted rectangle generate the internal noise created by the measurement system.

Having determined f_{int} we now turn our attention to calculating f_a from the power measured at the receiver. Multiplying all terms in (B-1) by kT_0b where k is Boltzman's constant in J/K, T_0 is 290K, and b is the noise equivalent bandwidth in Hz

$$kT_0fb = kT_0f_{ext}b + kT_0(f_{int} - 1) \tag{B-3}$$

and realizing that the left side is the power measured by the receiver and referred to the antenna terminals we have

$$P_{meas}l_t l_c = P_{ext} + P_{int} \tag{B-4}$$

or

$$P_{ext} = P_{meas} l_t l_c - P_{int}. \tag{B-5}$$

To estimate the E-field intensity, we recognize that external noise power is also

$$P_{ext} = S A_e l_c \tag{B-6}$$

where S is the external noise power density in Watts/ m^2 and A_e is the effective antenna aperture, including impedance matching losses, in m^2.

The power density is related to the electric field intensity by

$$S = \frac{|E|^2}{Z_0} \tag{B-7}$$

where E is the electric field intensity in RMS V/m and Z_0 is the 120π ohm intrinsic impedance of free space.

The effective aperture is related to the aperture of an ideal isotropic antenna by

$$A_e = g_p A_{iso} \tag{B-8}$$

where g_p is the practical gain,

$$A_{iso} = \frac{\lambda^2}{4\pi} = \frac{c^2}{4\pi f^2} \tag{B-9}$$

λ is the wavelength in m, c is the speed of light in m/sec, and f is the frequency in Hz.

Substitution of these expressions yields

$$P_{ext} = \frac{|E|^2}{Z_0} \frac{g_p c^2}{4\pi f^2} l_c \tag{B-10}$$

and rearranging to solve for the electric field gives

$$|E|^2 = \frac{P_{ext} f^2}{g_p l_c} \cdot \frac{4\pi Z_0}{c^2}. \tag{B-11}$$

In decibels

$$E\left(\frac{dBV}{m}\right) = P_{ext}(dBW) + 20\log_{10}\big(f(Hz)\big) - G_p(dBi) - L_c(dB) - 132.78 \tag{B-12}$$

Finally converting to decibels units of uV/m, mw, and MHz we add 60, 30, and 120 dB, respectively and have

$$E\left(\frac{dB\mu V}{m}\right) = P_{ext}(dBm) + 20\log_{10}\big(f(MHz)\big) - G_p(dBi) - L_c(dB) + 77.2 \tag{B-13}$$

If the antenna factor, k_a, is provided we can calculate g_p by

$$g_p = \frac{4\pi Z_0}{R_l c^2}\frac{f^2}{k_a^2} \tag{B-14}$$

or

$$G_p = 20\log_{10}\big(f(MHz)\big) - 20\log_{10}(k_a) - 29.8 \tag{B-15}$$

where R_l is the nominal 50 ohm receiver load resistance.

To convert to noise figure we substitute

$$P_{ext}(dBm) = F_{ext}(dB) + B(dBHz) + kT_0(^{dBm}/_{Hz}) \tag{B-16}$$

where kT_0 = -174 dBm/Hz so that for any antenna

$$E\left(\frac{dB\mu V}{m}\right) = F_{ext}(dB) + 20\log_{10}\big(f(MHz)\big) + B(dBHz) - G_p(dBi) - L_c(dB) - 96.8 \tag{B-17}$$

and

$$F_{ext}(dB) = E\left(\frac{dB\mu V}{m}\right) - 20\log_{10}\big(f(MHz)\big) - B(dBHz) + G_p(dBi) + L_c(dB) + 96.8. \tag{B-18}$$

To convert to F_a we substitute antenna directivity by

$$D(dBi) = G_p(dBi) + L_c(dB) \tag{B-19}$$

which for a lossless, short vertical monopole (SVM) on a ground plane receiving a surface wave is 3/4 or −1.25 dBi [B-1] so that

$$F_a(dB) = E\left(\frac{dB\mu V}{m}\right) - 20\log_{10}\big(f(MHz)\big) - B(dBHz) + 95.5. \tag{B-20}$$

This report uses F_a to report results. To convert F_a to E add the number in Figure B-2 and B in dBHz.

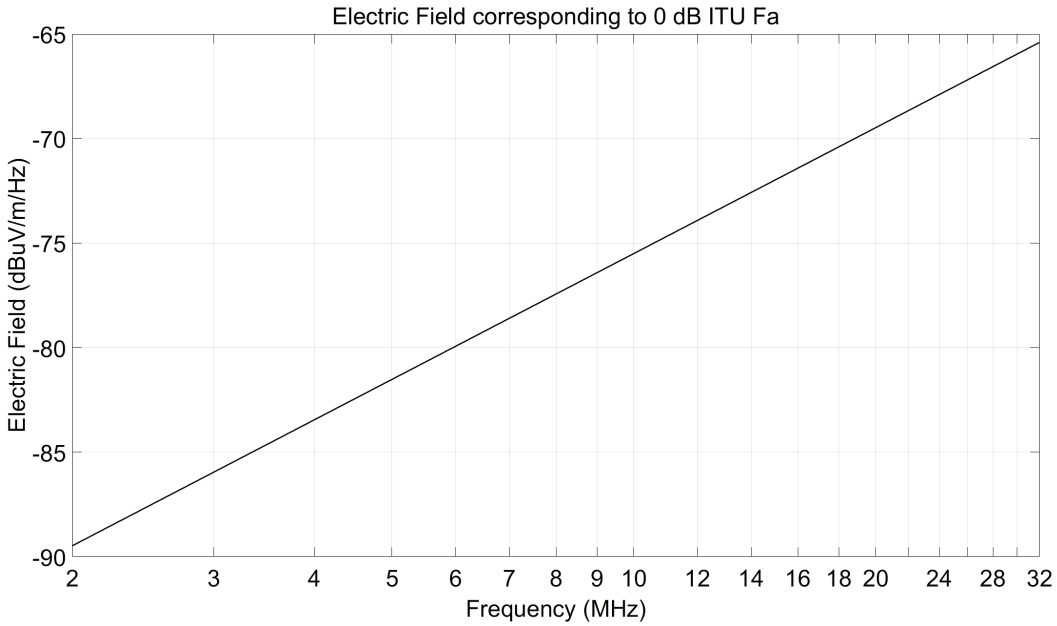

Figure B-2. Electric field in dBuV/m/Hz corresponding to 0 dB ITU F_a.

B.1 References

[B-1] John W. Ames, Willam A. Edson, "Gain, Capture Area, and Transmission Loss for Grounded Monopoles and Elevated Dipoles," RF Design, Part 1 Nov/Dec 1983 pp. 44-56, Part 2, pp. 12-23 Jan/Feb Year 1984.

Appendix C. Specifications

Table C-1. Receiver specifications.

Parameter	Value	Note
Manufacturer	CRFS	
Model	RFeye 50-8	
Frequency Range	9 kHz to 50 MHz	Baseband mode
VSWR	2.0	
IP3	5 dBm typical, 0 dB attenuation 10 dBm typical, 10 dB attenuation N.A. typical, 20 dB attenuation	LNA on
Noise Figure	9 dB typical, 0 dB attenuation 9.5 dB typical, 10 dB attenuation 16 dB typical, 20 dB attenuation	LNA on

Table C-2. Common mode noise filter.

Parameter	Value	Note
Manufacturer	Palomar Engineering	
Model	CMNF-500-50N	
Frequency Range	1–60 MHz	
Input Impedance	50 ohms	
Common Mode Rejection	21-38 dB	Over frequency range
Insertion Loss	0.01–0.04 dB	Over frequency range

Table C-3. HF bandpass filter.

Parameter	Value	Note
Manufacturer	K&L Microwave	
Model	8LB30-17.9/U28.2-O/O	
Center Frequency	17.9 MHz	
1.0 dB Bandwidth	28.2 MHz	
Input Impedance	50 ohms	
Insertion Loss	0.6 dB	
Return Loss	9.5 dB	2.0 VSWR
Passband Range	3.8 – 32.0 MHz	
Stopband Attenuation	38 dBc at 2.9 MHz 33 dBc at 52 MHz	

Table C-4. PR antenna DC bias unit specifications.

Parameter	Value	Note
Manufacturer	Rhode and Schwarz	
Model	IN600.11	
Frequency Range	1 to 30 MHz	
VSWR	<2.5, 1.5 typical	
Interference level	-130 dBm	

Table C-5. PR cable.

Parameter	Value	Note
Manufacturer	Talent Microwave	
Model	A40-NM-NM-1	
Frequency Range	DC-110 GHz	
Length	30.48 m (100 ft)	
Input Impedance	50 ohms	
VSWR	<1.25	
Attenuation	1.0 dB	RG-8 or RG-213 1 dB/100 ft at 30 MHz
Cable Diameter	3.6 mm	
Armor Diameter	9.0 mm	
Shielding Effectiveness	90 dB	

Table C-6. PR antenna specifications.

Parameter	Value	Note
Manufacturer	Rhode and Schwarz	
Model	HE010E	
Frequency range	0.083 to 100 MHz	
Input impedance	50 ohms	
VSWR	< 2	
IP3	> 30 dBm, 33 typical > 20 dBm	0.083 to 30 MHz 30 to 100 MHz
Noise Figure	47 dB at 3 MHz 27 dB at 30 MHz	
Height	1 m	
Ground Plane	Yes	20, 15.2 m (50 ft) radials

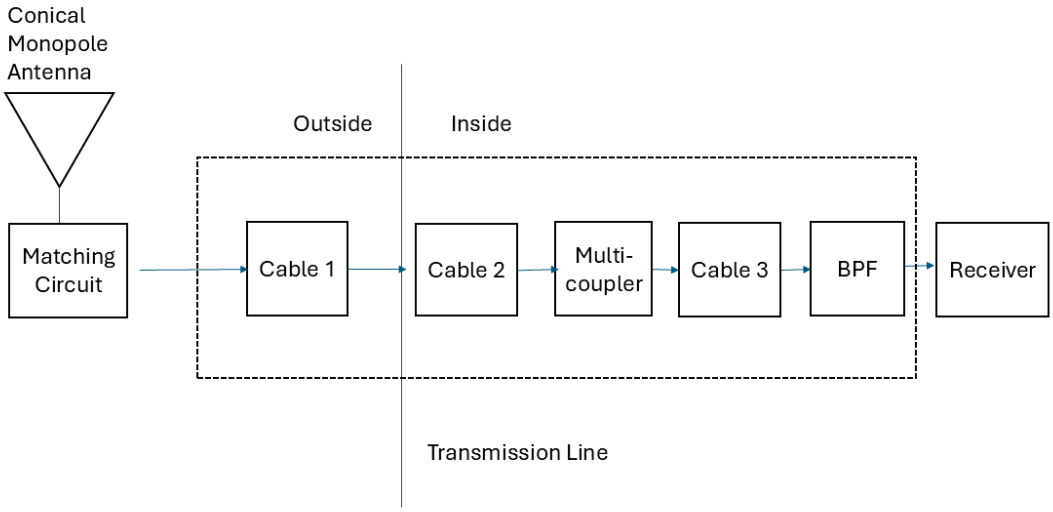

Figure C-1. Black Island system block diagram.

Table C-7. BITF CM antenna specifications.

Parameter	Value	Note
Manufacturer	TCI	
Model	550-04-02	
Frequency Range	3.8 to 32 MHz	
VSWR	< 2	
Height	62 ft or 18.9 m	
Diameter	127 ft or 38.7 m	Guy to guy
Ground plane	Yes	64, 19.7 m (64.6 ft) radials

Table C-8. BITF CM antenna gain at ground level with perfect ground plane.

Frequency (MHz)	3.8	7.6	13.3	17.1	26.6	38
Gain (dBi)	5	5	2.5	7.5	5	5

Table C-9. BITF multicoupler specifications.

Parameter	Value	Note
Manufacturer	Stridsberg	
Model	MCA108M	8 output ports
Frequency range	0.5 to 50 MHz	
VSWR	< 1.2	
IP3	> 32 dBm	
Gain	-1 to 2 dB	0.5 to 50 MHz
Noise Figure	3.0 dB	

Table C-10. BITF cable specifications.

Cable	Length	Loss	Note
1	167.6 m (550 ft)	1.2 dB	Heliax LDF5-50A 0.2 dB / 100 ft at 30 MHz
2	9.4 m (31 ft)	0.3 dB	RG-8 or RG-213 1 dB/100 ft at 30 MHz
3	3.1 m (10 ft)	0.1 dB	RG-8 or RG-213 1 dB/100 ft at 30 MHz

Table C-11. MACOPS CM antenna specifications.

Parameter	Value	Note
Manufacturer	TCI	
Model	506-06	
Frequency Range	5 to 30 MHz	
VSWR	< 2	
Height	32 ft or 9.8 m	
Diameter	66 ft or 20.1 m	Guy to guy
Ground plane	Yes	64, 15.2 m (50.0 ft) radials

Table C-12. MACOPS CM antenna gain at ground level with perfect ground plane.

Frequency (MHz)	5.0	7.5	15.0	17.5	20.0	25.0	35
Gain (dBi)	5	5	6.0	4.5	-7.0	5.0	7.0

Table C-13. MACOPS cable specifications.

Cable	Length	Loss	Note
1	45.7 m (150 ft)	0.3 dB	Heliax LDF5-50A 0.2 dB / 100 ft at 30 MHz

Appendix D. Radio Noise Measurement System Characteristics

Parameters used to calculate internal noise factor are provided in Figures D-1–D-5. The study described in this report used an active portable rod with an active transistorized impedance matching circuit. Parameters for a passive portable rod antenna operating over the same bandwidth with a non-transistorized passive impedance matching circuit composed of resistors, capacitors, and inductors are included for comparison purposes.

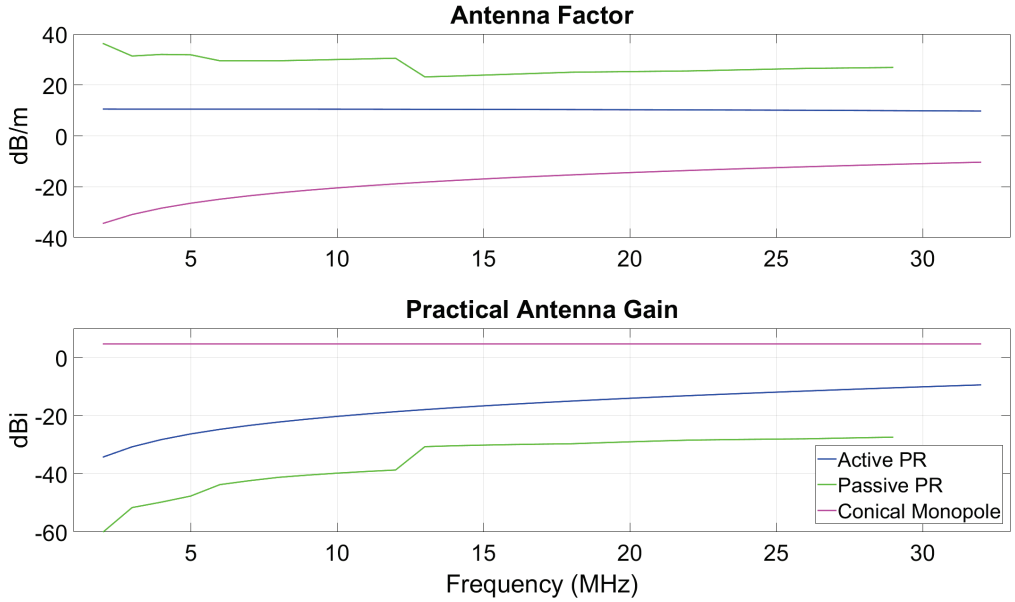

Figure D-1. Antenna factors and practical gains.

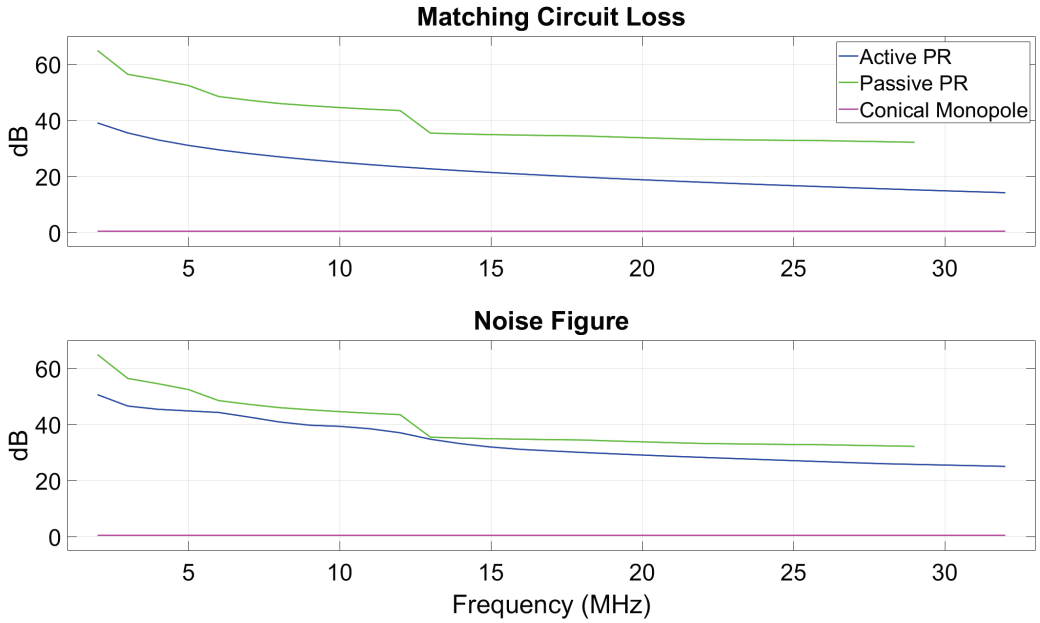

Figure D-2. Antenna matching circuit loss and noise figure.

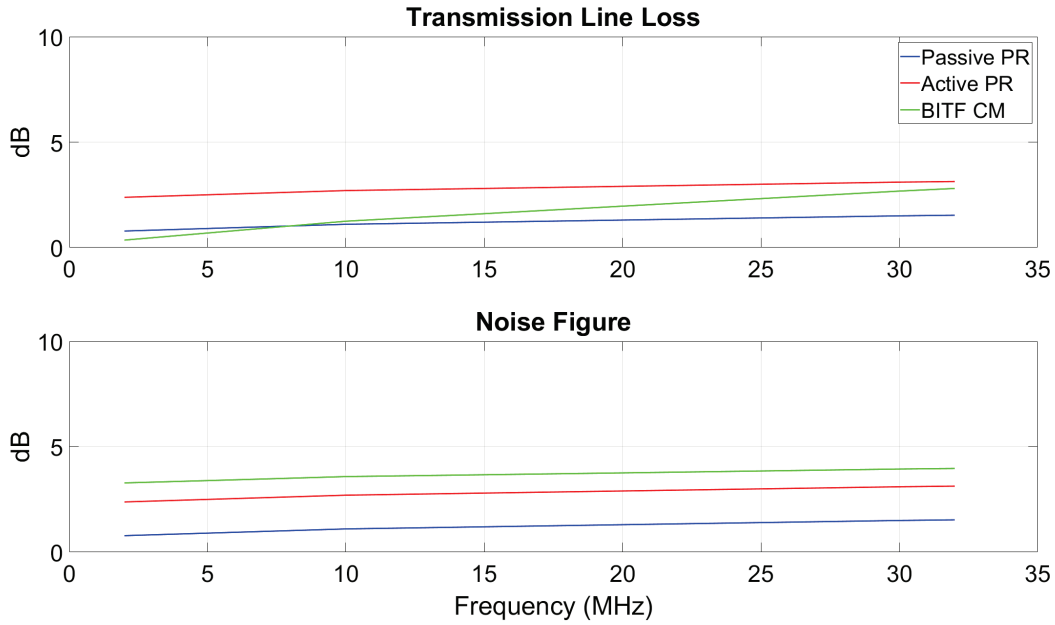

Figure D-3. Transmission line loss and noise figure.

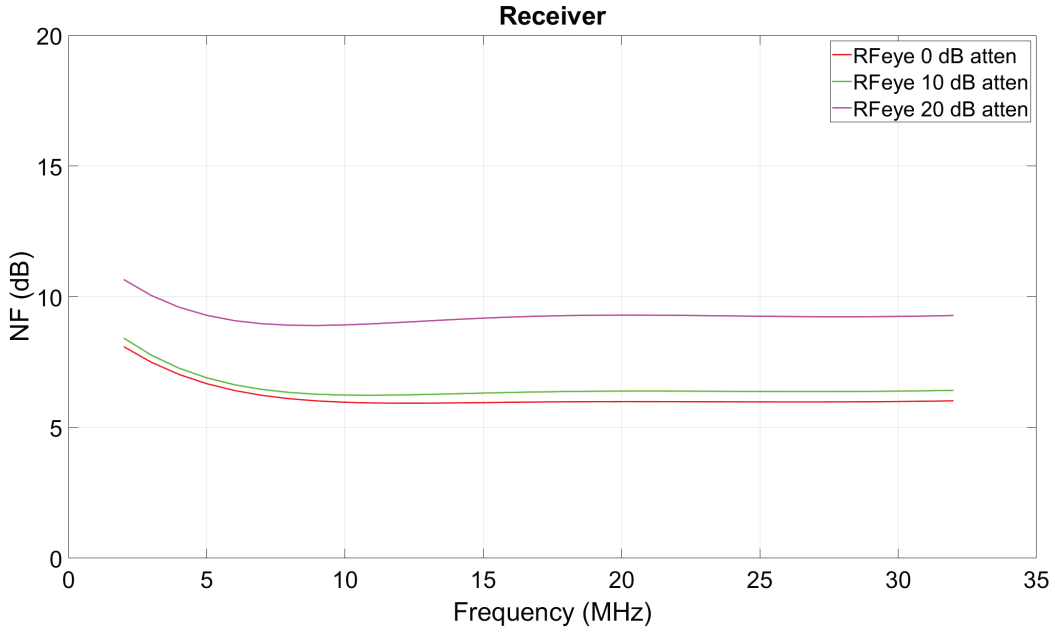

Figure D-4. Receiver noise figure for 3 different internal attenuator settings.

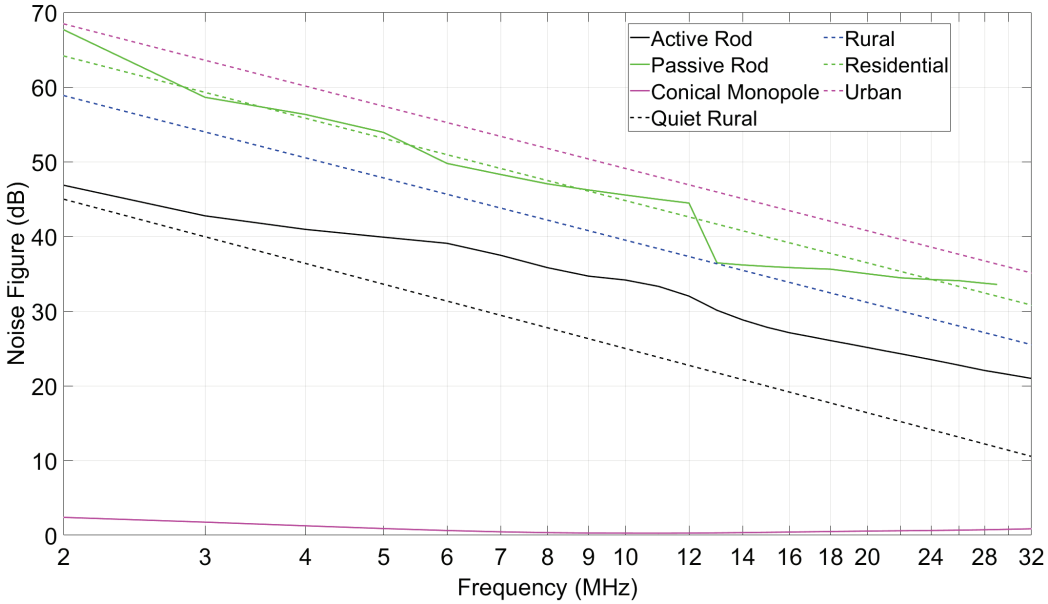

Figure D-5. Minimum measurable ITU noise figure assuming internal noise is external noise received by a lossless short vertical monopole antenna. RFeye, the receiver used in this study, attenuation is 0 dB.

Appendix E. Previous Stanford University Study Supplemental Information

Figure E-1 shows a map with the Stanford University (SU) measurement locations near MS. Figure E-1 provides a description of the locations.

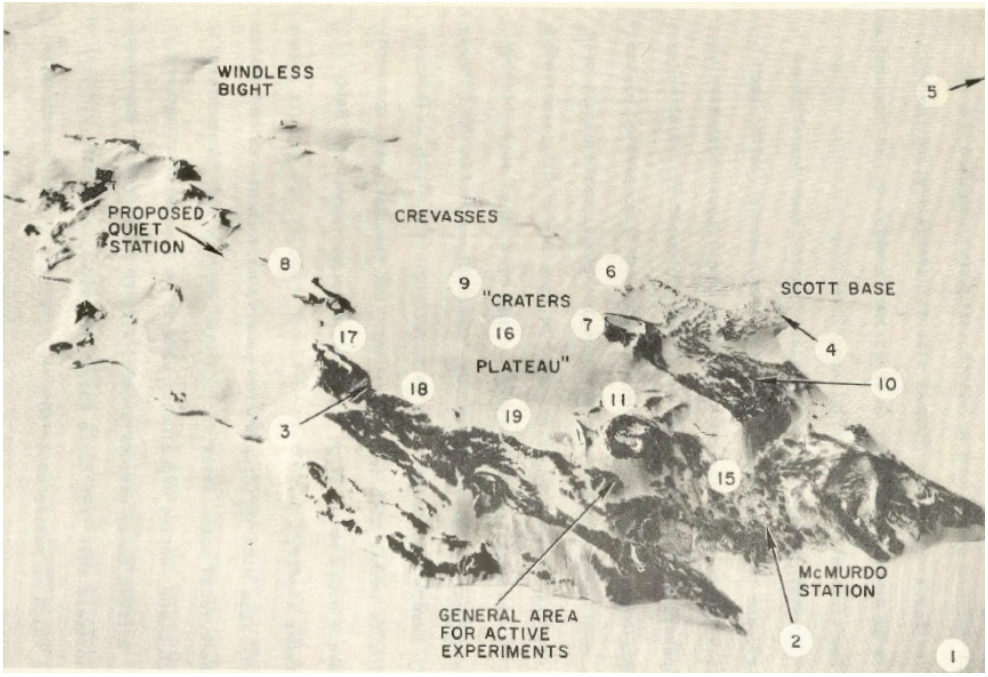

Figure E-1. Measurement locations for prior SU study. Map location indexes are identified in Table E-1. From Figure 13 "Aerial View of the Hut Point Peninsula Showing the Location of the Proposed Quiet Station" in [E-1]

Table E-1. Measurement location description.

Index	Location Description
1	On ice shelf about ½ mile from McMurdo
2	McMurdo Geodetic Satellite Hut
3	Wannagan, Second Crater
4	Scott Base Laboratory
5	Road to Williams Field
6	Scott Base Whistler Antenna
7	Crater Hill
8	Near Half Moon Crater
9	Midway Crater Hill – Half Moon Crater
10	Cosmic Ray Building
11	Riometer Building
12	Vanda Station (off map)
13	Marble Point (off map)

Index	Location Description
14	Black Island (off map)
15	Navy Antenna Field
16	Midway Crater Hill – Second Crater
17	Northeast Second Crater
18	Wannagan, Second Crater
19	Auroral Hut, Arrival Heights

Receiver dynamic range was reported to be -20 to 70 dBuV. The minimum detectable field strength in the measurement bandwidth is determined by adding the frequency dependent antenna factors in Table E-2 to the minimum detected voltage

$$E_{min}\left(dBuV/_{m}\right) = -20\ dBuV + AF(^{dB}/_{m}) \quad \text{(E-1)}$$

Table E-2. SU rod antenna factors, AF, in dB/m.

MHz	dB/m	MHz	dB/m	MHz	dB/m	MHz	dB/m
2	35	12	26	22	21	32	23
3	30	13	26	23	21.2		
4	30.5	14	26.3	24	21.4		
5	27	15	26.8	25	21.6		
6	27.5	16	27	26	21.8		
7	28	17	20.8	27	22		
8	28.5	18	21	28	22.5		
9	25	19	21	29	23		
10	25.25	20	21	30	23		
11	25.5	21	21	31	23		

Table E-3 contains original measurement results reported in field strength corresponding to the noise figures plotted in Figure 25. Measurements below minimum (BM) were plotted with minimum. Measurements with continuous tones (SW) were not plotted.

Table E-3. Electric field strength data in 5 kHz bandwidth in dBuV/m. BM represents below minimum, SW continuous tone, and NA not available.

Map Index	Frequency (MHz)									
	3.75	5.0	7.85	8.06	11.0	12.2	13.2	14.65	16.2	29.4
2	34	26	54	89	31	86	16	97	21	36
7	BM	BM	35	75	SW	90	10	96	86	38
10	23	18	59	103	102	18	18	88	75	21
11	NA	9	45	96	81	86	21	10	102	5
14	BM	BM	BM	39	37	27	BM	34	32	BM
15	BM	BM	52	93	81	88	BM	97	BM	31
19	BM	BM	SW	79	78	69	BM	91	SW	38

E.1 References

[E-1] M.J. Sites and G.F. Stuart, Table 3b "Observed levels at selected frequencies above 1 uV/meter (Corrected for Antenna Calibration Factor)", in "An Electromagnetic Survey of the Hut Point Peninsula and Adjacent Regions," Radioscience Laboratory, Stanford Electronics Laboratory, Stanford University, Stanford, California, Technical Report 3640-1, October 1971. (Prepared for The Office of Polar Programs, National Science Foundation under NSF Grant GA-19603.)

Appendix F. Previous ITS Study Supplemental Information

F.1 CM-5 Transmission Line Loss

T-Site CM-5 transmission line loss was measured by NIWIC. T-Site CM-5 antenna transmission line specifications and measured loss are provided in Table F-1 and Figure F-1, respectively. BITF CM transmission line loss was obtained from specifications.

Table F-1. T-Site CM-5 antenna transmission line specifications.

Cable	Length	Loss	Note
1	170.7 m (560 ft)	1.1 dB	Heliax LDF5-50A 0.2 dB / 100 ft at 30 MHz
2	4.3 m (14 ft)	0.1 dB	RG-8 or RG-213 1 dB/100 ft at 30 MHz

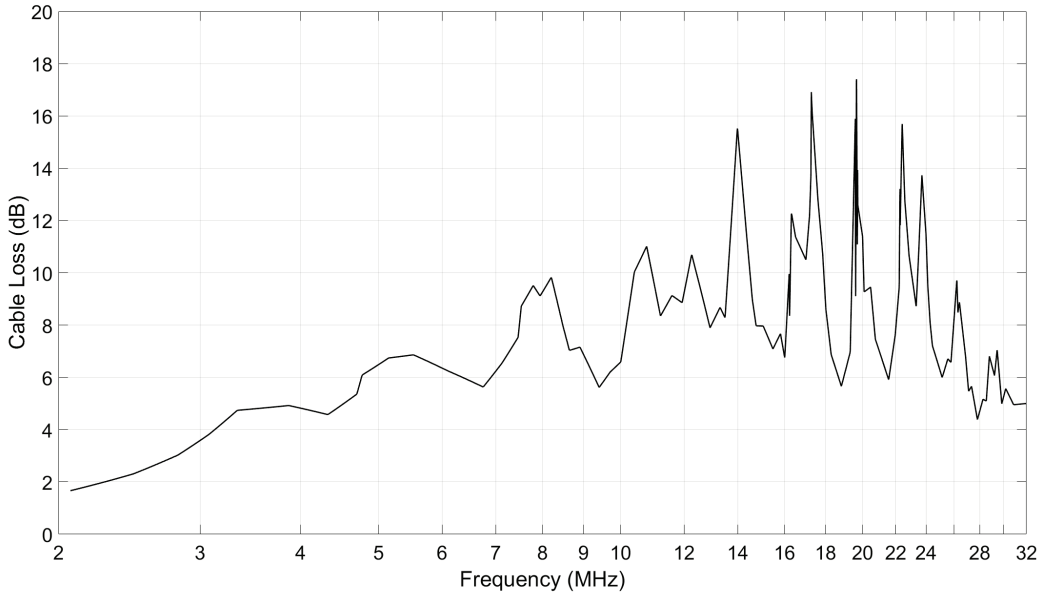

Figure F-1. Measured T-Site CM-5 antenna transmission line loss. (Credit Mike Goad).

F.2 Comparison of ATC channel power for BITF and T-Site CM antennas

Figures F-2–F-15 show ATC channel measured power times series with the same model of CM antenna at BITF and T-Site over a 24-hour period from 07:00. Solar noon is approximately 13:41. Time series for both locations at the same frequency are placed on the same page for direct comparison. Results are displayed as measured power at the receiver input.

The time series have gaps caused by overload. Overload can be caused by any signal in the receiver bandwidth. Out of 720 measurements collected at each location, BITF and T-Site measurements overloaded 130 and 627 times, respectively. The overload is evident from

hours 11:00 to 15:00 in the BITF results and 11:00 to17:00 in the T-Site results. The high T.Site 11.256 MHz ATC channel power is likely caused by a T-Site HF transmitter malfunction.

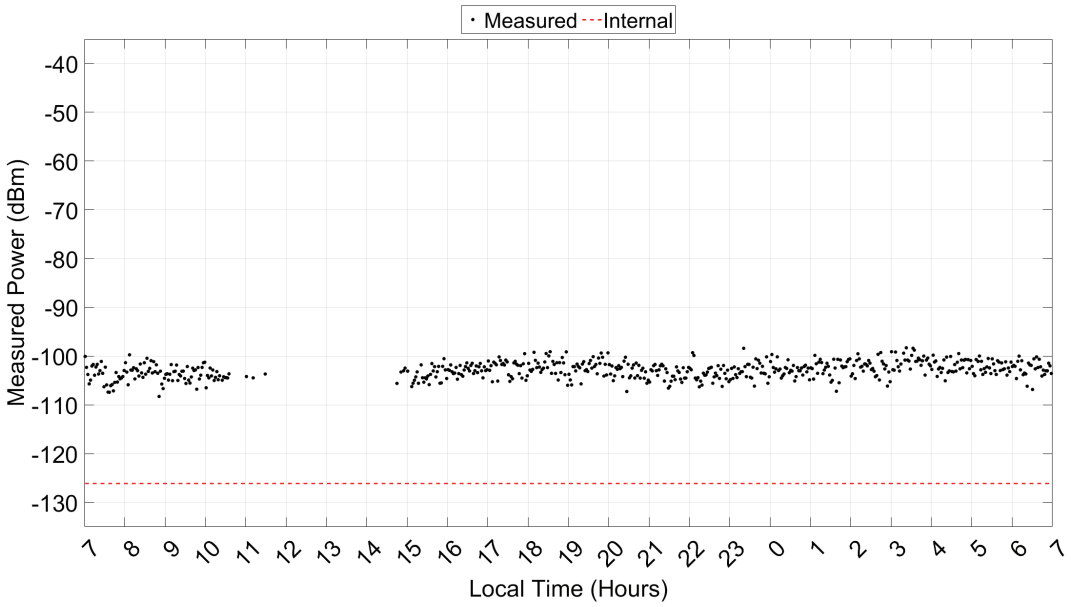

Figure F-2. BITF CM 4.718 MHz.

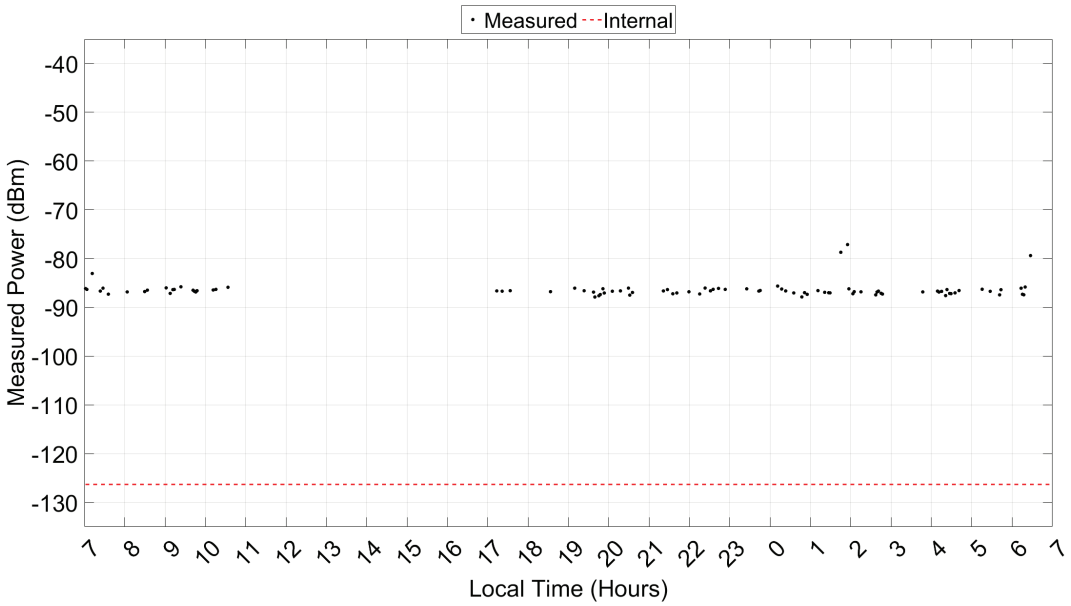

Figure F-3. T-Site CM5 4.718 MHz.

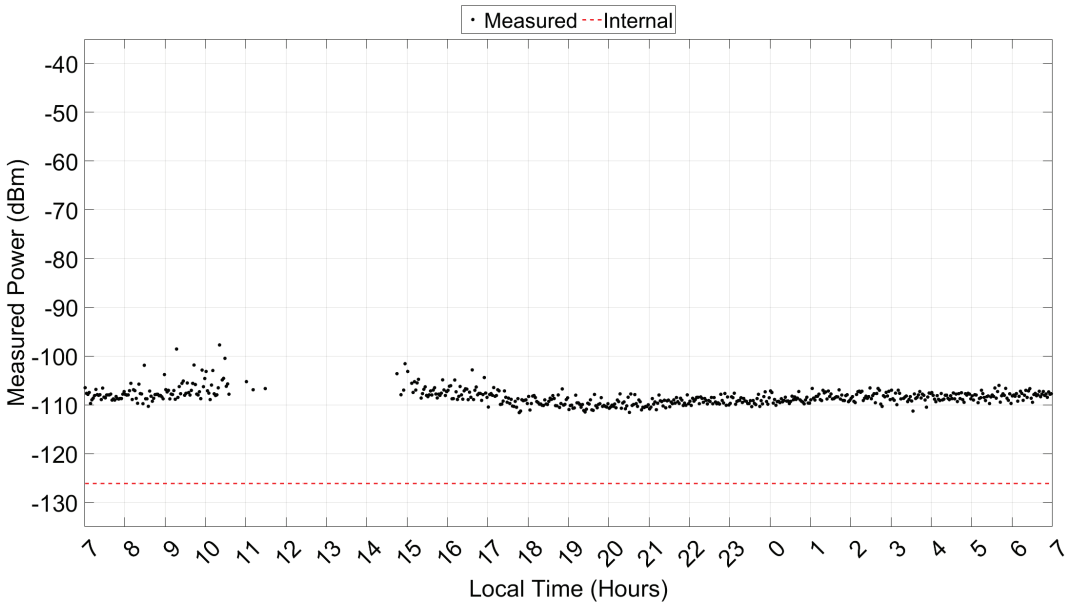

Figure F-4. BITF CM 5.726 MHz.

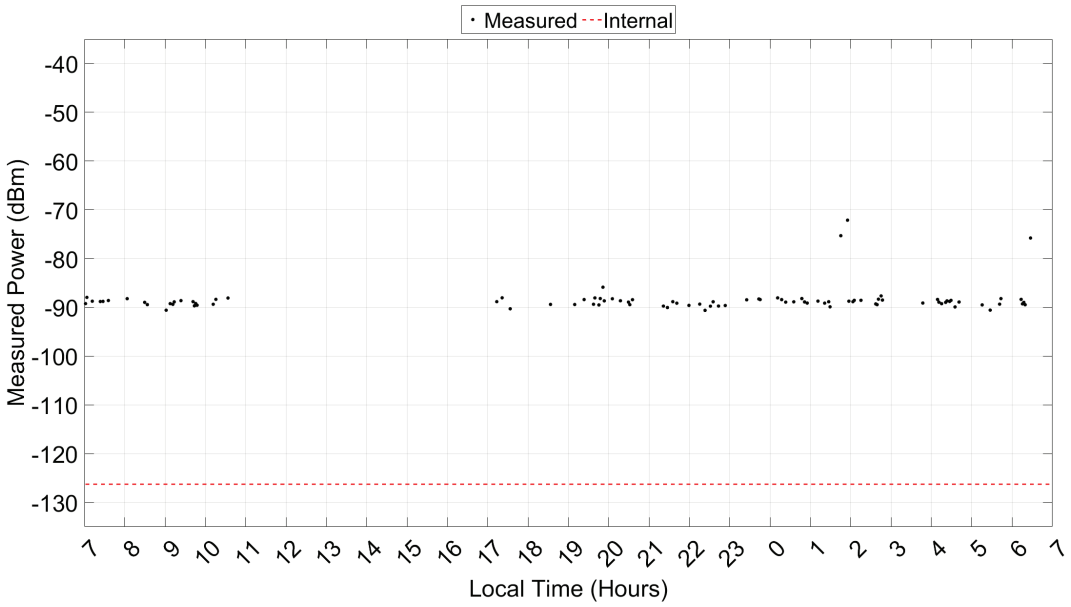

Figure F-5. T-Site CM5 5.726 MHz.

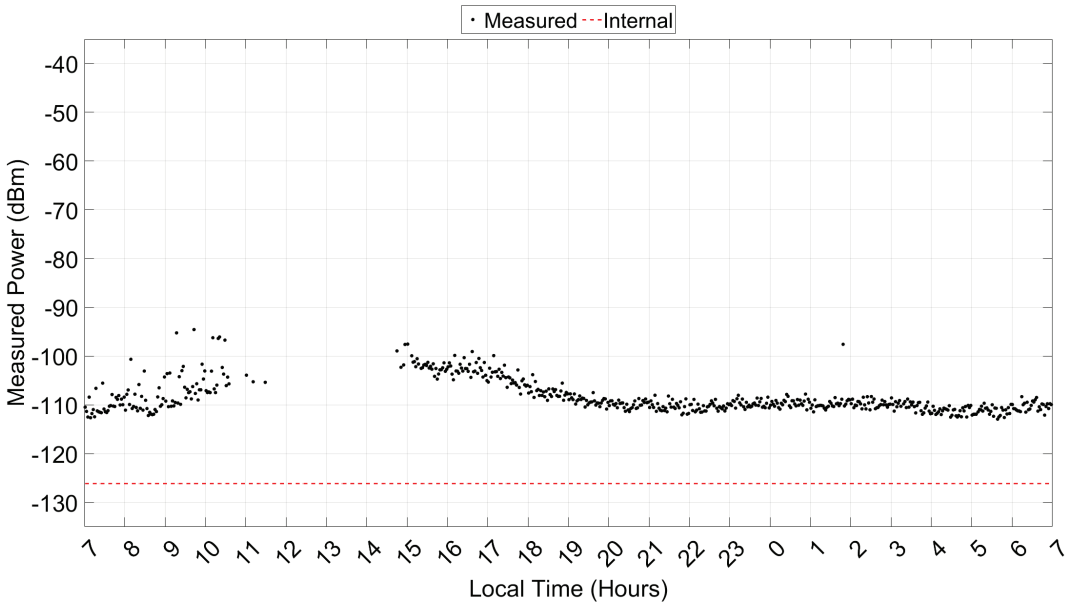

Figure F-6. BITF CM 6.708 MHz.

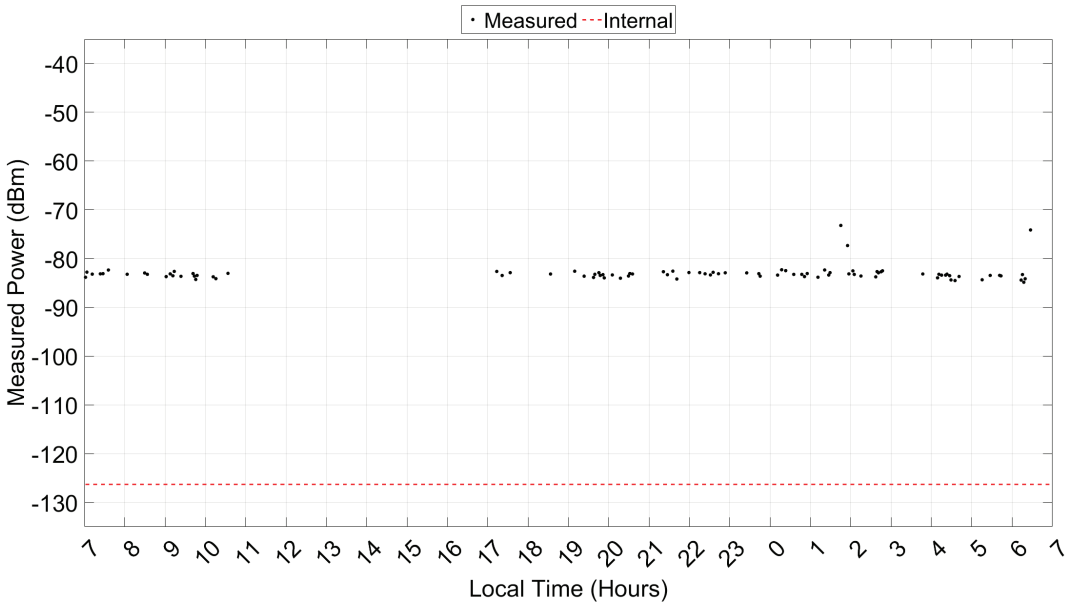

Figure F-7. T-Site CM5 6.708 MHz.

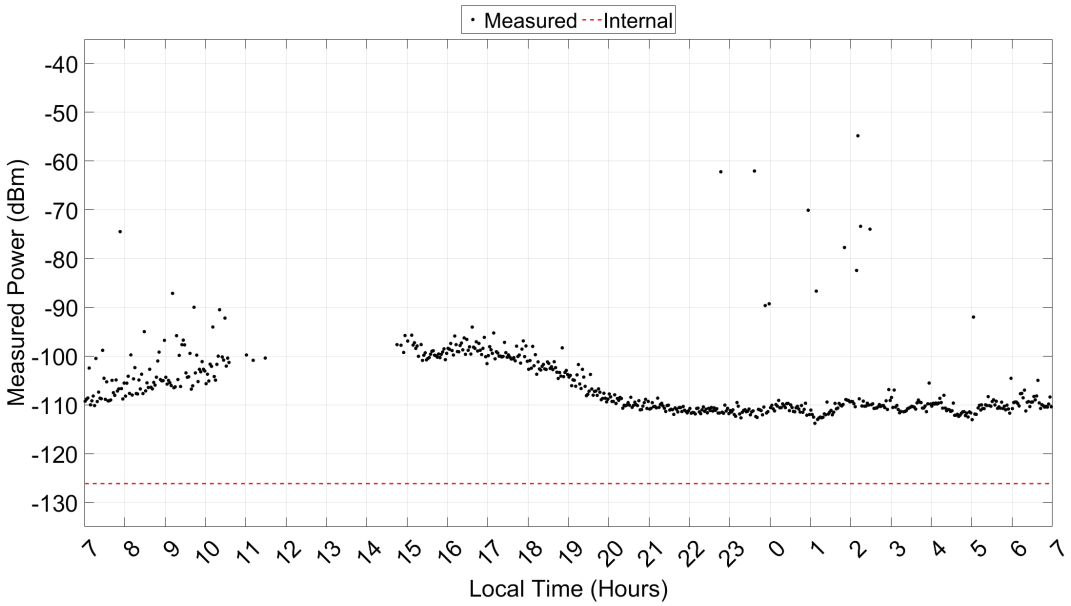

Figure F-8. BITF CM 9.032 MHz.

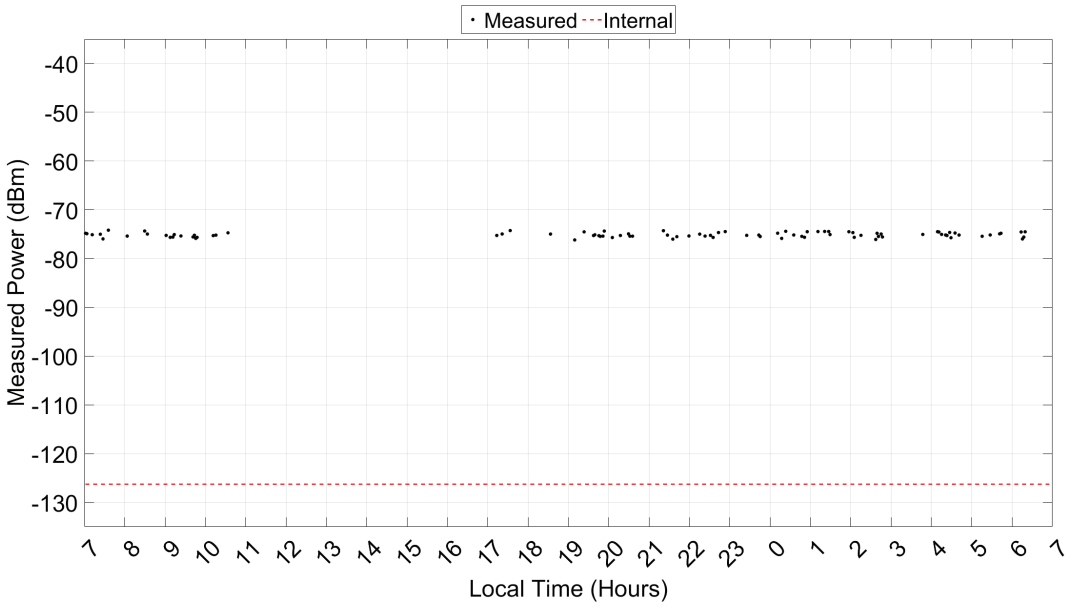

Figure F-9. T-Site CM5 9.032 MHz.

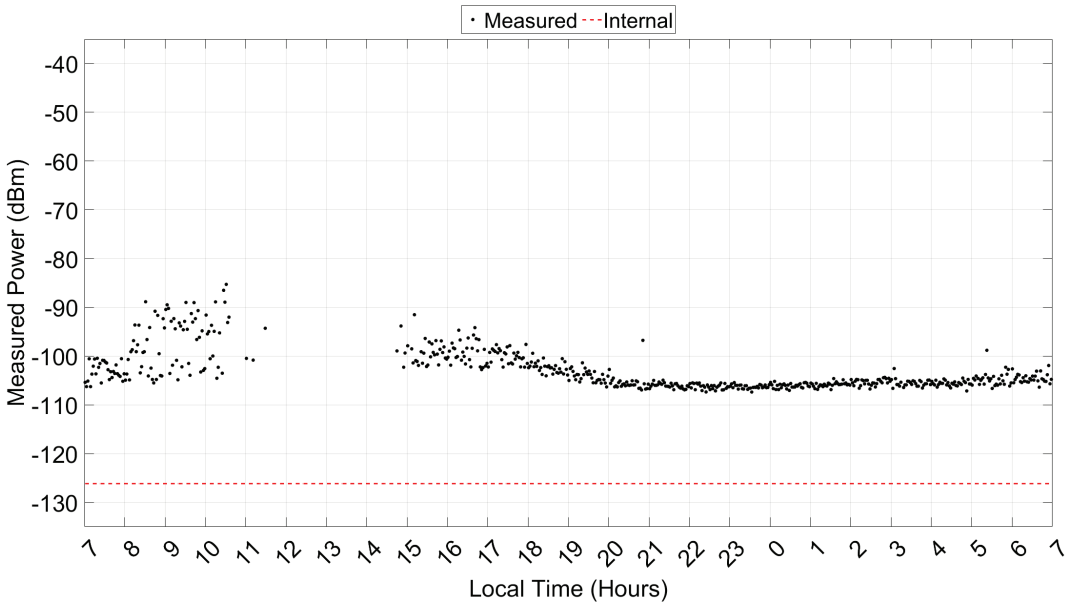

Figure F-10. BITF CM 11.256 MHz.

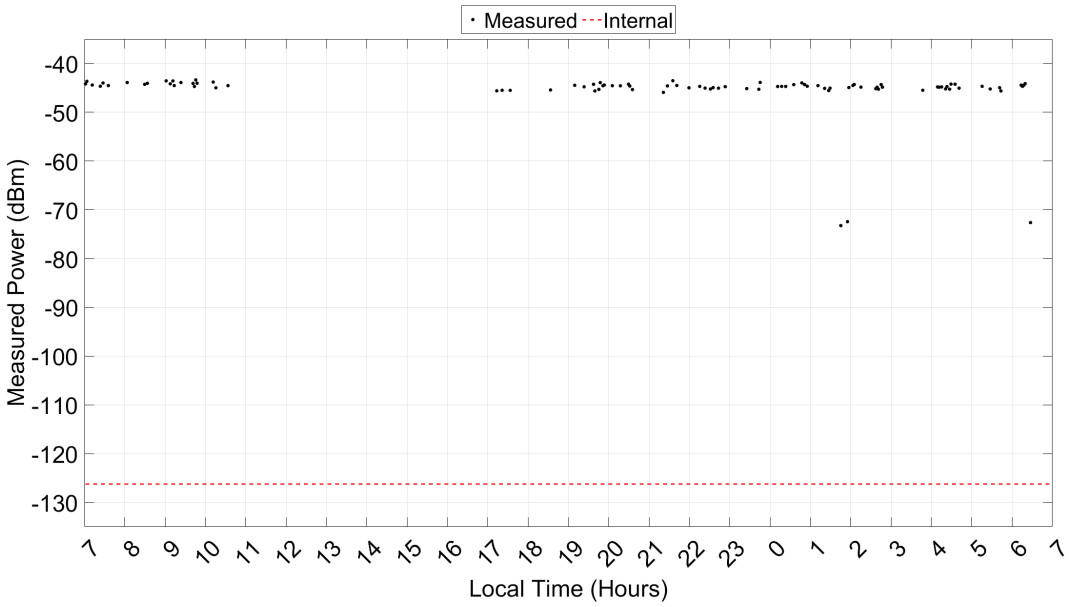

Figure F-11. T-Site CM5 11.256 MHz.

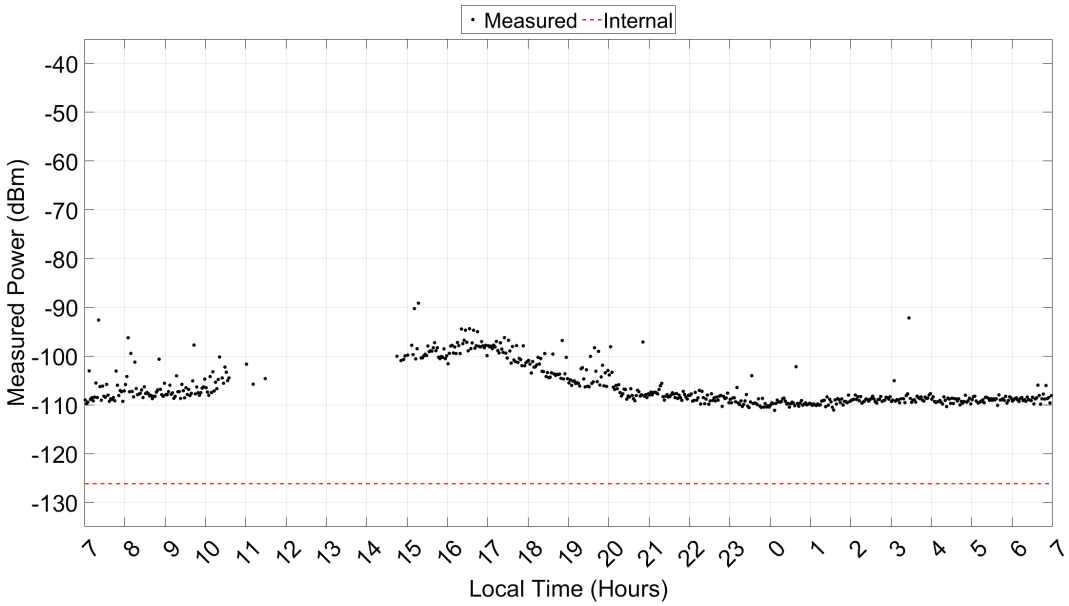

Figure F-12. BITF CM 13.251 MHz.

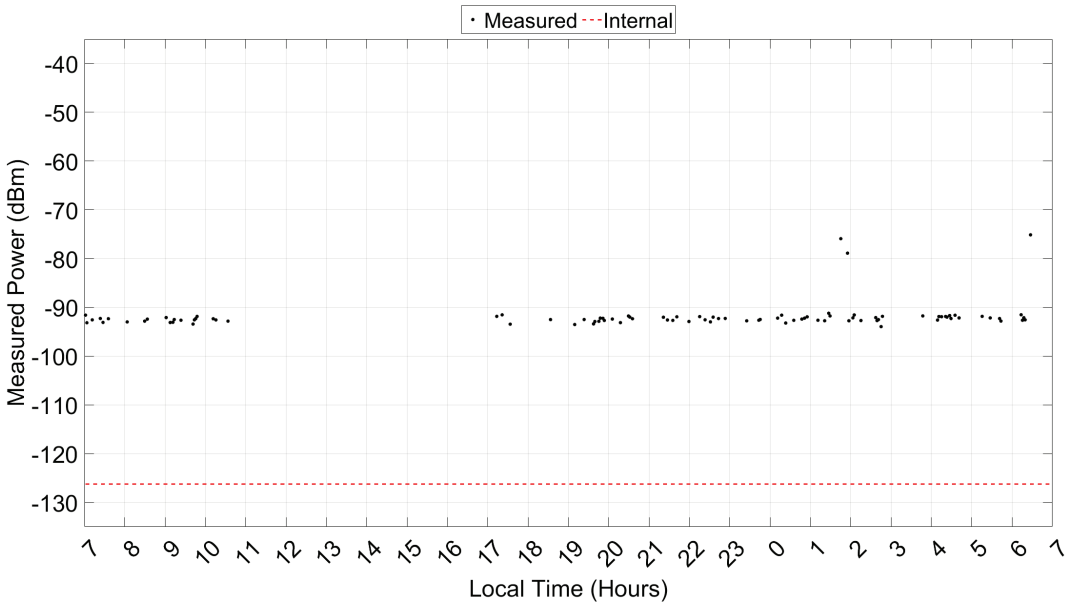

Figure F-13. T-Site CM5 13.251 MHz.

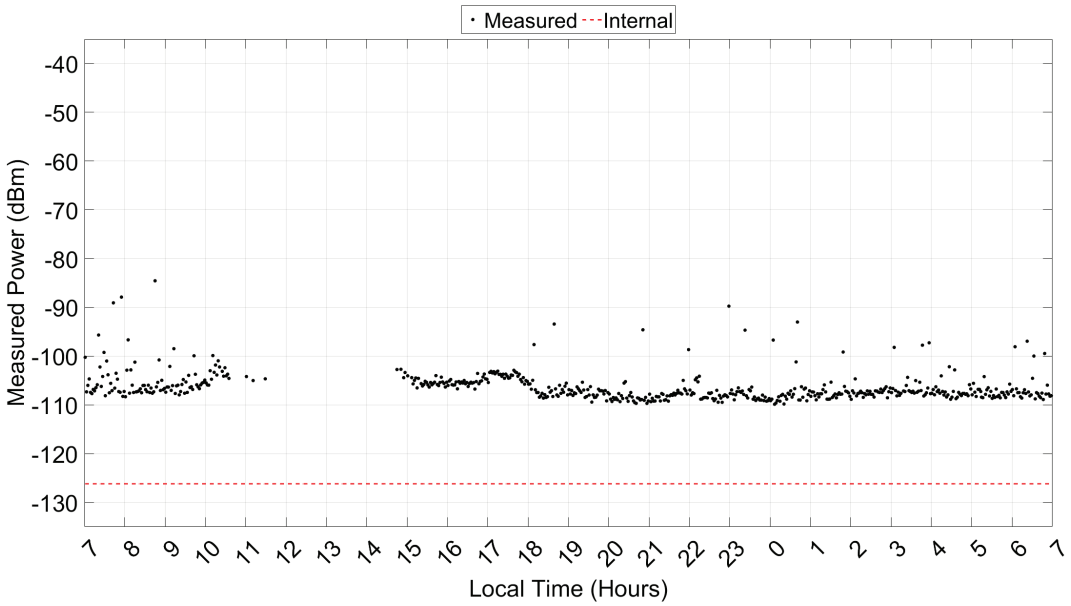

Figure F-14. BITF CM 18.0 MHz.

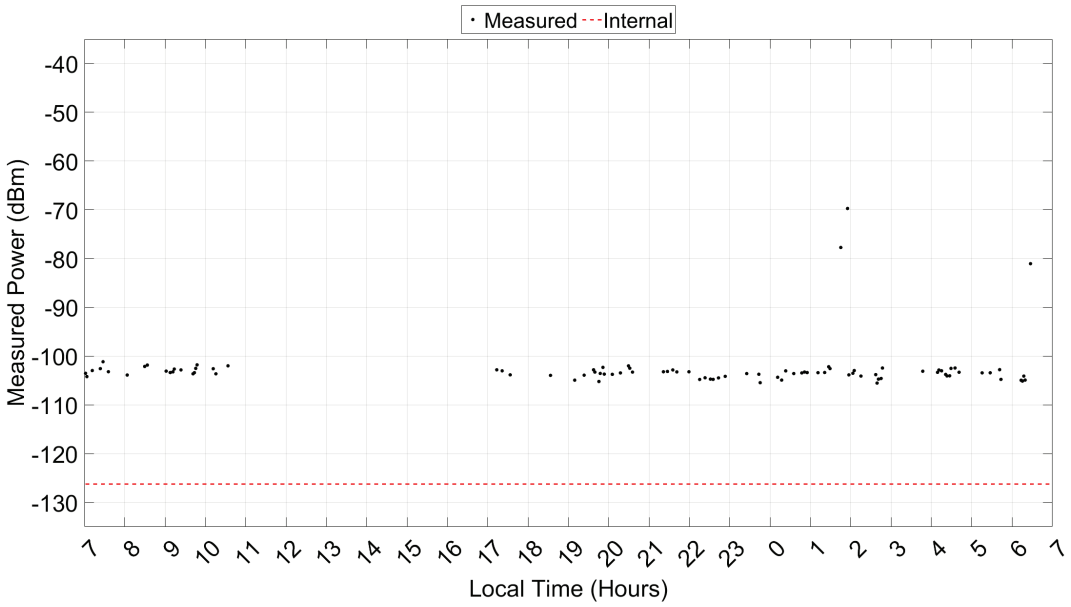

Figure F-15. T-Site CM5 18.0 MHz.

Appendix G. ATC Channel Noise Figure Data

Table G-1. Median noise figures in dB for all locations and ATC channel frequencies in MHz.

Frequency (MHz)	4.718	5.726	6.708	9.032	11.256	13.251	18.000
BITF	30.8	23.9	24.8	26.3	31.5	27.6	20.9
MACOPS	43.9	42.1	37.1	45.2	34.6	36.1	26.7
T-Site	NA	NA	NA	48.8	39.7	32.8	NA
MTRS-2	57.0	51.5	47.7	47.5	44.1	44.0	37.7
MGS	50.3	52.8	59.4	46.0	57.7	41.4	36.9
HS	53.8	52.3	51.7	50.1	43.4	41.4	37.7
AH	48.8	46.2	44.6	54.4	45.0	37.3	32.4

Appendix H. McMurdo Station Historical Photos

Figure H-1. McMurdo Station 1967. (Credit Dave Bresnahan USAP)

Figure H-2. McMurdo Station 2007 (Credit Alan Light USAP)

REPORT DOCUMENTATION PAGE

1. REPORT DATE	2. REPORT TYPE	3. DATES COVERED	
		START DATE	END DATE
September 2025	Technical Report	10/1/2024	9/30/2025

4. TITLE AND SUBTITLE
2024 McMurdo Area Radio Noise Measurements and Analysis

5a. CONTRACT NUMBER	5b. GRANT NUMBER	5c. PROGRAM ELEMENT NUMBER
A2307.049.013.047630		NSF O2406-049-013-032791

5d. PROJECT NUMBER	5e. TASK NUMBER	5f. WORK UNIT NUMBER
6130401-008	003	NTIA-ITS.T

6. AUTHOR(S)
Robert J. Achatz, Adam C. Hicks, Sarah L. Vasel, Ryan S. McCullough

7. PERFORMING ORGANIZATION NAME(S) AND ADDRESS(ES)
Institute for Telecommunication Sciences
National Telecommunications and Information Administration
U.S. Department of Commerce
325 Broadway
Boulder, CO 80305

8. PERFORMING ORGANIZATION REPORT NUMBER
NTIA TR-25-579

9. SPONSORING/MONITORING AGENCY NAME(S) AND ADDRESS(ES)
National Science Foundation
Spectrum Innovation Initiative
415 Eisenhower Avenue
Alexandria, VA 22314

10. SPONSOR/MONITOR'S ACRONYM(S)
NSF SII

11. SPONSOR/MONITOR'S REPORT NUMBER(S)

12. DISTRIBUTION/AVAILABILITY STATEMENT
Approved for public release. Distribution unlimited.

13. SUPPLEMENTARY NOTES

14. ABSTRACT
The Institute for Telecommunication Sciences (ITS) performed high frequency (HF) band (3–30 MHz) radio noise power measurements at six locations in the McMurdo Station (MS), Antarctica (AQ), area and one location at the Black Island Telecommunication Facility (BITF) 32 km (20 mi) from MS. The primary purpose of the measurements is to compare MS and BITF radio noise powers so that HF radio system designers can assess the feasibility of relocating BITF air traffic control (ATC) and field party communication HF antennas and receivers to MS. Measurements were performed with portable rod (PR) and fixed conical monopole (CM) antennas. Twenty-four–hour spectrum occupancy plots show most signals below 15 MHz at BITF and MS. Differences in signal populations between locations were observed. Taking into account the location variability endemic to radio noise, noise at the ATC channel frequencies was found to be generally higher at MS than at BITF. BITF noise was similar to what would be expected of a quiet rural noise environment. MS noise was similar to what would be expected of a rural or residential noise environment, although noise at 9 MHz was comparable to that of an urban setting.

15. SUBJECT TERMS
active rod antenna, air traffic control communications, Antarctica, high frequency radio, HF, man-made radio noise, McMurdo Station, radio noise, spectrum occupancy, Table Mountain Radio Quiet Zone

16. SECURITY CLASSIFICATION OF:			17. LIMITATION OF ABSTRACT	18. NUMBER OF PAGES
a. REPORT	b. ABSTRACT	C. THIS PAGE		
Unclassified	Unclassified	Unclassified	UU	121

19a. NAME OF RESPONSIBLE PERSON	19b. PHONE NUMBER (Include area code)
Robert J. Achatz	720-642-6705